Astronomy & Astrophysics

(CAUCASUS)

International Scientific Journal

1

SAMTSKHE-JAVAKHETI STATE UNIVERSITY PRESS

2016

UDC 52(050)(479.22)

A-89

Astronomy & Astrophysics

(CAUCASUS)

Samtskhe-Javakheti State University Press

Email: astronomy@sjuni.edu.ge

Our brief history

Our small university, in which 1,500 students are enrolled, is 26 years old. Initially, in 1990, Samtskhe-Javaketi State University was established as a branch of Ivane Javakhishvili Tbilisi State University. This establishment introduced and strengthened Tbilisi University traditions in Akhaltsikhe. From the beginning, we decided to pursue a scientific direction. The co-existence of learning and scientific development helped us to gain prominence in the region, which was a challenge during the economic, political, and social hardships of 1990s. From the outset, the local Georgian and non-Georgian population trusted us. Many collegiate, national, and international conferences were held at our University. Thus the University became the foundation of scientific intelligence of South Georgia.

The Abastumani Astrophysical Observatory was the only serious research institution in Samtskhe-Javakheti. It was known in scientific circles for its important scientific work. The University made close scientific contacts with the Observatory from the very first days of its existence.

Observatory staff started their pedagogical careers at our University. Academician Evgeni Kharadze, who led the Observatory from the date of its establishment, managed these relations and scientific contacts. At the same time, he was the rector of the Ivane Javakhishvili Tbilisi State University in 1959-1966. So, academic and scientific activities were very familiar to him.

In 1992, Evgeni Kharadze and George Tchoghoshvili supported the establishment of the Faculty of Mathematics and Astronomy at the Akhaltsikhe branch of Tbilisi State University. At the time, Revaz Chigladze was the head of the department.

Evkgeni Kharadze often visited the branch. Several times, he was a chairman of the State Examination Commission, where our graduates passed their final exams.

Professors Revaz Chigladze, Raguli Inasaridz , Lorand Sigua, Khvedri Inasaridze, Rolan Kiladze , Victor Japiashvil and others helped to promote close scientific and educational contacts between Astrophysical Observatory and the University. They worked in Akhaltsikhe and Abastumani. The geographical proximity of these two locations strengthened future research activities. Our university graduates Bidzina Kapanadze, Marekh Ivanidze and Diana Ivanidze defended their doctoral dissertations .

In 2014, Samtskhe-Javakheti State University was formed on base of the branch and the State Teaching University. Our doctoral program in astronomy was accredited, which was an important incentive, especially for the staff members who have done a lot of scientific work and have had many years of experience in astronomy, but could not manage to get their doctoral degrees due to the absence of the Doctoral Degree Defense Council. Among them are Givi Kimeridze, Eduard Janiashvili, Roman Ivanidze, Manana Vardosanidze, Maia Sikharulidze, and others.

In addition to our University professors, the Samtskhe-Javakheti Doctoral Council in Astronomy includes Javakhishvili and Ilia State University professors and researchers at the Abastumani Astrophysical Observatory. Samtskhe-Javakheti State University is the only university in Georgia that offers educational programs in astronomy at the Bachelor's, Master's, and Doctoral levels.

Scientists of the traditional Georgian Astronomical School have not had the opportunity to hold international scientific conferences in Georgia for many years. Samtskhe-Javakheti State University hosted an international conference on October 7-9, 2015. Conference organizers and participants decided to print the conference proceedings. Other scientists responded to this publication and expressed their desire to include their works in the publication. Our organization eagerly shared the relevant work, and today we have a collection of scientific works.

We want to thank all the authors, the organizational and editorial members of the group, the faculty of engineering, agricultural and natural sciences - Dean: Professor Giorgi Meskhi, Vice Rector Professor Maka Kachkachishvili-Beridze, Senior specialist Manana Ioseliani and especially, Editor Professor Revaz Chighladze, for their hard work.

Samtskhe-Javakheti State University Rector, Professor M. Beridze

Astronomy & Astrophysics (Caucasus) 1, (2016) 4-10

Research of the NH_3 Lines in the Region λ 6475 Å Band of Jupiter Spectrum

A. A. Atai, H. M. Mikhailov and Z. S. Farziyev
Azerbaijan National Academy of Science Shamakhi Astrophysical Observatory named after N. Tusi

Email: atai1951@yahoo.com

Received March 11, 2016; revised May 18, 2016

Abstract

In 2014, spectral observations of separate areas on the disk of Jupiter in the visible spectrum were made by means of the echelle-spectrometer installed in Cassegrain 2-meter mirror telescope's focus of Shamakhi Astrophysical Observatory. The echellespectrometer equipped with the CCD camera provided spectral resolution R=14000 with dispersion of 10 Å/mm. Aims. Features of the intensity change of the ammonia absorption lines at 6475 Å were studied for the spectra of different details of Jupiter's disk. The absorption line 6495.7 Å for ammonia was found only in the GRS spectrum of Jupiter. Methods. Earlier that line was noted in the laboratory spectrum of Giver; it was absent in the spectrum obtained by Mason; in the theoretical spectrum of ammonia it was noted at 6495.9 Å. Comparison of characteristics of the ammonia line in the spectra of various details allows investigating horizontal inhomogeneity of ammonia distribution on the Jupiter's disk. Results.
Key words: Jupiter, ammonia, absorption lines, NH3, 6475 Å band

1. Introduction

Studies of the planets atmospheres by high spectral resolution methods allow revealing of many factors acting in their atmospheres, which influence on the observed lines of molecular gases. For example, due to the known Doppler effect the lines should be expanded. On the other hand, hydrogen lines are also subject to the shock narrowing effect, because of which there is a distortion (compression) of the line profile caused by Doppler spread. In addition, at high pressures a shift effect occurs which causes asymmetrical broadening of the line.

The absorption bands in the spectra of Jupiter and other giant planets of the Solar system had been studied with small and average dispersion at the beginning of XX-th century by Slipher (1908, 1933)and Vildt; for more than 100 years, scientists try to specify chemical composition of the atmospheres of the planets for further tracking physical phenomena that occur in them. For example, in 1973, from the board of the Pioneer 10 space probe, helium glow was registered on Jupiter and it was defined that helium content is much less than that of hydrogen one. The most important discovery was detection of the water vapor in the Jupiter atmosphere.

One of the main tasks of the ≪Juno≫ spacecraft which took off to Jupiter on August 5, 2011 is studying chemical composition of the planet atmosphere.

It was succeeded to determine quite precisely the average molecular weight of Jupiter atmosphere by the aim of different observation methods. It is quite reliably revealed that the atmospheres of the Jupiter group planets consist of light gases (helium and hydrogen) mainly. Observing with telescopes equipped with fourier-spectrographs discovered also acetylene, ethane, deuteromethane, deuterohydrogen, phosphene, cyanogen-hydrogen, germanium tetra-hydride, carbon monoxide and other molecular compounds, which are present in the Jupiter atmosphere in insignificant amounts.

In the conditions of the Jupiter atmosphere, methane is not condensed and its content doesn't almost change from place to place. But ammonia, hydrogen sulfide and water are sensitive to temperature

changes in the Jupiter atmosphere; their content depends on the depth and the coordinates on the planet surface. It should be noted that ammonia plays an important role in the Jupiter atmosphere, almost like water vapor in the terrestrial atmosphere. This molecular gas actively participates in all kinds of chemical reactions with hydrocarbons and sulfur. In particular, it can form hydrosulfide of ammonium NH_4SH, which is considered to be, a major factor in formation of an intermediate cloud layer in the troposphere of Jupiter between ammoniac and water layers of clouds.

Inhomogeneous distribution of the ammonia over the Jupiter disk, and also the variation of its amount in vertical and horizontal directions in the atmosphere of the planet are of a great interest and the subject of research both due to ground-based observations and space missions (for more detailed information see monographs of V.D. Vdovichenko, G. A. Kiriyenko 2013, 201).

After putting into operation of the 2-meter telescope in Shamakhi Astrophysical Observatory, research of Jupiter and Saturn atmospheres were started (Ibragimov N.B. 1974, 1975) and new spectrograms of the equator and the central meridian of Jupiter were obtained in 1969-1974.

In this article, the results of analysis of the Jupiter's spectrograms were used for clarifying the peculiarities of the NH_3 absorption lines at 6475Å (traditionally referred to as the 6450 Å band or as $5\gamma_1$ after Badger) over the planet disk.

2. Observations

In February-March, 2014 (namely, 7/8.02.; 12/13.02 and 05/06.03 of 2014), observations of Jupiter were conducted with the use of the echelle-spectrometer equipped with the CCD camera (580×530 pixel) installed in the Cassegrains focus of the telescope (Kh.Mikayilov and al.). The processing of the eshelle- spectrograms CCD images were carried out by the DECH 20 software package developed in SAO of the Academy of Sciences of the Russian Federation by Galazutdinov. The DECH 20 program allows three possibilities for determination of the equivalent widths: direct integration, building the profile manually, and by the Gauss method. We used direct integration and the Gauss method. The difference in the results is not big because the lines are narrow and have a small half-width.

During each night of observation, 14 spectra of the planet and 2 spectra of the standard star were obtained in the region of wavelengths λλ 4700-6800 ÅÅ with dispersion of 10 Å/mm at Hα (spectral resolution R=14000).

As a rule, spectra obtained in one night were averaged and then, the resultant spectrum for every night was processed. In order to define new wavelengths taking into account shifting of Fraunhofer and planetary lines, a dispersive curve with high precision was plotted. The spectra of the daytime sky emission was used for creation of the dispersion curve.

3.Analysis

Experimentally defined and theoretically calculated wavelengths of ammonia absorptionlines at 6475 A are given in Table 1.

Wavelengths for absorption lines of ammonia gas theoretically calculated by R.M. Badger and S.H. Chao are given in columns 1 and 2, correspondingly. The respective data for the wavelengths, determined by laboratory measurements of H.P. Mason and L.P. Giver et al, D.H. Rank et al. , C.C. Kiess et al., are given in columns 3, 4, 5 and 6, accordingly.

As a result, the equivalent width of W(mÅ), half width of the NH_3 absorption lines at 6475 Å for different details of the Jupiter disk (Table 2) were determined by us.

Note:

EZ - Equatorial zone

STB - Southern Temperate Belt

NEB - Northern Equatorial Belt

SPR - Southern Polar Region

NTrZ - Northern Tropical Zone

GRS - Great Red Spot

NPR - Northern Polar Region

In the spectra of the planet obtained during three observation nights, 20 lines of ammonia proved to be suitable for con- fident enough processing (see Tab. 2). Different details on the Jupiter disk were chosen for having an opportunity to compare horizontal distribution of ammonia absorption (designation of the details is given in the Notes). The obtained values of depth and half-width of spectral lines are influenced by the tool pro- file of the spectrograph. To determine the tool contour half-width, those of telluric absorption lines of the atmospheric oxygen 6290 Å (the line - 6490.22 Å) were measured; as those lines are forbidden, their half-widths must be very narrow, so has to be defined by the half-width of the instrumental contour only.

4. Preliminary Results and Discussion

Measured half-widths and depths of ammoniac lines were recounted for the instrumental contour by the following approximate formulas (Kozhevnikov):

$$R = R_{obs}\left(1 + \frac{\gamma_{inst}^2}{\gamma^2}\right) \qquad (1)$$

$$\gamma = \sqrt{\gamma_{obs}^2 - \gamma_{inst}^2} \qquad (2)$$

where γ_{inst} is the half-width of the instrumental contour, R_{obs} and γ_{obs} are the observed depth and half-width of the line, R and γ are the true depth and half-width of the ammonia absorption lines.

For comparing and controlling the intensity change of the NH_3 absorption lines at 6475 Å in different details, Fraunhofer line FeI λ 6469.19 Å was chosen, as in the spectruma of the studied details, the intensity of that line remains almost constant. Observations of Jupiter in 2014 show that the intensity of the ammonia absorption line at 6475 Å is generally higher in the Northern part of the planet, than in the Southern part of the disk. In the Southern part of the disk, the greatest intensity is detected only in some lines of ammonia in the GRS spectrum. As the intensity of unsaturated lines of ammonia is directly proportional to the number of molecules , it is clear that the abundance of NH_3 in the Northern part of Jupiter's disk is more than in the Southern part of the sight beam disk; and in the Southern part of GRS, the abundance of NH_3 is less than in the surrounding area. These observation results coincide with data CA (Achterberg and al.).

The detected line 6495.7 Å for ammonium was mentioned in the laboratory list of Giver and others (Giver and al.); that line was noted as 6495.9 Å in Badger's and others' work (Rank and al.). In Ibragimov's list it was noted as 6496.0 Å and was clearly visible on the spectrogram taken in 1970 and on some spectrograms in 1971. However, in our observation in 2014, the ammonia line 6495.7 Å is detected only in the GRS spectrum on Jupiter. It should be noted that the ammonia absorption line 6495.7 Å is absent in the laboratory list of Mason. In spectruma of some Jupiter details, the NH_3 absorption lines 6490.47 and 6489.8 Å were blended with one-another, and to separate them was not possible, except spectruma of GRS and the Southern Polar Region of the planet.

Based on the results of those observations, the 6451.12 Å line contour for NH_3 was built (Fig. 1) with taking into account the tool contour according to the approximate formulas (1) and (2).

Comparison of ammonia lines spectruma for different details of Jupiter disk reflects strong change of their intensity. This defines horizontal inhomogeneities on the Jupiter disk at the depth of cloud layers where the observed ammonia absorption lines are formed. The obtained observation data allow to calculate the rotary temperature, the change of concentration of aerosol and gas components in structural formations, and also the degree of deviation from homogeneity in the Jupiter atmosphere. Determination of those parameters of the Jupiter atmosphere will be subject of the following article.

It is clearly seen from Fig. 2, that in the area of the GRS there is minimal absorption of ammonia. However, it should not be neglected that due to the insufficient high spatial resolution of the observation, those data present average information for the area of the studied cloudy formations.

Actually, based on the results of both CIRS and ground data, the structure of NH_3 distribution around GRS is complicated (Fletcher and al.). The maximum of information is obtained from the observations carried out by using 8-11 micron filters; those data belong to the pressure level of 550 mbar, i.e., to the intermediate heights. The content of ammonia along the GRS constantly reveals asymmetry in the direction of the North-South, raising on the most northern edge and in the whirlwind centre (~ 70 ppm) and going down to the South, in places of warmer periphery (~30 ppm). Nevertheless, all the information of the atmosphere parameters inside the "interior" of GRS demonstrate North-South asymmetry, showing higher degree of ammonia content towards the North from the warm centre, closest to the SEB, and the lowest contents in a symmetric arch which is close to the southern periphery near STrZ that is characterized by the highest temperatures.

Similar North-South asymmetry was observed by IRTF spectroscopy (Lara and al.); and a strong shortage of ammonia on the South edge of the GRS indicates strong subsidence of the atmospheric masses in this place. The lack of NH_3 around GRS is observed usually over wider spectrum of latitudes in comparison with two narrow ≪ruptures≫ of high transparency about which it was said above, and stretches inside the STrZ and inside the Southern Temperate Belt.

The analysis of the observation data on the ammonia absorption at the λ 6475 Å band shows strong variations of the line intensity over the Jupiter disk. Once again, it proves importance of the long-term ground based spectral observations of Jupiter (as well as Saturn) in the region of the ammonia absorption lines which are sensitive, in particular, to local temperature changes. In its turn, this helps to understand the essence of the dynamic processes that happen in the Jupiter atmosphere which lead to disappearance of the old and the birth of new details and formations on the planet disk. Of course, it would be better if those researches would be carried out with high spectral and spatial resolution during long time periods, i.e. patrol observations. Such an approach creates the necessary base for the disclosure of secrets of the unknown intermediate phenomena that play a big role in the evolution of the atmospheres of giant planets.

5. Acknowledgments

The authors express gratitude to V.D. Vdovichenko for valuable remarks and very useful suggestions.

Table 1. Wavelengths of ammonia absorption lines at the 6475 Å band

1[Badger]	2[Chao]	3[Mason]	4[Giver]	5[Rank]	6[Kiess]
Badger	Chaos	Mason	Giver	Rank ..	Kiess
6419.5	-	6419.4	-	6443.79	6433.6
6422.2	6425.87	6425.6	-	6444.63	6435.09
6423.3	6426.9	6426.8	-	6445.53	6435.92
6425.5	6429.26	6429	-	6446.41	6436.98
6426.5	6429.75	6429.5	-	6447.15	6437.86
6427.8	6433.64	6433.6	-	6449.19	6440.5
6428.6	6434.93	6435	-	6451.02	6442.43
6429.7	6435.38	6435.3	6443.79	6452.12	6443.73
6431.8	6437.04	6437.1	6444.63	6452.6	6444.56
6434.5	6437.5	6437.7	6445.53	6457.12	6445.49
6435.6	6441.51	6441.4	6446.41	6459.08	6446.38
6438.2	6441.07	6441.9	6447.15	6460.5	6446.55
6442.5	6442.52	6442.5	-	6465.42	6447.13

6446.2	**6442.97**	**6442.9**	**6449.19**	**6469.64**	**6448.45**
6449.5	**6493.84**	**6443.8**	**6449.92**	**6479.3**	**6449.01**
6450.4	**6444.63**	**6444.5**	**6451.02**	**6488.24**	**6450.32**
6453.1	**6445.59**	**6445.6**	**6452.12**	**6489.86**	**6451.04**
6455.4	**6446.42**	**6446.4**	**6452.6**	**6490.45**	**6452.02**
6457.4	**6447.21**	**6447.2**	**6454.06**		**6452.51**
6460.1	**6448.37**	**6448.5**	**6454.36**		**6453.95**
6460.8	**6451.04**	**6451.1**	**6455.84**		**6454.32**
6463.6	**6451.12**	**6452.1**	**6457.12**		**6457.11**
6464.7	**6452.62**	**6452.6**	**6459.08**		**6458.16**
6464.9	**6454.45**	**6454.3**	**6460.5**		**6459.06**
6465.6	**6455.9**	**6455.8**	**6465.42**		**6460.42**
6467.9	**6457.16**	**6457.1**	**6467.45**		**6461.27**
6468.2	**6458.61**	**6458.1**	**6469.64**		**6465.34**
6470.3	**6460.5**	**6460.5**	**6470.71**		**6466.49**
6474	**6465.39**	**6465.4**	**6474.24**		**6467.42**
6474.7	**6470.74**	**6470.7**	**-**		**6468.27**
6475.7	**6472.04**	**6472**	**6479.3**		**6469.64**
6478.8	**6478.07**	**6477.9**	**6488.24**		**6470.02**
6479.6	**6478.45**	**6478.3**	**6489.86**		**6470.65**
6483.2	**-**	**6478.8**	**6490.45**		**6471.94**
6485.3	**6488.26**	**6488.4**	**6495.7**		**6472.74**
6485.8	**6489.86**	**6489.9**	**6498.73**		**6473.03**
6486.9	**6490.53**	**6490.6**	**6500.2**		**6474.16**
6488.5	**6493.8**	**6493.8**	**6501.16**		**6474.78**
6489.5	**6498.74**	**6498.9**	**6510.97**		**6476.69**
6492.4	**6500.01**	**6500.1**			**6477.05**
6494.9	**6505.12**	**6505.2**			**6483.36**
6495.9	**6505.55**	**6505.7**			**6484.01**
6498.2	**6505.1**	**6506.1**			**6485.74**
6499.3	**6506.56**	**6506.6**			**6486.18**
6501	**6509.23**	**6509.3**			**6488.23**
6501.8	**6511.01**	**6511.1**			**6488.81**
6506.6	**6511.52**	**6511.6**			**6489.85**
6510.9	**6520.56**	**6520.5**			**6490.34**
6512.9	**6521.46**	**6521.3**			**6498.87**
6514.9	**-**	**6531.4**			
6517.1	**6536.42**	**6536.4**			
6519.9					
6522.7					
6525.9					
6528					
6529.4					

Table 2. The equivalent width of W(mÅ) and half width of the NH3 absorption lines at 6475 Å for different details of the Jupiter disk

	EZ	EZ	NEB	NEB	NTrZ	NTrZ	NP
λ(Å)	Δλ(Å)	W(mÅ)	Δλ(Å)	W(mÅ)	Δλ(Å)	W(mÅ)	Δλ(Å)
6433.6	0,55	36,8	0,53	33	0,51	30,6	0,4
6435	0,23	13,8	0,25	12,3	0,25	9,3	0,3
6437.8	0,50	53	0,60	59,8	0,64	51,9	0,6
6444.6	0,47	41	0,60	44	0,57	34,5	0,6
6445.5	0,52	49,4	0,46	41	0,60	42	0,6
6446.4	0,52	52,7	0,44	41,8	0,44	35,6	0,5
6451.12	0,44	42,7	0,42	37,3	0,40	30,8	0,5
6452.6	0,38	44,8	0,41	43,2	0,39	17,6	0,5
6454.36	0,55	50,4	0,49	41,8	0,52	19,9	0,4
6457.12	0,50	56,3	0,54	56,4	0,50	46,3	0,4
6459,08	0,38	20,1	0,40	21,4	0,47	18,5	0,4
6460,50	0,42	19,4	0,28	13,8	0,39	16,1	0,4
6465,40	0,46	29,8	0,44	33,1	0,41	23,8	0,4
6479,30	0,49	36,3	0,71	47,3	0,63	40,1	0,5
6488,24	0,48	36,9	0,41	28	0,48	30	0,2
6489,80	0,64	55,2	0,73	59,4	0,67	54	0,7
6490,47							
6495,70	-	-		-		-	-
6498,70	0,63	74	0,60	71,3	0,55	61	0,6
6501,60	0,49	37,7	0,54	35,9	0,48	29,1	0,5
6469,19	0,60	66,8	0,57	67	0,57	61	0,6

	STB	STB	SPR	SPR	GRS	GRS
λ(Å)	Δλ(Å)	W(mÅ)	Δλ(Å)	W(mÅ)	Δλ(Å)	W(mÅ)
6433.6	0,41	22,1	0,41	23	-	-
6435	0,19	7,2	0,16	7,3	0,17	6,5
6437.8	0,59	49,6	0,47	30,7	0,43	30,1
6444.6	0,45	23,7	0,46	22,1	0,64	27,5
6445.5	0,45	27,2	0,66	33,5	0,64	35
6446.4	0,44	29,7	0,54	30,1	0,65	34
6451.12	0,25	16,9	0,47	32,3	0,37	19
6452.6	0,43	36	0,42	34	0,32	19
6454.36	0,37	24,6	0,52	31,4	0,64	37
6457.12	0,43	40,8	0,49	40	0,65	51
6459,08	0,31	12,8	0,44	14,5	0,40	11,3
6460,50	0,23	9,1	0,43	16	0,37	8,6
6465,40	0,39	23,8	0,44	22,4	0,29	11,4
6479,30	0,53	32,6	0,53	25	0,41	21
6488,24	0,66	40,7	0,63	34	0,37	17,9
6489,80	0,66	53	0,44	33,2	0,43	21

6490,47			**0,39**	**27**	**0,36**	**22**
6495,70	**-**	**-**	**-**	**-**	**0,83**	**16,5**
6498,70	**0,69**	**72**	**0,76**	**76,8**	**0,65**	**47,9**
6501,60	**0,41**	**22,6**	**0,49**	**40,8**	**0,29**	**17,4**
6469,19	**0,58**	**63**	**0,65**	**60**	**0,63**	**57**

References

Achterberg R. K., Conrath,, B. J., Gierasch P. J., 2006, Cassini CIRS retrievals of ammonia in Jupiters upper troposphere, Icarus, V.182. p. 169-180.
Astron.Zh., V.52 ,N 4, p. 895-898.
Astrophysical Observatory, Astron.Zh., V.51, N 1, p. 178-186.
Badger R.M., 1930, Absorption bands of ammonia gas in the visible , // Physical Rev. , May 1, V. 35, p. 1038-1046.
Chao S., 1936, The photograph infrared spectrum of gaseous ammonia, Phys. Rev., 50, p. 27-37.
Fletcher Leigh N., G. S. Orton, O. Mousis, P. Yanamandra-Fisher, P. D. Parrish, P. G. J. Irwin, B. M. Fisher, L. Vanzi, T. Fujiyoshi, T.Fuse, A.A. SimonMiller, E. Edkins, T.L. Hayward, J. De Buizer, 2010, Thermal Structure and Composition of Jupiters Great Red Spot from High-Resolution Thermal Imaging, Icarus 208, p. 306-328.
Galazutdinov G.A. , Eshele spectra processing system DECH20, Preprint No. 92 (Spec. Astrophys. Observ)., Nizhny Arkhyz, p. 52.
Giver L.P., Miller J.H., Boese R.W., 1975, A laboratory atlas of the 5 ν1 NH_3 absorption band at 6475 Å with application to Jupiter and Saturn, Icarus, 25, N1, p. 34-48.
Ibragimov N.B., 1974, Investigation of Jupiter and Saturn with the 2-m reflector of the Shemakha
Ibragimov N.B., 1975, Determination of the abundance of ammonia in the atmosphere of Jupiter,
Kh.Mikayilov, V.M.Khalilov and I.A.Alekberov, 2005, Echelle spectrometer for Cassegrain fokus of 2-meter telescope of the Shamakhy Astrophysical Observatory Tsirk. ShAO 109, p. 21-29.
Kiess C.C.,.Corliss C.H. and Kiess H.K., 1960, High-dispersion spectra of Jupiter, Ap.J., V.132, p. 221-231.
Kozhevnikov, N. I., Sitnik G. F., Khlystov,1972, I. Profiles and half-widths of telluric lines , So Sht. N. 180 p.3-19.
Lara L., Bezard B., Griffith C., Lacy J., Owen T., 1998, High-resolution 10- micronmeter spectroscopy of ammonia and phosphine lines on jupiter. Icarus 131 (2),p. 317-333.
Mason H.P.,1970, The abundance of ammonia in the atmosphere of Jupiter, Astrophys. and Space Sci., 7, N.3, p. 424-436.
Rank D.H., Fink U. and Wiggins T. A., 1966, Measurements of spectra of gases of planetary interest. II. H2, CO2, NH3 and CH4, Astrophys. J., V. 143, N.3, p. 980-988.
Slipher V.M., 1908, "The Spectrum of the Major Planets," Lowell. Observ. Bull., no. 42, l, p. 231.
Slipher V.M.,1933, Spectrographic studies of the planets, Monthly Notices Roy. Astron. Soc, v. 93, p. 657-668.
Smith W.H.,.Macy W., Cochran W., 1980, Ammonia in the atmospheres of Saturn and Jupiter, Icarus, V.42. p. 93-101.
Vdovichenko V.D., Kirienko G.A., 2013, The investigation of Jupiter, Mars,Titan and Vesta, LAP LAMBERT Academic Publishing, LAP LAMBERT Academic Publishing, p. 386.
Vdovichenko V.D., Kiriyenko G.A., 2014, The atmosphere of Jupiter. The Great Red Spot, LAP LAMBERT Academic Publishing, p. 275.
Vildt R.,1932, Note on the spectra of Jupiter and Saturn, Veroff. Univ. Sternwarte Gottingen, N. 22.

Astronomy & Astrophysics (Caucasus) 1, (2016) 11-16

Electropolarimetric Study of Jupiter's Galilean Satellites

R. A. Chigladze
Samtskhe-Javakheti State University, Kharadze Abastumani Astrophysical Observatory, Georgia

Email:**revazchigladze@ yahoo.com**

Received March 12, 2016; revised May 18, 2016

Abstract

In the indicated work polarization properties of the light, reflected from Jupiter's satellites, are studied. Maximum difference is noticeable between polarization degrees of light, reflected from the front and rear hemispheres of the satellite. For the satellites, located relatively close to Jupiter (Io, Europe, Ganymede), the magnitude of polarization degree of light, reflected from the front hemisphere, is comparatively less than that the magnitude of polarization degree of light, reflected from the rear hemisphere, and vice versa for the satellite Callisto. In the presented paper an acceptable hypothesis is presented in order to explain the mentioned differences.

Key words: Galilean satellites, polarization degree, front and rear hemispheres

1.Introduction.

It is possible to name only several scientific works (Dolffus.1975, Geake, Dollfus.1979, Veverka.1971, Botvinova, Kucherov.1980,Bolkvadze.1973,Bolkvadze et al. 1986) in which polarization properties of Jupiter's Galilean satellites are studied insufficiently.

Proceeding from the above stated since 1981 the author has set his mind on the investigation of polarization properties of Jupiter's Galilean satellites in the alpha angle of each phase and in ten different areas of visible spectrum (Chigladze.1984,1985,1987). The observed material was obtained at Abastumani Astrophysical Observatory on both 40-cm refractor and 125-cm reflector, to which the polarimeter ASEP-78 was attached during observations.

Due to the fact that consideration of the effect of Jupiter's surrounding background is rather complicated, we have not conducted Jupiter's observations from limb along 2-3 radii vision ray. It should also be mentioned here that a mean square error of one measurement during observation without filter does not exceed 0.05%. The observational method is described in the work in detail. (R.A.Chigladze 2001).

Taking all the above stated in the account a relatively reliable observation of Jupiter's Galilean satellites is possible when they are within the following orbital intervals:

Io	$]30^o; 150^o[$ and $]210^o; 330^o[$
Europe	$]19^o; 161^o[$ and $[119^o; 341^o[$
Ganymede	$]12^o; 168^o[$ and $]192^o; 348^o[$
Callisto	$]7^o; 173^o[$ and $[187^o; 353^o[$

In general the magnitude of polarization degree of the light, reflected from the satellite's surface, must vary depending on α-phase angle, satellite orbital longitude L, wave length λ and observation period t, or $P = P(\alpha, L, \lambda, t)$.

2.Observations.

In the indicated work polarization properties of the light, reflected from Jupiter's satellites, are studied. Maximum difference is noticeable between the polarization degrees of the light, reflected from satellites' front and rear hemispheres. For the satellites, located relatively close to Jupiter (Io,

Europe, Ganymede), the magnitude of polarization degree of light, reflected from the front hemisphere, is comparatively less than the magnitude of polarization degree of light, reflected from rear hemisphere, and vice versa for satellite Callisto. An acceptable hypothesis is presented in order to explain the mentioned differences.

Based on the processing of obtained material we deduce that:

The magnitude of polarization degree of the light, reflected from the front side ($L \approx 90^o$) of the satellite Io during observations without filter is in absolute magnitude by 0.15 – 0.20% less than the magnitude of the polarization degree of the light, reflected from the rear side ($L \approx 270^o$) when the phase angle $\alpha \approx 5^o$, while the magnitude of polarization degree of the light, reflected from satellite Io's rear hemisphere is equal to $P(\alpha) = P(5^o) = -0{,}38\%$ (Table 1).

Table 1

Io

Data	Telescope (cm)	α^o	L^o	P%
1981 March 0.909	40	4.9	100	-0.20
1982 March 27.960	125	5.6	270	-0.38
28.875	125	5.2	114	-0.21
1985 July 8.836	125	5.6	70	-0.18
1987 September 24.958	40	5.3	280	-0.39
25.948	40	5.2	123	-0.20

The magnitude of polarization degree of light, reflected from satellite Europe's front side during observations without filter is in absolute magnitude by 0.12% less than the magnitude of polarization degree of light, reflected from the rear side, when phase angle $\alpha \approx 3^o.5$, and the magnitude of polarization degree of light, reflected from satellite Europe's rear hemisphere, is equal to $P(\alpha) = P(3^o.5) = -0.25\%$ (Table 2).

Table 2

Europe

Data	Telescope (cm)	α^o	L^o	P%
1982				
May				
16.881	125	4.0	322	-0.24
21.911	125	4.9	113	-0.12
1984				
June				
7.801	40	4.6	263	-0.24
9.941	40	4.0	120	-0.15
1985				
July				
10.854	40	3.5	262	-0.25
1987				
September				
27.875	125	4.7	124	-0.13

The magnitude of polarization degree of the light, reflected from satellite Ganymede's front side during observations without filter in absolute magnitude is by 0.15 – 0.18% less than the magnitude of polarization degree of light, reflected from the rear, when phase angle $\alpha \approx 5^o$, while the magnitude of polarization degree of the light, reflected from satellite Ganymede's rear hemisphere, constitutes $P(\alpha) = P(5^o) = -0.40\%$ (Table 3).

Table 3

Ganymede

Data	Telescope (cm)	α^o	L^o	P%
1981				
March				
3.952	40	4.4	289	-0.42
1982				
May				
16.923	125	4.0	3.2	-0.18
18.896	125	4.4	131	-0.22
21.952	125	4.9	284	-0.40
1985				
July				
7.870	40	5.8	91	-0.15
10.813	40	5.3	239	-0.35
1987				
September				
25.844	125	5.2	95	-0.21
28.903	125	4.5	249	-0.36

The magnitude of polarization degree of light, reflected from satellite Callisto's front side during observations without filter in absolute magnitude is by 0.65% more than the magnitude of polarization degree of the light, reflected from the rear side, and constitutes 0.35% (Table 4).

Table 4

Callisto

Data	Telescope (cm)	α^o	L^o	P%
1982				
July				
12.946	125	10.6	89	-0.98
August				
15.790	40	10.1	97	-0.95
1984				
August				
29.849	40	10.1	268	-0.42
1985				
June				
12.818	40	9.4	295	-0.43
1988				
September				
12.917	40	11.3	277	-0.26
13.042	40	11.3	280	-0.29
22.024	40	10.6	93	-1.08

3.Analysis .

It is evident that the magnitude of polarization degree of the light, reflected from the front hemisphere of the first three satellites (Io, Europa, Ganymede), is less than the magnitude of polarization degree of the light, reflected from the rear hemisphere, while in the case of satellite Callisto it is vice versa. One of the possible hypotheses for explaining this phenomenon is the following: as is known there is a shower of a multitude of meteorites, moving both on circular and elliptic orbits. Showers of meteors, moving on elliptic orbits in the direction, coinciding with that of the satellite direction, must be the reason of the above mentioned exposed difference. These showers are falling asymmetrically upon the satellites' front and rear hemispheres.

In order to facilitate our calculations let us review meteor showers, the pericenter of which is ~$6R_J$ close to the satellites' (specifically Io's) orbit, located near the planet, and the apocenter ≈ $26R_J$ close to satellite Callisto's orbit.

In such a case, as is well-known from celestial mechanics, velocity of a body's movement in perocenter and apocenter is calculated using the following formulae:

$V^2 = V^2_c (1+ e)/(1 – e)$ (in pericenter), $V^2 = V^2_c (1- e)/(1 +e)$ (in apocenter), where V_c is main velocity of an object, moving on the orbit, and e – orbit's excentricity.

On the one hand, it may be easily obtained that the velocity of meteoric bodies, having the above mentioned properties, will equal to V = 22.50 km/sec. in pericenter and V = 5.04 km/sec. in apocenter.

On the other hand, optimum velocities of Galilean satellites, moving on circular orbits, are: for Io 16.94 km/sec., Europa 13.43 km/sec., Ganymede 10.63 km/sec. and Callisto 8.01 km/sec. Evidently, the indicated meteoric bodies are falling upon Io from the rear side ($V_{Flow}>V_{Io}$), while in the case of Gallisto ($V_{Cal} > V_{Flow}$) we have the opposite picture. Callisto is gathering on and overtaking meteor showers, which bombard it from the front side due to the fact that the majority of meteoric bodies are dark (have less albedo and a high polarization degree). Consequently the light, reflected from the satellite's indicated side corresponds to the higher polarization degree (Chigladze,2006,2012,2015). As the mentioned effect lasts for billions of years, the satellite's front and rear sides differ from each other.

REFERENCES

Bolkvadze O, University of Helsinki, 1981. 73.
Bolkvadze, O.I.Kvaratskhelia, A.N.Korol, A.K.Maier L.A. Sigua R.A.Chigladze, Bull. Abastumani Astrophysikal Observatory, 1986. 61, 269.
Botvinova V., V.A . Kucherov, Astron-Astrophys , 1980.
Chigladze R, Astron.Cirk, 1984. 1320, 4.
Chigladze R, Bull.of the Academy of Sciences of Georgia, 1985. 118, 513.
Chigladze R, Proceedings of Tbilisi University, 1987. 270, 240.
Chigladze R,Poceedings of Akhaltsikhe Branch of Tbilisi State University. 2001. 2, 170.
Chigladze R, Dissertation. Abastumani, 2006. 186.
Chigladze R, Bull.Georgian National Sciences, 2012. 6 , 96.
Chigladze R,Electropolarimetric and Electrofotometric Investigation of Jupirer's Galilian Setellites". International Scientific Conference „Problems of Modern Astrophysics" Akhaltsikhe.2015.
Dolffus A, Icarus., 1975. 25, 416.
Geake, K, A.Dollfus. Icarus., 1979. 343.
Veverka I, Icarus,1971. 14, 355.

Astronomy & Astrophysics (Caucasus) 1, (2016) 17-23

Period Lengthening in the V444 Cyg System and the Mass Loss by the Wolf- Rayet Component

E. B. Janiashvili[1,2], T. V. Urushadze [2]

[1] Samtskhe-Javakheti State University, Georgia

[2] E. Kharaze National Astrophysical Observatory, Georgia

Email: edik_var@yahoo.com

Received March 14, 2016 ; revised May 18, 2016

ABSTRACT

The phenomenon of mass loss of Wolf-Rayet stars have an important role in the evolution of these massive objects. The article describes the pace of substance loss of one of the eclipsing binary V444 Cyg system in real time. Observational data are in good agreement with earlier estimates of the loss of solid matter around the star speed.

Key words: **stars, Wolf-Rayet – stars,Mass loss from stars – stars, evolution WR stars**

1. Introduction.

Studies of the period fluctuations of eclipsing binaries with Wolf-Rayet components are of fundamental value for determining the rate at which Wolf-Rayet stars lose mass. Among the five known eclipsing systems of this kind, the most promising for such studies are *CQ* Cephei and *V444* Cygni, whose periods were first suspected to vary by Gaposhkin(1944) and Koch(1970), respectively. The first reliable dynamical estimate of the mass-loss rate $\dot{M}_{WR}$, being an important quantity for stellar evolution theory, was obtained in Khaliullin(1974) by one of us with the rate at which the period of the eclipsing binary $V444\ Cyg\ (WN5+O6, P=4^{d}_{.}2)$ was found to be lengthening:
$P = 0.22 \pm 0.04$ sec/yr. For the most possible model, that of spherically symmetric outflow beyond the system, the corresponding intensity of mass loss by the WN5 component was found to be $\dot{M}_{WN5} = 1.09 \cdot 10^{-5} M_{\odot}$/yr. This change in the period of $V444\ Cyg$ was subsequently confirmed by Kornilov et. al. (1979), Hirv (2006), and shown evidently to result from actual mass loss rather than from the presence of a possible third body in the system.

To refine the value of $\dot{M}_{WN5}$ and to establish more definitely whether the system lacks third component, we thought it advisable to make a further analysis of the changes in the $V444\ Cyg$ orbital period.

2. Observations. The new photoelectric observations of V444 Cyg have confirmed the increase of the period found earlier, giving $\dot{P} = 0.202 \pm 0.019$ s/yr. The mass loss by the MN5 star of $\dot{\mathfrak{M}} = -(1.01 \pm 0.22) \cdot 10^{-5} \mathfrak{M}_{\odot}$/yr is obtained.

In 1990 we observed the object photoelectrically in an effort to establish its epoch of primary minimum. The observations were carried out with the 48-sm reflector at the Abastumani Astrophysical Obsevatory, equipped with a photon-counting photometer operating in the V band.

Table I. Individual V-Band Observations of V444 Cyg, 1990

$JD_{\odot}$2448000+	Phase	ΔV	$JD_{\odot}$2448000+	Phase	ΔV	$JD_{\odot}$2448000+	Phase	ΔV
56.3455	0.1240	0.567	136.4932	0.1505	0.556	157.2369	0.0749	0.672
56.3462	0.1241	0.565	136.4939	0.1507	0.565	157.2377	0.0751	0.669
56.3468	0.1243	0.564	136.4951	0.1510	0.547	157.2383	0.0753	0.669
56.3514	0.1254	0.583	153.3245	0.1461	0.576	157.2421	0.0762	0.677
56.3521	0.1255	0.575	153.3269	0.1467	0.582	157.2427	0.0763	0.677
56.3528	0.1257	0.570	153.3275	0.1469	0.576	157.2473	0.0774	0.677
56.3562	0.1265	0.576	153.3319	0.1479	0.599	157.2651	0.0816	0.650
56.3568	0.1266	0.585	153.3327	0.1481	0.594	157.2658	0.0818	0.648
56.3574	0.1268	0.576	153.3336	0.1483	0.590	157.2665	0.0819	0.648
106.3757	0.0008	0.764	153.3540	0.1531	0.586	157.2733	0.0836	0.643
106.3763	0.0009	0.765	153.3547	0.1533	0.586	157.2740	0.0837	0.641
106.3769	0.0011	0.768	153.3553	0.1535	0.585	157.2748	0.0839	0.640
106.3798	0.0018	0.769	153.3685	0.1566	0.581	157.2973	0.0893	0.631
106.3804	0.0019	0.784	153.3692	0.1568	0.580	157.2978	0.0894	0.629
106.3810	0.0021	0.777	153.3698	0.1569	0.582	157.2984	0.0895	0.627
106.3841	0.0028	0.774	153.3789	0.1591	0.564	157.3562	0.1032	0.594
106.3847	0.0029	0.788	153.3795	0.1592	0.559	157.3568	0.1034	0.590
106.3853	0.0031	0.787	153.3803	0.1594	0.567	157.3608	0.1043	0.594
136.4779	0.1469	0.546	153.3841	0.1603	0.557	157.3713	0.1068	0.585
136.4784	0.1470	0.557	153.3847	0.1604	0.574	157.3722	0.1070	0.592
136.4790	0.1471	0.558	153.3853	0.1606	0.578	157.3728	0.1072	0.582
136.4873	0.1491	0.558	157.2305	0.0734	0.686	157.3783	0.1085	0.576
136.4880	0.1493	0.562	157.2311	0.0735	0.681	157.3790	0.1087	0.573
136.4903	0.1498	0.555	157.2316	0.0737	0.681	157.3795	0.1088	0.578

JD⊙2448000+	Phase	ΔV	JD⊙2448000+	Phase	ΔV	JD⊙2448000+	Phase	ΔV
174.1926	0.1001	0.608	182.2326	0.0087	0.814	182.3501	0.0366	0.844
174.1932	0.1002	0.606	182.2331	0.0089	0.815	182.3507	0.0368	0.846
174.1938	0.1004	0.601	182.2372	0.0098	0.817	182.3525	0.0372	0.845
174.1970	0.1011	0.605	182.2406	0.0106	0.832	182.3558	0.0380	0.818
174.1976	0.1013	0.604	182.2411	0.0108	0.834	182.3563	0.0381	0.824
174.1982	0.1014	0.606	182.2417	0.0109	0.829	182.3572	0.0383	0.819
174.2084	0.1038	0.603	182.2573	0.0146	0.838	182.3631	0.0397	0.824
174.2091	0.104	0.605	182.2578	0.0147	0.831	182.3649	0.0401	0.821
174.2098	0.1042	0.605	182.2592	0.0150	0.832	182.3663	0.0405	0.816
174.2130	0.1049	0.607	182.2622	0.0158	0.834	182.3738	0.0423	0.827
174.2136	0.1051	0.602	182.2628	0.0159	0.834	182.3744	0.0424	0.822
174.2142	0.1052	0.609	182.2641	0.0162	0.836	182.3750	0.0425	0.814
174.2174	0.1060	0.591	182.2673	0.0170	0.833	182.3800	0.0437	0.803
174.2180	0.1061	0.595	182.2679	0.0171	0.831	182.3806	0.0439	0.804
174.2186	0.1063	0.594	182.2685	0.0173	0.835	182.3811	0.044	0.804
174.2310	0.1092	0.599	182.2849	0.0211	0.853	182.3843	0.0447	0.808
174.2306	0.1091	0.594	182.2854	0.0213	0.848	182.3848	0.0449	0.805
174.2340	0.1099	0.595	182.2860	0.0214	0.844	182.3854	0.0450	0.795
174.2346	0.1101	0.591	182.2892	0.0222	0.846	186.2392	0.9599	0.625
174.2352	0.1102	0.597	182.2898	0.0223	0.845	186.2403	0.9601	0.641
174.2385	0.1110	0.604	182.2903	0.0224	0.846	186.2409	0.9603	0.638
174.2391	0.1111	0.604	182.2936	0.0232	0.847	186.2414	0.9604	0.636
174.2397	0.1113	0.603	182.2943	0.0234	0.848	186.2435	0.9609	0.635
182.1714	0.9942	0.745	182.3081	0.0267	0.846	186.2441	0.9610	0.628
182.1720	0.9943	0.748	182.3087	0.0268	0.848	186.2446	0.9612	0.631
182.1726	0.9945	0.749	182.3092	0.0269	0.846	186.2495	0.9623	0.638
182.1757	0.9952	0.736	182.3126	0.0277	0.835	186.2554	0.9637	0.625
182.1763	0.9954	0.741	182.3132	0.0279	0.842	186.2565	0.9640	0.626
182.1769	0.9955	0.742	182.3138	0.028	0.849	186.2570	0.9641	0.631
182.1812	0.9965	0.756	182.3185	0.0291	0.837	186.2576	0.9642	0.624
182.1818	0.9967	0.757	182.3191	0.0293	0.833	186.2668	0.9664	0.633
182.1892	0.9984	0.757	182.3197	0.0294	0.836	186.2680	0.9667	0.635
182.1899	0.9986	0.763	182.3269	0.0311	0.827	186.2686	0.9669	0.629
182.1905	0.9987	0.763	182.3275	0.0313	0.827	186.2692	0.9670	0.636
182.1940	0.9996	0.773	182.3281	0.0314	0.833	186.2712	0.9675	0.636
182.1947	0.9997	0.773	182.3312	0.0321	0.834	186.2718	0.9676	0.644
182.1953	0.9999	0.772	182.3318	0.0323	0.832	186.2723	0.9677	0.632
182.2000	0.0010	0.780	182.3324	0.0324	0.838	186.2730	0.9679	0.642
182.2007	0.0012	0.781	182.3369	0.0335	0.822	186.2740	0.9681	0.622
182.2014	0.0013	0.779	182.3376	0.0337	0.830	186.2756	0.9685	0.629
182.2320	0.0086	0.811	182.3382	0.0338	0.829	186.2762	0.9687	0.629

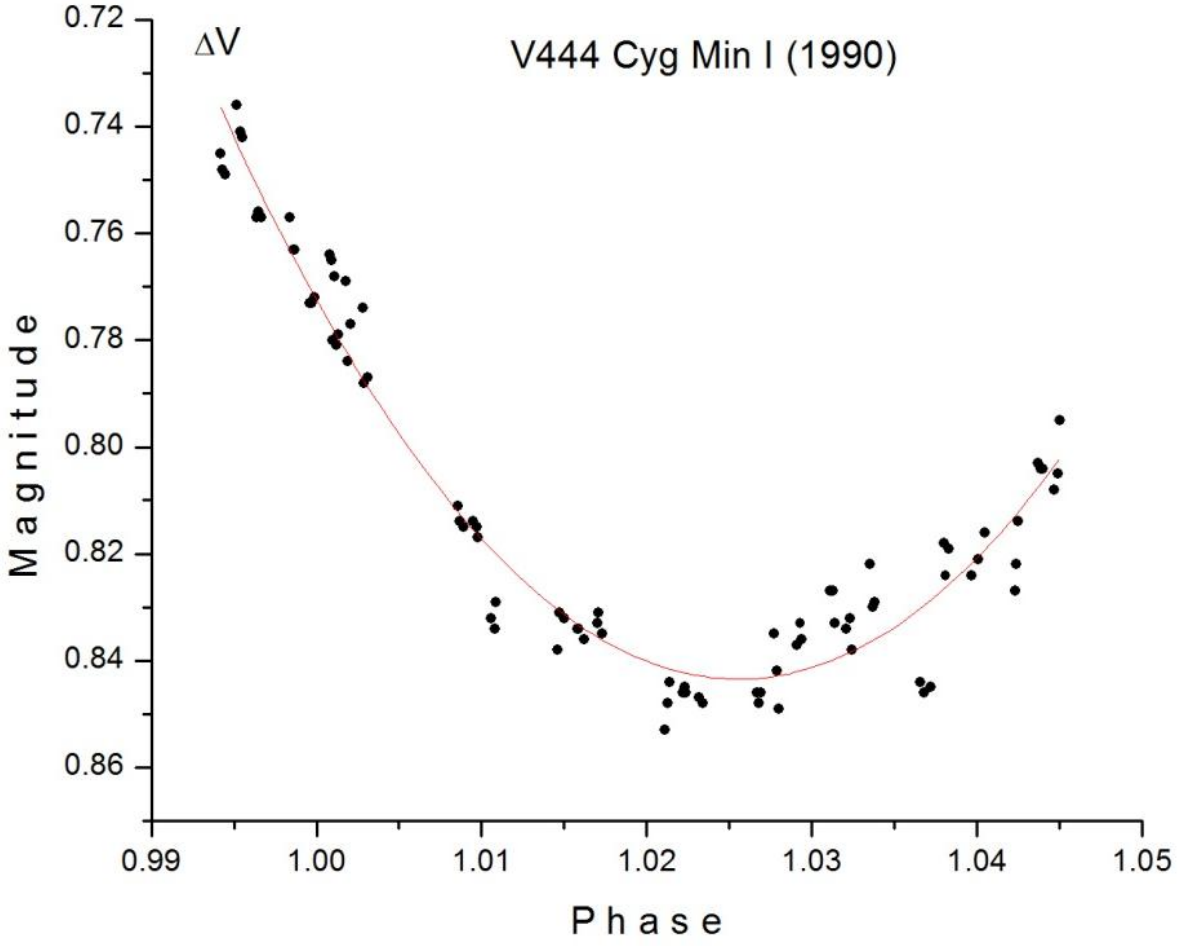
ΔV
V444 Cyg Min I (1990)
Magnitude
0.72
0.74
0.76
0.78
0.80
0.82
0.84
0.86
0.99
1.00
1.01
1.02
1.03
1.04
1.05
Phase

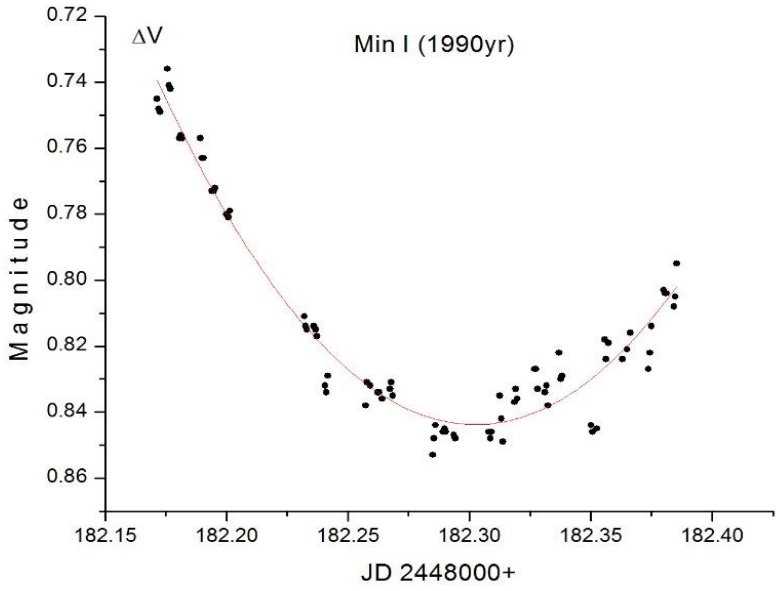

Fig.1. Individual V-band measurements of V444 Cyg at the primary minimum of 1990.

The Standard differential procedure was used, with HD 193514 ($7^m_.5\ pg, Sp = O8k$) as the comparison star and HD 193595($9^m_.0\ pg, Sp = B$) as a control. Table I and Fig. 1 present the results. The rms error of a single measurement is $\sigma = 0^m_.006$.

From the light curve of Fig. 1 we obtain the heliocentric epoch of primary minimum:

$Min\ I = JD_\odot 2448182^d_.251 \pm 0^d_.004.$

3. Mass Loss Rate of WN 5 Stars. Table II gives a series of heliocentric epochs of primary minimum for V444 Cyg and the corresponding residuals $(O-C)_1$ based on theoretical epochs of the minimum computed from the Linear elements Khaliullin (1973)

$C_1 = JD_\odot 2441164^d_.337 \pm 4^d_.212435 \cdot E.$

Table II. Heliocentric Epochs of Primary Minimum of V444 Cyg, 1902 – 2002

$JD_\odot$ 2400000+	O-C	Probable error
15902.585	0.220	0.050
23000.421	0.103	0.040
29900.294	0.008	0.004
30700.643	-0.006	0.005
32103.376	-0.014	0.004
32701.537	-0.019	0.006
37903.892	-0.021	0.003
38603.167	-0.010	0.006
39003.346	-0.012	0.004
39003.341	-0.017	0.004
40903.163	-0.004	0.003

41164.342	0.005	0.003
43700.254	0.032	0.005
45528.460	0.040	0.003
44913.424	0.017	0.004
45528.460	0.040	0.004
45972.860	0.032	0.004
47394.562	0.034	0.004
47773.678	0.031	0.004
48182.251	0.051	0.004
52105.429	0.067	0.004

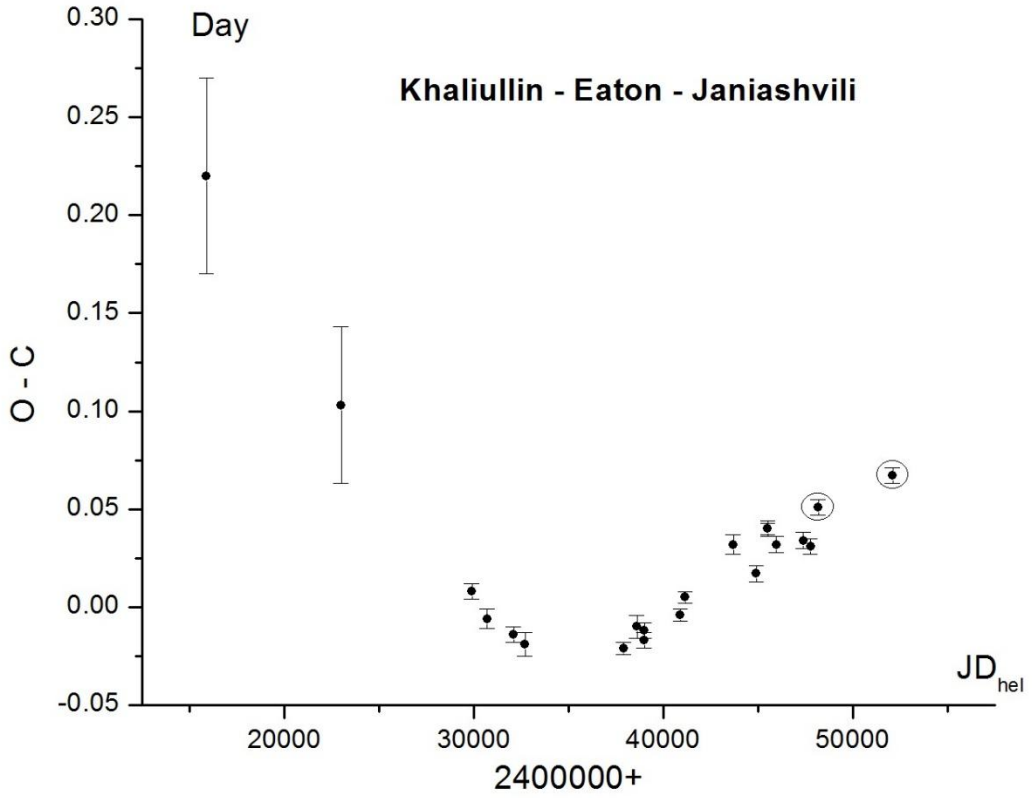

Fig.2. Dependence of residuals $(O-C)_1$ from linear elements on the Julian data of observation of V444 Cyg.

The observed times of minimum quoted in Table II have been obtained by a modified Hertzsprung method from analisis of all available photometry of V444 Cyg. References and a full explanation will be found in the papers cited above Khalliullin (1974, 1979,1973). We have omitted from Table II the ultraviolet photometry by Eaton and the authors Eaton et. al.(1982), in order that the lower accuracy of these satellite measurements and the pronounced disparities in the V444 Cyg light

curves at different wavelengths Cherpashchuk (1975) might not distort the homogeneity of our series of data.

In Fig.2 we have plotted the dependence of (O-C) of the Julian data of observation. Notice that our new measurements confirm the period-variation law found earlier. If we fit a quadratic dependence on epoch number E (TableII) to these heliocentric times of minimum by least squares, we obtain the following nonlinear elements:

$$C_2 = Min\, I_{\odot} = JD_{\odot} 2441164^d.337 + 4^d.2124694 \cdot E + 1^d.37 \cdot 10^{-8} \cdot E^2 \qquad (2)$$

So that the period is currently lengthening at a rate

$$\dot{P} = (2^d.33 \pm 0^d.24) \cdot 10^{-6} yr^{-1} = (0.202 \pm 0.019) sec \cdot yr^{-1} \qquad (3)$$

The residuals $(O-C)_2$ corresponding to these nonlinear elements are given in the fourth column of table II.

In the model of radially symmetric outflow of matter beyond the binary system we would have an estimate.

$\dot{M}_{WR} = -(1.01 \pm 0.22) \cdot 10^{-5} M_{\odot} \cdot yr^{-1}$.

For the rate of mass loss by the WN 5 component is in good accord with the theoretical moedel (Janiashvili 2015).

References

Cherepashchuk A.M., Khaliullin Kh. F., Astron. 1975. 52.. 1214.

Eaton J.A., Cherepashchuk A.M., Khaliullin Kh. F. In: Advances in ultraviolet astronomy.

Goddard Space Flight Cen., 1982. 525.

Gaposchkin S., Astrophys.J., 1944 . 100. 242.

Hirv A, Annuk K, et.all. Orbital elements and mass-loss rate of V444 Cyg. Baltic Astronomy, 2006. 15, 405.

Janiashvili , E.B., „A Study of Eclipsing Star Sistems with the WR type Component ” (report).

International Scientific Conference ,,Problems of Modern Astrophysics” Akhaltsikhe.2015.

Khaliullin Kh. F., Astron. Zh. 1974. 51. 395.

Khaliullin Kh. F., Perem. Zvezdy. 1973. 19.73.

Kornilov V.G., Cherepashchuk A.M., Pis’ma Astron. Zh.1979. 5. 398.

Koch R.H., In: Mass Loss and Evolution in Close Binaries. Proc. IAU Coll. №6. Copenhagen Univ. 1970. 65.

Astronomy & Astrophysics (Caucasus) 1, (2016) 24 - 33

Real-Time Polarization-Holographic Stokes-Astropolarimeter For Observations Of Stars And Fxtended Objects

G. Kakauridze[1], B. Kilosanidze[1], T. Kvernadze[2], G. Kurkhuli[2]

[1] Laboratory of Holographic recording and processing of Information, Institute of Cybernetics of the Technical University, Georgian
[2] Kharadze Abastumani Astrophysical Observatory ,Georgia

Email:solar-corona@yahoo.com

Received March 18, 2016; revised May 18, 2016

Abstract

An innovative real-time imaging Stokes spectropolarimeter is presented. The main unit of the polarimeter is an integral polarization-holographic diffraction element, which enables one to carry out a complete analysis of the eight polarization state in real time. An element is recorded by a special polarization-holographic schema using circularly and linearly polarized beams. It decomposes the incoming light into orthogonal circular and linear basis. The simultaneous CCD intensity measurements of the corresponding points or areas in the diffraction orders and further data reduction through the calibration parameters we get real-time Stokes images of a light source that allows to determine detailed polarization state of a light coming from a point or extended space object in a narrow or a wide spectral range. The operating spectral range of the polarimeter is 500-1600 nm with diffraction efficiency equal to 20% at 532 nm, 16% at 635 nm and 2% at 1550 nm. The theoretical model of relations between measured intensities in different diffraction orders and Stokes parameters, earlier developed by the authors, were used to calibrate the polarimeter. The laboratory tests show that the resulting errors are near of 10^{-2}. The polarimeter is very compact, light weight and could be installed both on ground-based large or small and airborne telescopes

Key words: Polarization-holographic element, Polarization-sensitive materials. Stokes astropolarimeter

1. Introduction

The polarimetry still remains one of the key tools for astronomers since the first polarization observations of Francois Arago in 1811 and spectropolarimetric observations of George Hale in 1908. Almost all astronomical sources radiate polarized light of certain state and degree. Knowledge of the polarization state of radiation along with the intensity measurements and spectrometry provides far more astrophysical information to understand physical processes occurring in the space objects or environment.

Astronomical polarimetry is still a very much developing field. New observational possibilities are ensured by the use of novel components and material and by the application of different mathematical techniques.

Currently used polarimeters are complicated and expensive devices and most of them contain mechanically rotating or electronically tunable optical elements. From this point of view, the development of compact, precise, sensitive and light-weight polarimeter is of great importance.

The polarization-holographic method was first proposed by prof. Sh.Kakichashvili in 1972 (Kakichashvili 1972, Kakichashvili 1989). By the methods of polarization holography the unique polarization-holographic elements can be created that are capable of making a full analysis of the state and degree of polarization in real time and working in a wide spectral range including the near infrared. Namely the element, developed by the authors (Kilosanidze & Kakauridze 2007, Kilosanidze & Kakauridze 2009, Kakauridze & Kilosanidze 2011) decomposes the incident light of any polarization state into the orthogonal circular and linear basis, forming diffraction orders.

Simultaneous measurement of the corresponding point intensities of the diffracted beams and using of the formulae obtained by Kilosanidze & Kakauridze (2009) and Kakauridze & Kilosanidze (2011), allow to determine all four Stokes parameters and the corresponding ones of the polarization ellipse: ellipticity, azimuth and the direction of rotation as well as the degree of polarization.

The polarimetric devices on the basis of such polarization-holographic element will not have mechanically moving or electrically tunable optical elements, but only one basic element connected with a couple of lenses and a photodetector will be used. This device will be compact, relatively cheap and light-weight, the latter being especially important for its installation on the airborne space telescopes. The speed of the operation of this device is limited only by a computer processing. Besides, such devices will give the possibility of simultaneous investigation of spectral dispersion of polarization properties of the objects.

In this work we consider the possibility of application of integral polarization-holographic elements developed by us for astropolarimetric investigations. A theoretical description of an element and a process of diffraction on it are given. Requirements for the characteristics of such an element are discussed. The results of the laboratory tests are given as an illustration.

2. Polarization-holographic Element

It is possible to create polarization-holographic elements in the form of gratings with a different profile of anisotropy, depending on the polarization state of the beams during the recording of the polarization sensitive materials using polarization-holographic method (Kakichashvili 1972, Kakichashvili 1989).

Besides, in polarization holography there is a possibility of recording several polarization gratings on the same area of polarization-sensitive material,so that holograms will be absolutely independent of each other, while the special technology of shooting is used. We use this property for obtaining the integral polarization-holographic element on which several gratings are recorded so that the beams diffracted on each grating are spatially divided. Simultaneously measuring the intensities of diffracted beams by a photometric detector ,a complex analysis of the light polarization state in real time can be done.This means that all four stokes parameters: ellipticity, direction of rotation, azimuth and polarization degree and those of the polarization ellipse are observed at the same time

It should be noted that such an element is able to work in a wide optical spectral range which gives a possibility to determine the spectral dispersion of polarization state as well. It is possible to use

several configurations of the integral polarization-holographic element, depending on the type of gratings.

For a theoretical description of the functioning of such an element it is necessary to obtain Jones matrices of gratings. In Kilosanidze & Kakauridze (2007) the general case of the recording of polarization-holographic gratings by two coherent beams of the arbitrary elliptic polarization is considered. The Jones vectors of the recording beams are (Jones 1941)

$$\psi = \begin{pmatrix} \psi_x \, exp(ia_x) \\ \psi_y \, exp(ia_y) \end{pmatrix} exp(i\omega t), \quad \xi = \begin{pmatrix} \xi_x \, exp(ib_x) \\ \xi_y \, exp(ib_y) \end{pmatrix} exp \; i(\omega t + \delta), \tag{1}$$

where $\tilde{\psi}_x = \psi_x exp(ia_x)$ and $\tilde{\psi}_y = \psi_y exp(ia_y)$ are x and y components of the complex amplitude of the first recording beam, $\tilde{\xi}_x = \xi_x exp(ib_x)$ and $\tilde{\xi}_y = \xi_y exp(ib_y)$ are the same for the second recording beam, ω is the frequency and δ is the phase shift that occurs at a certain angle between the beams during recording. These beams are added in the plane of the recording medium and the summary field has the form of

$$E_\Sigma = \begin{pmatrix} \psi_x \, exp(ia_x) + \xi_x \, exp(ib_x) \cdot exp(i\delta \\ \psi_y \, exp(ia_y) + \xi_y \, exp(ib_y) \cdot exp(i\delta) \end{pmatrix} exp(i\omega t) \tag{2}$$

Polarization-sensitive material, in which corresponding anisotropy and gyrotropy of the optical parameters are induced under the action of actinic polarized light, is used for the recording of polarization-holographic gratings. The regularity of the connection of anisotropy and gyrotropy induced by polarized light with the polarization characteristics of the inducing light were obtained by Kakichashvili (1982). This regularity is of universal character irrespective of the mechanism of anisotropy and gyrotropy induction. The complex coefficients of the photoinduced linear and circular birefringence appear in this regularity and functions of the scalar (isotropic) reaction $\hat{s} = s' + is''$ on the acting intensity of light and two vector reactions – the anisotropic reaction $\hat{v}_L = v'_L + iv''_L$ on linearly polarized light and the gyrotropic reaction $\hat{v}_G = v'_G + iv''_G$ on circularly polarized light are introduced to describe the photo response of the polarization-sensitive medium

$$\hat{n}^2_{1,2} = \hat{n}^2_0 + \hat{s}(I_1 + I_2) \pm \sqrt{[\hat{v}_L(I_1 - I_2)]^2 + [\hat{v}_G(I^+ - I^-)]^2}, \tag{3}$$

where $\hat{n}_1$ and $\hat{n}_2$ are the complex coefficients of elliptical birefringence of the medium; $\hat{n}_0$ is the complex refractive index of the medium in the initial non irradiated state; a complex refractive index is given in the form of $\hat{n}_1 = n - in\tau$ (n is the real refractive index and τ is the extinction coefficient); $I_1 + I_2$ is the first Stokes parameter, $I_1 - I_2$ is the second Stokes parameter, and $I^+ - I^-$ is the fourth Stokes parameter of the inducing light.

The photoinduced anisotropy and gyrotropy of the medium can be described by Jones matrix (Jones 1941), which in the linear approximation has the following form:

$$M \approx exp(-2ikd\hat{n}_0) \, exp\left[-\frac{ikd\hat{s}}{2\hat{n}_0}(I_1 + I_2)\right] \begin{pmatrix} m_{11} & m_{12} \\ m_{21} & m_{22} \end{pmatrix}, \tag{4}$$

where $m_{11,22} = 1 \mp cos\,\theta \left[\frac{ikd\hat{v}_L}{2\hat{n}_0}(I_1 - I_2)\right]$ and

$m_{12,21} = -sin\,2\theta \left[\frac{ikd\hat{v}_L}{2\hat{n}_0}(I_1 - I_2)\right] \mp \frac{kd\hat{v}_G}{2\hat{n}_0}(I^+ - I^-)$; θ is the angle of orientation of the major axis of the polarization ellipse, measured counter-clockwise relative to the x axis; $k = 2\pi/\lambda$; λ is the wavelength, and d is the thickness of the medium.

The following expression was obtained for the grating matrix:

$$M = M_0 + M_{-1} + M_{+1} \tag{5}$$

where

$$M_0 \approx exp(-2ikd\hat{n}_0)\begin{pmatrix}1 & 0\\ 0 & 1\end{pmatrix}$$

$$M_{-1} \approx -\frac{ikd}{2\hat{n}_0} exp(-2ikd\hat{n}_0)\, exp(i\delta) \times \begin{pmatrix}(\hat{s}+\hat{v}_L)\hat{\psi}_x^*\hat{\xi}_x + (\hat{s}-\hat{v}_L)\hat{\psi}_y^*\hat{\xi}_y & (\hat{v}_L+\hat{v}_G)\hat{\psi}_x^*\hat{\xi}_y + (\hat{v}_L-\hat{v}_G)\hat{\psi}_y^*\hat{\xi}_x\\ (\hat{v}_L-\hat{v}_G)\hat{\psi}_x^*\hat{\xi}_y + (\hat{v}_L+\hat{v}_G)\hat{\psi}_y^*\hat{\xi}_x & (\hat{s}-\hat{v}_L)\hat{\psi}_x^*\hat{\xi}_x + (\hat{s}+\hat{v}_L)\hat{\psi}_y^*\hat{\xi}_y\end{pmatrix}$$

$$M_{+1} \approx -\frac{ikd}{2\hat{n}_0} exp(-2ikd\hat{n}_0) exp(-i\delta) \times \begin{pmatrix}(\hat{s}+\hat{v}_L)\hat{\psi}_x\hat{\xi}_x^* + (\hat{s}-\hat{v}_L)\hat{\psi}_y\hat{\xi}_y^* & (\hat{v}_L+\hat{v}_G)\hat{\psi}_y\hat{\xi}_x^* + (\hat{v}_L-\hat{v}_G)\hat{\psi}_x\hat{\xi}_y^*\\ (\hat{v}_L-\hat{v}_G)\hat{\psi}_y\hat{\xi}_x^* + (\hat{v}_L+\hat{v}_G)\hat{\psi}_x\hat{\xi}_y^* & (\hat{s}-\hat{v}_L)\hat{\psi}_x\hat{\xi}_x^* + (\hat{s}+\hat{v}_L)\hat{\psi}_y\hat{\xi}_y^*\end{pmatrix}$$

Here matrix M_0 is responsible for forming of the non diffracted order, matrices M_{-1} and M_{+1} are, responsible for forming orders -1 and +1. With Eq. (5) it is easy to obtain Jones matrices of gratings for different combinations of the polarization state of recording beams. Substituting the concrete values of the components of Jones vectors of the recording beams and the characteristics of the recording medium, into Eq. (5) we can obtain matrices M_0, M_{-1} and M_{+1} for various polarization-holographic gratings that use media with various characteristics for the recording and can describe the diffraction process on them. As follows from Eq. (5), the recording media have the decisive influence on the properties of polarization-holographic gratings.

Let us consider the polarization-holographic gratings which decompose the incoming wave onto an orthogonal circular and linear basis (gratings *C* and *L*). Particularly, if the polarization-holographic grating is recorded by two orthogonal circularly polarized beams and the functions of reaction of a recording medium obey the condition $\hat{s} = \hat{v}_L$, $\hat{v}_L = -\hat{v}_G$ then we get Jones matrices for grating *C* from Eq. (5)

$$M_{\mp 1,C} \approx -\frac{ikd\hat{v}_L\psi_C^2}{2\hat{n}_0} exp(-2ikd\hat{n}_0) exp[\mp i(a_x - b_x)] exp(\pm i\delta)\begin{pmatrix}1 & \mp i\\ \mp i & -1\end{pmatrix} \tag{6}$$

The determination of the ellipticity and the direction of rotation of the polarization ellipse is possible by the grating *C* . For determination of the azimuth of linearly and elliptically polarized light has been offered to the using of two gratings recorded by beams with parallel linear polarization.

If we consider the recording of the polarization-holographic grating by two parallel linearly polarized beams with azimuth α and as a recording medium using of the material with functions of reaction obey the condition $\hat{s} = \hat{v}_L, \hat{v}_L = -\hat{v}_G$, we get from the matrices for grating L (Kilosanidze & Kakauridze 2007). Eq. (5)

$$M_{\mp 1,L} \approx -\frac{ikd\hat{v}_L\psi_L^2}{\hat{n}_0} exp(-2ikd\hat{n}_0) exp[\mp i(a_y - b_y)] exp(\pm i\delta)\begin{pmatrix}cos^2\alpha & sin\alpha\, cos\alpha\\ sin\alpha\, cos\alpha & sin^2\alpha\end{pmatrix} \tag{7}$$

In the special cases of α we get the following:

$$\alpha = 90°,\ M_{\mp 1,90} \approx -\frac{ikd\hat{v}_L\psi_{90}^2}{\hat{n}_0} exp(-2ikd\hat{n}_0)exp\left[\mp i(a_y - b_y)\right]\exp(\pm i\delta)\begin{pmatrix}0 & 0\\ 0 & 1\end{pmatrix} \quad (8)$$

$$\alpha = 45°,\ M_{\mp 1,45} \approx -\frac{ikd\hat{v}_L\psi_{45}^2}{2\hat{n}_0} exp(-2ikd\hat{n}_0)exp\left[\mp i(a_x - b_x)\right]exp(\pm i\delta)\begin{pmatrix}1 & 1\\ 1 & 1\end{pmatrix} \quad (9)$$

Let the light beam incoming onto the element is elliptically polarized with Jones vector $\begin{pmatrix}E_x\exp(i\varepsilon_x)\\ E_y\exp(i\varepsilon_y)\end{pmatrix}$. In the process of diffraction, the element decomposes the light incoming on them onto orthogonal circular and linear basis. As a result the element forms 3 beams in +1 and 3 beams in -1 orders of diffraction: two orthogonal circularly polarized beams I_{+C} and I_{-C} , two linearly polarized beams I_{45} with an azimuth +45° with equal intensities and two linearly polarized beams with an azimuth +90° with equal intensities I_{90} and also none diffracted beam with a state of polarization identical to incoming beam by a state of polarization. Jones vectors of diffracted orders are derived from multiplication of the appropriate Jones matrices (6), (8) and (9) by Jones vector of the incoming wave. As a result we have obtained the following expressions for intensities of the beams diffracted on the gratings C, L_{90} and L_{45}

$$I_{\mp 1,C} \approx \frac{(kd)^2(v'^2_L+v''^2_L)\psi_C^4}{2\left[n_0^2+(n_0\tau_0)^2\right]} exp(-4kdn_0\tau_0)\left[E_x^2 + E_y^2 \pm 2E_xE_y\sin(\varepsilon_y - \varepsilon_x)\right] \quad (10)$$

$$I_{\mp 1,90} \approx \frac{(kd)^2(v'^2_L+v''^2_L)\psi_{90}^4}{4\left[n_0^2+(n_0\tau_0)^2\right]} exp(-4kdn_0\tau_0)E_y^2 \quad (11)$$

$$I_{\mp 1,45} \approx \frac{(kd)^2(v'^2_L+v''^2_L)\psi_{45}^4}{2\left[n_0^2+(n_0\tau_0)^2\right]} exp(-4kdn_0\tau_0)\left[E_x^2 + E_y^2 + 2E_xE_y\cos(\varepsilon_y - \varepsilon_x)\right] \quad (12)$$

Simultaneously measuring the intensities of four diffracted orders using photodetectors, we can determine all four Stokes parameters. In addition, since the element has an angular dispersion, it decomposes each diffraction order in the spectrum. This gives the possibility to determine also the dispersion of the polarization state.

It is known (Born & Wolf, 1975) that for the light beam with Jones vector $\begin{pmatrix}E_x\exp(i\varepsilon_x)\\ E_y\exp(i\varepsilon_y)\end{pmatrix}$ the appropriate Stokes parameters is expressed as follows:

$$S_0 = E_x^2 + E_y^2,\quad S_1 = E_x^2 - E_y^2,\quad S_2 = 2E_xE_y\cos(\varepsilon_y - \varepsilon_x),\quad S_3 = 2E_xE_y\sin(\varepsilon_y - \varepsilon_x) \quad (13)$$

Using Eqs. (10) – (12) in (13) we easily obtain all the four Stokes parameters of the light that is being analyzed through the intensities of the beams diffracted on the polarization-holographic element taking into account the spectral dispersion of an element as well:

$$S_{0,\lambda} = k_{C,\lambda}(I_{+C} + I_{-C}),\quad S_{1,\lambda} = k_{C,\lambda}(I_{+C} + I_{-C}) - 2k_{90\lambda}I_{90}$$
$$S_{2,\lambda} = 2k_{45,\lambda}I_{45} - k_{C,\lambda}(I_{+C} + I_{-C}),\qquad S_{3,\lambda} = k_{C,\lambda}(I_{+C} - I_{-C}) \quad (14)$$

where $k_{C,\lambda} = \frac{2\left[n_0^2+(n_0\tau_0)^2\right]}{(kd)^2(v'^2_L+v''^2_L)exp(-4kdn_0\tau_0)\psi_C^4}$, $k_{90,\lambda} = \frac{4\left[n_0^2+(n_0\tau_0)^2\right]}{(kd)^2(v'^2_L+v''^2_L)exp(-4kdn_0\tau_0)\psi_{90}^4}$, $k_{45,\lambda} = \frac{2\left[n_0^2+(n_0\tau_0)^2\right]}{(kd)^2(v'^2_L+v''^2_L)exp(-4kdn_0\tau_0)\psi_{45}^4}$ are coefficients connected with absorption of light in an element, the diffraction efficiency of an element and the optoelectronic transformations by a

photodetector. The values of these coefficients are determined experimentally during calibration of the device.

From here, it is possible to determine the following parameters of polarization ellipse under investigation

ellipticity $\varepsilon = \frac{S_3}{1+\sqrt{S_1^2+S_2^2}}$, azimuth $\alpha = \frac{1}{2} arctg \frac{S_2}{S_1}$, degree of polarization $DOP = \frac{\sqrt{S_1^2+S_2^2+S_3^2}}{S_0}$.

The diameter of an element typically is about 20 mm, the operating spectral range varies between 500-1600 nm with diffraction efficiency equal to 20% at 532 nm, 16% at 635 nm and 2% at 1550 nm.

3. Laboratory Tests of a Polarization-holographic Element

Detailed laboratory tests were performed to study the behavior of a polarization-holographic element for different polarization state of incoming light from point-like source.

From the practical point of view we recorded and used the element with special configuration of C, $L_{45}$and L_{90} gratings resulted in the certain positions of 0 and 1st diffraction orders: the 0 order (I_0) is located in the center of an image, the 1st orders of L_{90} grating ($I_{+1,90}$ and $I_{-1,90}$) are positioned in the vertical direction and the 1st orders of L_{45} grating ($I_{+1,45}$ and $I_{-1,45}$) are positioned in the horizontal direction of the image, the 1st orders of C grating (I_{+C} and I_{-C}) are positioned with 45° angle to the vertical axes of the image (see Figure 1).

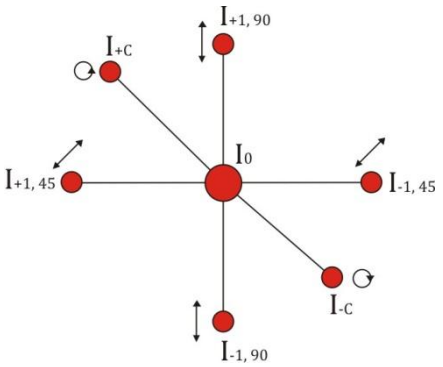

Figure 1. Schematic representation of diffraction orders. I_0 is an 0 order located in the center of an image, the 1st orders of L_{90} grating ($I_{+1,90}$ and $I_{-1,90}$) are positioned in the vertical direction and the 1st orders of L_{45} grating ($I_{+1,45}$ and $I_{-1,45}$) are positioned in the horizontal direction of the image, the 1st orders of C grating (I_{+C} and I_{-C}) are positioned with 45° angle to the vertical axes.

Equation (14) shows that the intensities of 4 orders - I_{+C}, I_{-C}, $I_{+1,90}$ and $I_{+1,45}$ fully and unambiguously describe all 4 Stokes parameters through the corresponding coefficients. So if we know exactly the polarization state, i.e. the Stokes parameters of the incoming light and measure these intensities , the values of the corresponding coefficients can be estimated: (14).

For laboratory tests we used the optical schema consisting of the laser with wavelength of 635 nm, a pack of polarizing optics and collimating lens to get a monochromatic parallel light beam with known circular or linear polarization which would be possible to change arbitrarily (see Figure 2).

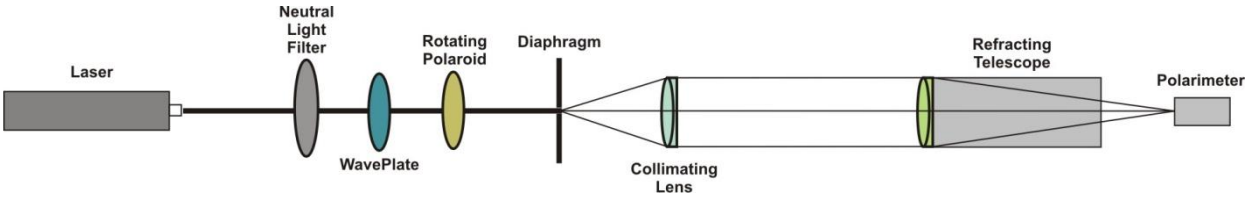

Figure 2. Optical schema of laboratory tests of the polarization-holographic Stokes-astropolarimeter.

To analyze the light beam we built a prototype of a polarization-holographic Stokes-astropolarimeter consisting of entrance diaphragm (or slit in case of non monochromatic light source), collimating lens, narrow interference light filter (optional for non monochromatic light source), polarization-holographic element, objective and CCD camera (see Figure 3). The astropolarimeter is attached to the refracting telescope (see Figure 2) with the aperture of 100mm and focal length of 1000mm.

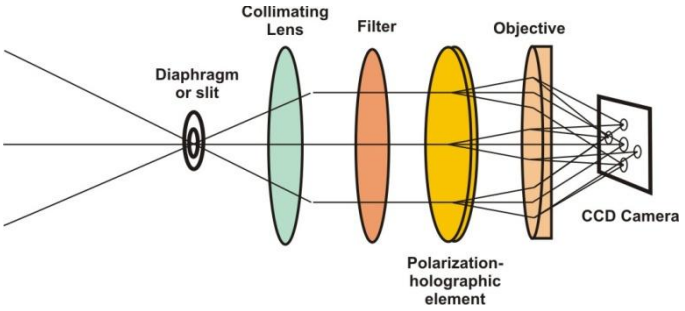

Figure 3. Optical schema of a polarization-holographic Stokes-astropolarimeter.

The series of CCD images were captured for different polarization states of the incoming light, both circular and linear. The special attention was paid to the linear polarization analyze - light source linear polarization phase angle was changed using rotating polarizer with steps of 5 or 10 degrees and consequently captured with CCD. Such a detailed analysis allows to trace the variation of diffraction order intensities along all the possible values of the phase angle and reveal some systematic deviations from the theoretical values of Stokes parameters for the same polarization states.

Figure 4 shows typical Starlight Express Trius SX-36 (array of 36.3 x 24.2 mm, 4904 x 3280 pixels, 7.4 μm pixel size) CCD image used to get during laboratory tests.

The CCD camera control, CCD image data acquisition and processing and further aperture photometry of the 1st orders were performed using MaxIm DL Pro 5 software.

Figure 4. Starlight Express Trius SX-36 (array of 36.3 x 24.2 mm, 4904 x 3280 pixels, 7.4 μm pixel size) CCD image of diffraction orders. The binning of 3 is applied and the image is cropped accordingly.

4. Data Reduction and Results

To adequately represent any systematic linear deviations from theoretical relations, we transform equations 14 into more general linear form below

$$S_0 = k_{+C} I_{+C} + k_{-C} I_{-C}, \quad S_1 = S_0 - 2k_{90} I_{90} + C_1$$
$$S_2 = 2k_{45} I_{45} - S_0 + C_2, \qquad S_3 = k_{+C} I_{+C} - k_{-C} I_{-C} \tag{15}$$

Here k_{+C} and k_{-C} are the corresponding coefficients of *C* grating orders, which are not necessarily equal to each other. Also C_1 and C_2 represent some constant shifts of measured $S_1$and S_2 from theoretical values and appeared non-zero in practice.

The diffraction order intensities for different phase angles of linearly polarized light source measured from CCD images were further processed to estimate the coefficients in equations 15.

As the first step, we need to calculate the possible changes in the integral intensity of the incoming light into the polarimeter and correct the intensities of all orders for such changes correspondingly. As the zero order is always saturated on the CCD images, it is not appropriate to use it forthe light source intensity measurements.Instead we used the geometric mean of I_{+C} and I_{-C} as an estimator of the first Stokes parameter S_0, which apparently is proportional to the light source intensity. As a result we get the corrected order intensities which are further processed for estimation of coefficients for known Stokes parameters. The multi-parametric iterative least square fitting was used to get the best estimates.

Figure 5 shows the variations of all 4 Stokes parameters with phase angle of the linearly polarized incoming light. For calculation of theoretical Stokes parameters the same coefficients were used together with the average value of measured S_0.

For a quantitative estimation of the Stokes parameter fitting the deviation of the measured and calculated ones were averaged. The results for S_1 and S_2 are shown in Figure 6. The deviations show no significant trace of systematic errors within current accuracy of measurements. The simple statistics is shown in the table below:

	Mean value	Standard error
ΔS_1	0.005	±0.021
ΔS_2	0.007	±0.026

We calculated also the degree of polarization and phase angle using measured Stokes parameters, which should be around 100% for DOP and equal to the same values for the phase angle as it has the incoming light. The results are shown below:

	Mean value	Standard error
DOP, %	99.9	±2.0
Phase angle deviation, degree	0.03	±0.8

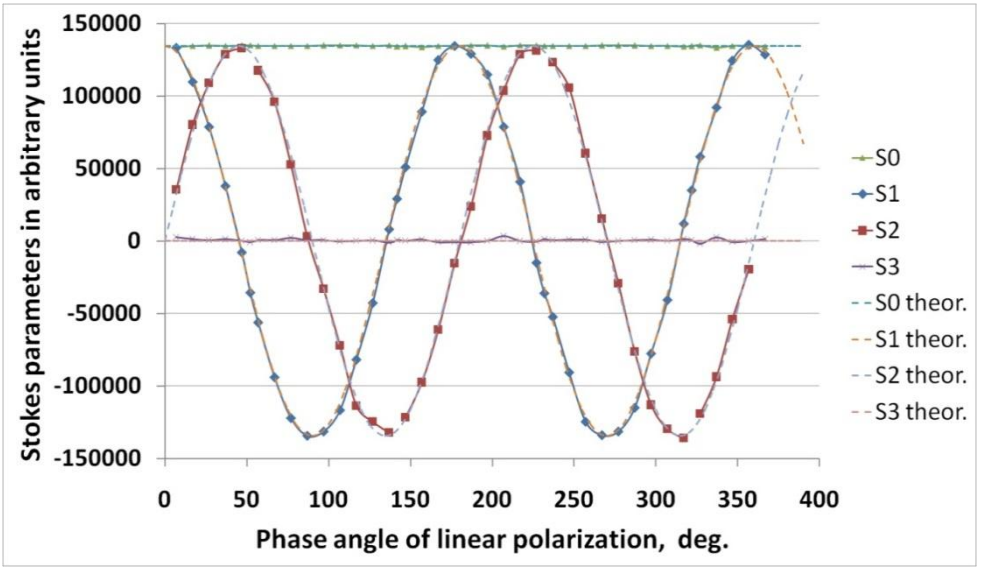

Figure 5. Variation of theoretical and measured Stokes parameters for different phase angle of linearly polarized light source. The theoretical Stokes parameters are calculated using the average of measured S_0 and the same coefficients as used for measured parameters.

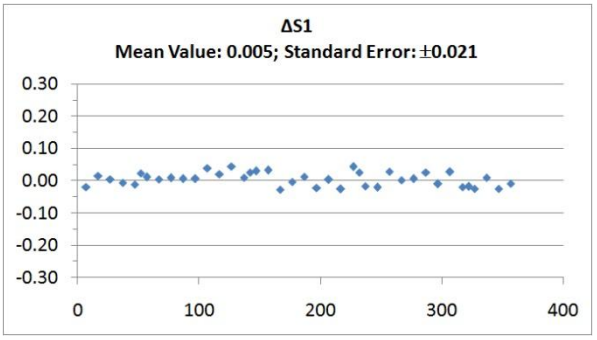

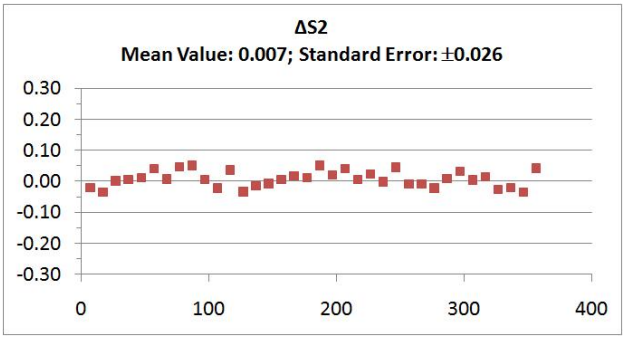

Figure 6. Deviation of measured Stokes parameters from the theoretical ones. Stokes parameters are normalized to S_0. Left drawing represents Stokes parameter S_1, right drawing - S_2. Horizontal axis is ticked with phase angle of linear polarization in degrees. Ordinate axis has normalized values of ΔS_1 and ΔS_2.

Our investigations show that the further development of technologies of polarization-sensitive material preparation and polarization-holographic element recording is possible to improve the diffraction efficiency of an element and increase the accuracy of determination of the Stokes parameters.

5. Conclusions

The theoretical basis, development, design and the results of laboratory tests of the innovative real-time polarization-holographic imaging Stokes astropolarimeter are discussed in the present paper.

The first prototype of the astropolarimeter were built according to the developed principal schema and specially designed and recorded polarization-holographic element. Experimental results show that the resulting errors are near 10^{-2} and prove the great potential of such astropolarimeter proved to be very compact, working in real time, light weight and suitable to be installed both on ground-based large or small and airborne telescopes. Also it is extremely important to continue the further investigations to improve the efficiency of the suggested method.

Acknowledgement

The authors gratefully acknowledge support by the Shota Rustaveli National Science Foundation of Georgia (Grant No. AR/209/6-120-14).

References

Born, M., Wolf, E. 1975, Principles of Optics, Pergamon Press, New York.
Jones, R.C. 1941, J. Opt. Soc. Am., 31, 488.
Kakichashvili, Sh. 1972, J. Opt. Spectrosc., 33(2), 324.
Kakichashvili, Sh. 1982, J. Opt. Spectrosc., 52(2), 317.
Kakichashvili, Sh. 1989. Polarization holography, Nauka, Leningrad.
Kakauridze, G. Kilosanidze, B. 2011, Proc. SPIE, 7957, 7957-28.
Kilosanidze, B., Kakauridze, G. 2007. Appl. Opt. 46(7), 1040.
Kilosanidze, B., Kakauridze, G. 2009, Proc. SPIE, 7358.

Astronomy & Astrophysics (Caucasus) 1, (2016) 34-37

Optical Study of TeV Blazars

G. N. Kimeridze

Samtskhe-Javakheti State University, E. Kharadze National Astrophysical Observatory, Georgia

givikimeridze@gmail.com

Received March 19, 2016; revised May 18, 2016

Abstract

BL Lacertae objects are the most enigmatic ones in astrophysics.They are the most powerful particle accelerators and most luminous sources in the Universe.Their energy density reaches the physically permitted maximum value.Although being the subject of intense study last thirty years,it is not clear,however,how this extremaly high efficiencies are reached and maintained over long periods of time.Several fundamental issues of blazar physics are still poorly understood.This is partly due to the fact that previous observations could not resolve the compact central structure.Time scales and higher order moment of the statistical characteristics of temporal variations provide the strongest constraints on the linear sizes and geometric properties of the emitting regions.

Key words: TeV gamma-ray, BL Lacertae objects, active galactics

1. Introduction

Active galactic nuclei (AGNs) were among the first sources detected at TeV energies and have remained as the largest source population for TeV gamma-ray astronomy. Initially, the TeV gamma-ray emitting AGNs found were exclusively in BL Lac objects at relatively low red-shifts (). With lower energy thresholds and better sensitivities offered by the new generation of ground-based gamma-ray observatories, a significant progress has been made in recent years on three fronts: much improved quality of multiwavelength data on a few bright TeV blazars for detailed studies (Horan et al. 2009; Donnarumma et al. 2009; Abdo et al. 2011bc; Abramowski et al. 2011, 2012); detection of flat-spectrum radio quasars whose gamma-ray output peaks at lower energies than BL Lac objects (Albert et al. 2008; Mariotti 2010; Wagner 2010); and detection of AGNs at higher red-shifts.
BL Lac objects and flat-spectrum radio quasars both belong to a sub-class of AGNs, which are known as blazars. Blazars are known to be highly variable across nearly the entire electromagnetic spectrum, producing flares of duration as short as a few minutes or outbursts of duration as long as many months. This, coupled with the non-thermal nature of their emission, implies that the photons from blazars most likely originated in the jets that are directed roughly towards us .
Such jet emission, Doppler-boosted in intensity as well as in energy, dominates over radiation from all other sources.Therefore, blazars are excellent laboratories for studying physical processes in the jets of AGNs. Not all blazars have been established as TeV gamma-ray emitters. The two peaks are seen to shift in a correlated manner during a major flare/outburst. Moreover, both the Xray and gamma-ray spectra of a blazar tend to become flatter as the source brightens.
Various models have been proposed to account for the broadband SED of TeV gamma-ray blazars. Both leptonic and hadronic models attribute the lower-energy SED peak to synchrotron radiation from relativistic electrons (and positrons) in the jets, but they differ on the origin of the higher-energy peak. Also, as the quality of multiwavelength data improves, it has become apparent that the X-ray and

gamma-ray correlation is fairly loose or even absent in some cases.Perhaps, the most serious challenges come from the discovery of TeV gamma-ray flares that either have no counterparts at Xray energies or are significantly offset in time from their X-ray counterparts . The latter are sometimes referred to as “orphan TeV flares”, even though they might not be genuinely orphans.
TeV gamma-ray variability has been observed on a time scale of minutes in PKS 2155–304 . The amplitude and duration of flares probably reflect the energetics and physical timescales involved in the processes. The SED of a TeV gamma-ray blazar is known to evolve significantly during a major outburst (or flare with a duration of weeks to months).
Until very recently, BL Lac objects represented the only type of AGN that is seen to emit TeV gammarays . With the detection of 3C 279 , flat-spectrum radio quasars have now emerged as a viable source population for TeV gamma-ray astronomy. Equally significant is the discovery of BL Lac objects, such as W Comae and 3C 66A , whose SED peaks are located in between the traditional TeV BL Lac objects and flat-spectrum radio quasars, as the observation begins to cover the entire continuum of the blazar phenomenon.
The main contribution to the γ-ray emission of blazars is generally thought to result from either inverse Compton scattering (high energy peak in the SED) by relativistic electrons in the jet of lower energy photons, produced either by synchrotron emission (low energy peak in the SED) within the jet or by emission external to the jet, for example from the accretion disk around the central engine, or from photoninduced cascades.
It is widely accepted that the variations recognizable in the Blazar light curves are due to the superposition of two (or more) components: in general, one can say that a long-term trend, maybe achromatic, possibly periodic, determines the base-level flux oscillations; faster variations, often implying spectral changes, are likely caused by a different physical mechanism. The violent flux variations observed in blazars have been explained in a variety of ways: shocks travelling down the jet, changes of the Doppler factor due to geometrical reasons, accretion disc instabilities, or as gravitational microlensing. The observation of micro/intraday variability, that is, of flux changes on time scales of less than few days , raises the questions of what is the smallest time scale of variability in blazars and, if the variations are of intrinsic nature, of how small the size of the emitting region can be.
The increased sensitivity of ground-based Cherenkov telescopes and the successful launch of FERMI/LAT ushered in a new era of observational astronomy in the energetic γ-ray band. The AGNs, and in particular blazars, are the most prominent class of associated sources in 2FGL and 2 TeV list . In total, 2FGL contains 917 sources that are associated with AGNs, of which 894 are blazars and over 95% of extragalactic populations of TeV sources are also blazars. Fermi/LAT, with its wide FoV, angular resolution and energy range increase over EGRET have allowed AGN/blazar variability to be monitored over a wide range of timescales for a large number of sources . Simultaneous multi-wavelength observations of a large number of these sources are crucial for determining the emission mechanisms in order to infer the physics of the luminous portions of jets. Also, observations of these extragalactic sources will lead to an understanding of their contribution to the isotropic, apparently diffuse, extragalactic high-energy γ-ray radiation .
The scientific impact of high-energy instruments such as Cherenkov telescopes and FERMI/LAT will be greatly increased if an efficient program for fast follow-up and monitoring observations from radio to TeV is carried out. The new generation space and ground-based Cherenkov telescopes allow the study of flux variations down to the minute timescales for the brightest sources. The best hope for understanding the mechanisms at work in blazars comes from the combination of observational data over the whole electromagnetic spectrum. Since such objects vary very rapidly at all wavelengths, to be meaningful, the spectra should be measured simultaneously at each wavelength. Therefore, only by coupling spectral and temporal information one can constrain the jet physics, so that a detailed sampling, both in time and energy, of the blazar spectrum can critically direct the interpretation to the correct scenario. Elucidating the structure of blazar jets, possible through multi-wavelength monitoring, is an essential precursor for understanding their formation and thus the extraction of energy from central engine. This allows one to know the energetics involved in the flare as a function of frequency, the relative amplitude of variability at different energies, and possibly time delays

between flux variations at different frequencies. Resolving the flux variability and detecting spectral correlations in the radio, mm, optical, x-ray and γ-ray regime will give a definitive answer to the question about the emission mechanism. The continuum production mechanism is critical for understanding the central engine in AGNs, a fundamental goal in extragalactic astrophysics .
Greatly increased numbers of γ-ray blazars and more sensitive observations of individual sources are the keys to answering fundamental questions about blazars: What is the global structure of the AGN jet? What are the sources of variability? Is the broad-band energy distribution pure Synchrotron Self-Compton (SSC), or are the External Compton Scattering (ECS) models, where the seed photons come from the accretion disk or are scattered off broad-line region clouds more correct? Is a one-zone model adequate or is an inhomogeneous jet model required? What are the red-shift dependencies of the γ-ray emission from blazars? Answering these questions requires corresponding instruments at different wavebands. Consequently, Cherenkov telescopes and FERMI/LAT will provide a tremendous opportunity for future, systematic studies addressing important, still open questions about the physical processes involved.
Variability of γ-ray emitting blazars on scales ranging from hours to years is a surprising feature in some respect because it implies a small emission region. Long-term variability time scales can tell us about how often certain objects, or certain classes of objects are in flaring state and how long these flares typically last. We also learn about flare evolution from one frequency domain to other. Therefore, it is also necessary to determine the wide-band energy distribution across a range of variability timescales.
Although previous multi-wavelength campaigns have shown interesting correlations (and anticorrelations) across the spectrum , their interpretation has been difficult because the overlapping coverage has been limited and piecemeal. So far, this was usually limited to particular well suited cases, often combining not truly simultaneous broadband data. The demand for quasi-simultaneity is important in view of the high activity and rapid variability of the sources. The lack of continuous, (quasi-) simultaneous observations at all wavebands and the historical lack of sufficient γ-ray data hampered past efforts to understand and study in detail the broad-band jet emission.
Understanding blazar variability is one of the major issues of active galactic nuclei studies. Blazars, i.e. BL Lac objects and flat-spectrum radio quasars exhibit strong flux variations across all the electromagnetic spectrum, on different time scales from years down to hours or less. A powerful tool in the study of relativistic jets is the analysis and modeling of the simultaneous spectral and temporal behaviour of blazars, over frequency as broad as possible – ideally covering the whole SED from radio to TeV energies.
One of the most important classes of Fermi and Cherenkov sources are blazars in which a relativistic boosting results in a very luminous and highly variable emission. These sources are thus ideal for studying the physics of the ubiquitous, but poorly understood astrophysical jets. We now have a basic understanding 3 of blazars, including rough scenarios for jet geometry, bulk speeds, and at least some of the relevant physical processes and radiation mechanisms . The spectral energy distributions (SEDs) are dominated by two components, one at lower energies (radio-opticalUV), and one at higher energies (X-ray/gamma-ray). The lower energy component is generally agreed to be due to synchrotron radiation from relativistic electrons accelerated at shocks in the jet, but the source of the high energy component of blazar SEDs is still disputed, with both leptonic and hadronic models able to fit many current constraints.
One key approach to this problem is to search for temporal correlations between the flux and spectra of the two major emission components. In hadronic models the high-energy and low energy components are produced by different particle populations that are not necessarily simply related. In contrast, in the simplest leptonic models (e.g., synchrotron self-Compton or inverse Compton) the two components are produced by the same particles, which lead to very specific predictions for correlations, lags and leads between the components, and spectral responses within each component. Observations across a sample of sources should be able to strongly restrict the available parameter space, and thus test the viability of the models generally. Such observations also serve as a starting point for constructing detailed physical models of relevant effects.

Now, for the first time, we have the possibility to have truly simultaneous data in the radio, optical, xray, GeV and the TeV bands. The FERMI/LAT and Cherenkov telescopes will offer opportunities to study relation between radio to γ-ray activity, and possibly to locate of the γ-ray emission. Therefore, the scientific impact will be greatly increased if an efficient program for fast follow-up and monitoring observations by radio (ALMA, VLBA, Metsähovi, MOJAVE, TANAMI, UMRAO, OVRO, Effelsberg, IRAM and other), optical (WEBT/GASP, ATOM, PANs, KANATA, SMARTS, MAPCAT, TUORLA_OMP, PERUGIA_OMP, SO_OMP and others), ground-based Cherenkov (Whipple, HESS, VERITAS and MAGIC) and space instruments (FERMI/LAT, AGILE, Chandra, SWIFT, INTEGRAL and other) is carried out. Some of the most interesting results on these sources have come through observations where several telescopes operating at different wavelength (quasi-) simultaneously monitor the activity of a blazar .

2. Analysis

Variability studies are thus a powerful tool to investigate blazar emission and to discriminate among the various theoretical models interpretations, in particular when observations are done in a continuous way and simultaneously at different wavelengths.

In the frame of the project we will continue active collaboration with different institutuions over the wolrd.we took part in the new campaigns on extragalactic TeV sources which use all be observing facility available ,from the radio to TeV energies.This allow us to conduct continuous and well-sampled simultaneous monitoring campains and to study the emission variability in detail and thus physics of the jets.The research has done on to the following topics:

1)Search for periodic time scales of variability
2)Study of spectral changes and their correlation with the flux density vatiations
3)Understanding the cross-correlation and time lags of flux changes at different frequencies
4)Separating intrinsic versus extrinsic intraday variability(IDV)
5)Distinguishing energetic processes versus geometrical effects
6)Broad-band spectral energy distributions(SEDs).

References

Abdo A.A., Ackermann, M., …, Kurtanidze O., Nikolashvili M., et al. 2011a, ApJ 726, 43 7. Abramowski A., Acero F., Aharonian, F., et al. 2011, A&A 533, A110 10. Abramowski A., Acero F., Aharonian, F., et al. 2012, A&A 539, A149 11.
Albert J., Aliu E., Anderhub H., et al. 2008, Science 320, 1752 22.
Donnarumma I., Vittorini V., Vercellone S., …, Kurtanidze O., et al. 2009, ApJ 691, L13 Principal Investigator, (Project Manager) Project Director VLBA, OVRO Key Personnel , EFFELSBERG Assistant Personnel Optical Observatories FERMI/LAT, SWIFT, AGILE Cherenkov Telescopes Master and PhD students Undergraduate and Graduate students 13 43. Horan D., Acciari V. A., Bradbury, S. M., …, Kurtanidze O. et al. 2009, ApJ 695, 596 64.
Mariotti M. 2010, ATel 2684, 1 78. Marscher A., Jorstad S., ..., Kurtanidze O., Nikolashvili M., et al. 2008a, Nature 452, 966 79.
Wagner R. 2010, 11th HEAD, BAAS 42, #2 134.

Astronomy & Astrophysics (Caucasus) 1, (2016) 38-44

Observations of Near-Earth Asteroids at Abastumani Astrophysical Observatory

Yu. N. Krugly[1], V. R. Ayvasian[2], R. Ya. Inasaridze[2], V. G. Zhuzhunadze[2], I. E. Molotov[3], V. A. Voropaev[3], V. V. Rumyantsev[4], and A. R. Baransky[5]

[1]Institute of Astronomy of V. N. Karazin Kharkiv National University, Kharkiv, Ukraine

[2]Kharadze Abastumani Astrophysical Observatory , Georgia

[3]Keldysh Institute of Applied Mathematics, RAS, Moscow, Russia

[4]Crimean Astrophysical Observatory, Nauchnyi, Crimea

[5]Astronomical Observatory of Kyiv National University, Kyiv, Ukraine

Email: krugly@astron.kharkov.ua

Received March 20, 2016; revised May 18, 2016

Abstract

Over the past five years physical properties of near-Earth asteroids are investigated in the Kharadze Abastumani Astrophysical Observatory. The work was launched in the collaboration with Kharkiv Institute of Astronomy within the Memorandum on scientific cooperation between Ilia State University (Georgia) and V. N. Karazin Kharkiv National University (Ukraine) in 2011. In the framework of this study the regular observations of several dozen asteroids per year are carried out to determine the rotation periods, size and shape parameters of these celestial bodies. A broad international cooperation is involved in order to improve the efficiency of the study. Abastumani is included in the observatory network called the *Gaia*-FUN-SSO, which was created for the ground support of the ESA's *Gaia* space mission.

Key words: Asteroid, photometry, CCD observations, albedo

1. Introduction

Presently mankind has realized and assessed the probability and the scale of the effects of a possible fall of large asteroidal or cometary bodies to the Earth. Recognition of the impact hazard is based on the facts of numerous falls of celestial bodies to the Earth, the Moon and other bodies of the Solar system, which happened in the past and continues to occur today. In the frame of Spaceguard efforts numerous survey projects regularly scan the sky, discovering dozens of near-Earth asteroids (NEAs) each month. Hundreds of professional and amateur observatories around the world are following up newly discovered NEAs getting both astrometric and photometric data for these bodies.

Our work is devoted to the study of physical properties of NEAs through regular photometric observations, which allow us to determine the rotational parameters, size and shape of these bodies, the optical properties of their surfaces etc. NEAs are small bodies from a few meters to several kilometers in diameter. The main objects of observations are NEAs closely approaching the Earth. First of all, the program of observations includes the newly discovered NEAs which are bright enough to be reachable for high-precision photometric observations.

Study of asteroids began in Kharadze Abastumani Astrophysical Observatory within the Memorandum on scientific cooperation between Ilia State University (ISU, Georgia) and V. N. Karazin Kharkiv National University (KhNU, Ukraine). The investigation is carried out in the collaboration with a number of observatories in the world. The Abastumani Observatory is involved in observations of asteroids in the frame of the International network ISON (International Scientific Optical Network). Abastumani is also a part of cooperation within the *Gaia*-FUN-SSO (the *Gaia* Follow-Up Network for Solar System Objects), created to support the observations of the Solar system bodies by the European space mission *Gaia* (Krugly et al. 2011, 2015)

2. Program of Study the Physical Characteristics of NEAs

Among many causes of the emergency facing humanity in recent years, much attention is paid to the problems of a possible collision of asteroids and comets with the Earth (e.g., Shustov et al. 2013). Even a small body with the diameter of 100-200 meters can cause a catastrophic destruction in an area of thousands of square kilometers. There are a few hundred thousand of such natural bodies in the space surrounding the Earth's orbit (Morbidelli et al. 2002). To date (October 2015) a little more than 12 thousand NEAs have been discovered (MPC 2015). Also, cosmic body drop to the Earth may be associated with the presence of a large number of space debris in the Earth orbit, which was formed as a result of space exploration (Molotov et al. 2013).

The median lifetime of NEAs in their orbits is about 10 Myr (Gladman et al. 2000; Morbidelli et al. 2002). Eventually these bodies collide with large planets or burn down in the Sun or go away to the distant region of the Solar system. The main source of replenishment of the NEAs is the main-belt of asteroids, in which there are millions of asteroidal bodies, being the remnants of the formation of the large planets at the early stage of formation of the Solar system more than 4.5 billion years ago. Currently orbits of 674 thousand asteroids are known, of which over 420,000 objects were numbered (MPC 2015).

Potentially hazardous asteroids (PHAs) among NEAs are defined based on 2 parameters: being larger than 100-150 m in size (H < 22.0), and approaching the Earth at distances closer than 0.05 AU (less than 10 Earth-Moon distances). 1546 PHAs were known at the beginning of October 2015. The most hazardous objects are the large bodies with diameters more than 1 km. There are about 1000 ± 100 such bodies from expert's estimates (NEO-Report 2003). Currently 870 objects with diameters greater than 1 km are known (MPC 2015).

The average time of a possible NEA fall on the Earth depends on the size of the body. Small bodies of a few meters in size fall to the Earth more often than larger ones. A body more than 1 km in size falls very rarely, aproximately once in the tens and hundreds of million years. A typical form of the dependence of expected impact time interval is shown in Fig. 1 (Chapman 2004).

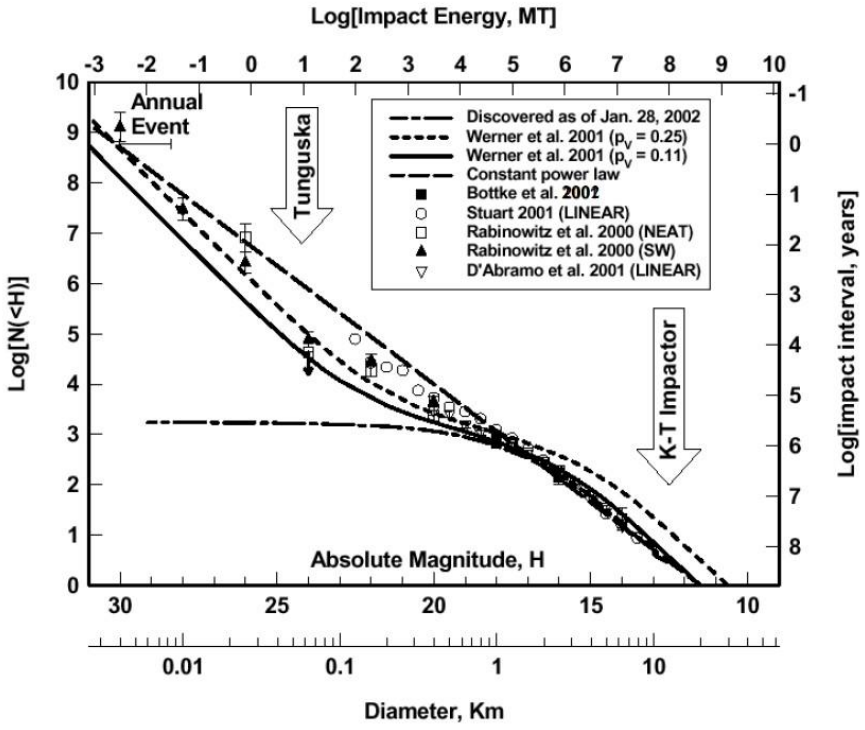

Fig. 1. Cumulative distribution of near-Earth asteroids vs their absolute magnitudes, and a scale for the diameters. Also impact energy and expected impact time interval are shown (Chapman 2004).

CCD observations of near-Earth asteroids at Abastumani Observatory were started in 2010. First of all a group of researchers was created. They have prepared the 70 cm and 1.25 m telescopes for the photometric observations. The test observations of several asteroids were carried out. Since 2011 the regular work on study of asteroids started in Abastumani within the Memorandum on scientific cooperation between ISU (Georgia) and KhNU (Ukraine). In the frame of this Memorandum, the Abastumani Observatory of ISU and the Institute of Astronomy of KhNU perform joint studies of potentially hazardous NEAs. The collaboration involves organizing cooperative observation projects, developing instrumental base, and training highly qualified specialists. The joint program of the asteroid study includes the next directions:

- Monitoring of potentially hazardous and newly discovered NEAs;
- Identification and study of binary NEAs by photometric method;
- Support for radar observations of NEAs by optical observations;
- Study of the YORP-effect (Yarkovsky-O'Keeffe-Radzievskii-Paddack), in particular detection variations of the rotation period of NEA under the influence of thermal photons re-emitted from its surface heated by the sun;
- Astrometry and photometry of asteroids, which will be observed and newly discovered during the *Gaia* mission (ongoing project of European Space Agency) in the frame of the International network *Gaia*-FUN-SSO.

3. Instruments and Technique of Photometric Observations

Recently the optical observations of celestial bodies are carried out using CCD cameras which are highly sensitive panoramic photodetectors of light. At the Abastumani Observatory observations of asteroids are performed with two telescopes: the 1.25 m telescope AZT-11 and the 70 cm Maksutov meniscus telescope AC-32. The telescopes were eqiupped with modern CCD camera manufactured by FLI firm (Finger Likes Instrumentation, USA) in 2010.

The CCD camera PL4301E and a filter-wheel with Bessell's *UBVRI* filters were installed in the Cassegrain focus of AZT-11 (f/12.8). The CCD has dimensions 2084 by 2084 pixels with 24 by 24 μm per pixel that gives a field of view 10.5' by 10.5' in 16 m focus. The limiting magnitude of this instument is 20.5 mag with *R*-band 3-minite exposure.

The AC-32 telescope was modernized in such a way that a flat diagonal secondary mirror was installed in front of the primary mirror to realize a Newtonian focus. The CCD camera IMG-6303E is fixed on a focusing mechanism which has been made and mounted on the telescope tube near the focal plane of the Newtonian focus (the effective focus is equal to 2141 mm). The CCD covers a field of view 44.4' by 29.6' with 3072 by 2048 pixels, with each pixel 9 by 9 μm subtending 0.87". The observations were mostly done in an unfiltered mode in white light. The R filter was used to implement the R-band close to the Johnson-Cousins photometric system. The limiting magnitude in white light was reached 20 mag using this set-up.

All observations of asteroids were carried out in order to obtain lightcurves. The observations were held as a continuous series for several hours. In most cases, observations of each asteroid included several nights of observations. Especially a lot of lightcurves are necessary for binary asteroids (Scheirich et al. 2015; Pravec et al. 2016). Exposure time was chosen in the range from 20 s to 5 min, depending on the brightness of the asteroid and the angular speed of its sky motion (Krugly 2004). During observations only R.A. tracking at the sidereal rate was used at both telescopes, therefore the limited exposure time is used for fast moving asteroids to obtain their images as a trace with a length of 2-3 seeing diameters of a fixed star (Krugly 2004).

Initial reduction of CCD images includes subtracting the average dark image and the average flat-field (commonly they referred to as the master dark and the master flat). The dark images are averaged using more than 10 ones, usually a few dozen. Images in the opposite to the sun side of the sky obtained during evening and morning twilight in clear conditions are used to calculate the master flat. Magnitudes of an asteroid and comparison stars are measured on calibrated images by a

technique of aperture photometry using the AstPhot software (Mottola et al. 1985). More details on the reduction are described in Krugly et al. (2002, 2007).
Attention was paid to obtain high-precision photometric measurements, for which observations are made with an optimal exposure and often without a filter. Average precision of brightness measurements of an asteroid is 0.01-0.02 mag and usually no worse than 0.04 mag.
To show accuracy of asteroid photometry made at Abastumani, we present observations of NEA (3554) Amun obtained at several observatories during its appearance in 2011. The asteroid was observed with 70 cm telescopes at the Abastumani Observatory, at the Chuguev Observatory (Ukraine), and at the Lisnyky Observatory (Ukraine) in February-March 2011. The parameters of setups used at Lisnyky and Chuguev observatories are given in Krugly et al. (2015). Figure 2 shows the obtained lightcurves. On February 14, the asteroid had brightness of 15.8 mag and was observed with an accuracy of 0.03 mag at Chuguev near the bright moon (Fig. 2A). At Lisnyky the lightcurve obtained in the next night on Feb. 15 in clear conditions had better accuracy of 0.02 mag (Fig. 2A). On Feb. 27 the asteroid was as bright as 15.0 mag, and the observations at Chuguev showed the precise data with RMS of 0.01 mag (Fig. 2C). On March 14 Amun's brightness was close to maximum in the 2011 opposition of 13.9 mag, and the observations at Abasumani were carried out with a high accuracy of about 0.007 mag (Fig. 2D).

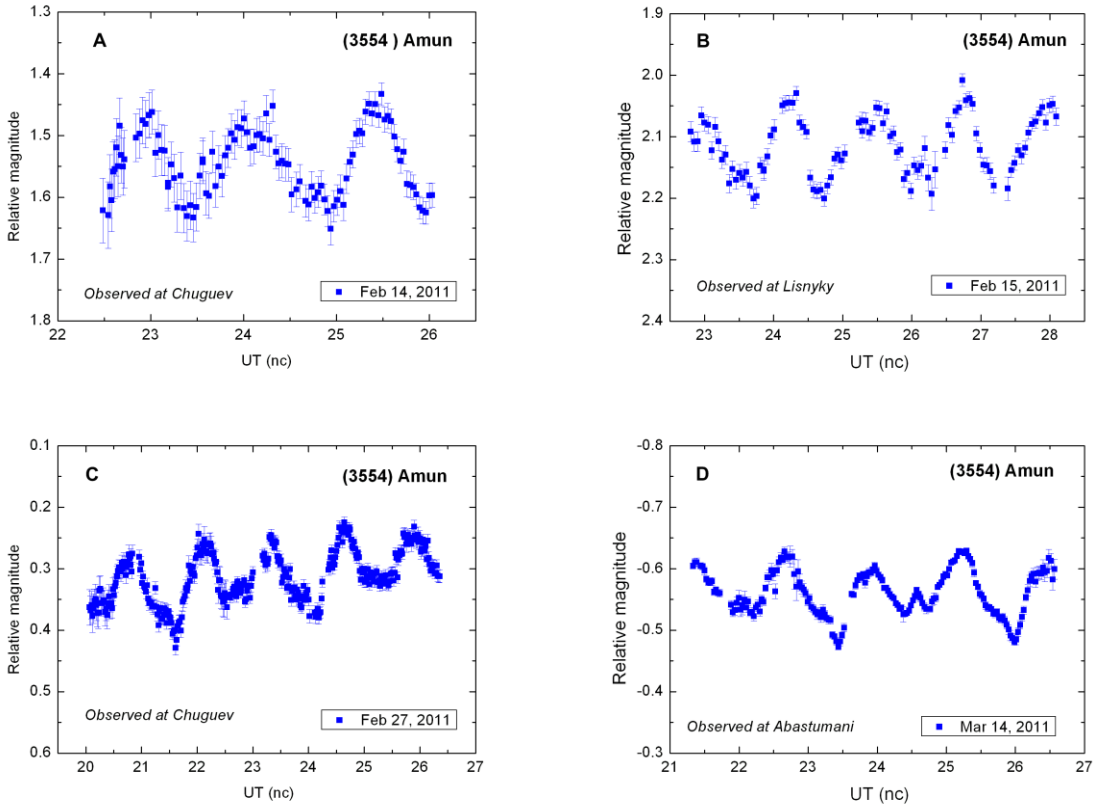

Fig. 2. Lightcurves of the asteroid (3554) Amun obtained in 2011 opposition: A) in Chuguev on February 14; B) in Lisnyky on Feb. 15; C) in Chuguev on Feb. 27; D) in Abastumani on March 14.

4. Results of Photometry

Regular CCD observations of asteroids have been started in Abastumani since the beginning of 2011. Each year about 25-35 NEAs are observed photometrically. More than hundred NEAs have been investigated in 2011-2015. Among the observed NEAs there are potentially hazardous objects, such as the asteroid (99942) Apophis. For more than thirty NEAs the rotation periods have been determined or substantially improved, and sizes and shapes of the observed bodies have been estimated. During the work 14 binary NEAs were observed, and Abastumani participated in the

discovery of 6 of them (Krugly et al. 2010; Pilcher et al. 2012; Pravec et al. 2016). More than 15 NEAs have been observed in parallel with the radar observations (among them 3 binary asteroids discovered from the radar observations). Several asteroids were observed to detect the YORP effect including NEAs (1862) Apollo (Kaasalainen et al. 2007), (1620) Geographos (Durech et al. 2008), and (3103) Eger (Durech et al. 2012) for which the effect was discovered. The photometric data were obtained for two well-known binaries (88710) 2001 SL9 and (175706) 1996 FG3 (Scheirich et al. 2015) to verify the existence of the Binary YORP effect (BYORP, see in Cuk & Burns 2005), which supposes orbital variation of a synchronously rotating secondary in a binary system under the YORP influence.

Below, we present observations of four NEAs which demonstrate results obtained on different tasks of our research.

(4055) Magellan discovered by Helin E. F. at Palomar Observatory in 1985 belongs to the Amor asteroids. The orbit of the asteroid lies beyond the Earth orbit with the following parameters: semi-major axis a = 1.8201 AU, eccentricity e = 0.326, inclination i = 23.258 deg, and perihelion q = 1.22 AU. The asteroid is known as the V-type asteroid (a possible source of the basaltic meteorites on the Earth) with albedo p_v = 0.36 and diameter D = 2.46 +0.53/-0.41 km. (Thomas et al. 2011, 2014). Taxonomic type is defined based on observations of the color indices and spectra (Visible + NIR) of the asteroid. The asteroid was firstly classified as the V-type by Cruikshank et al. (1991) due to measurements of color indices U-B = 0.52, and B-V = 0.22. Pravec et al. (2000) obtained lightcurves of the asteroid and determined a rotation period of P = 7.496 hours in 2000, and determined parameters of the phase-relation in the R band to be equal to Hr = 14.45, G = 0.25. In January-February 2014 the asteroid was observed by Warner (2014) which obtained a wrong period of 6.384 h, because of very sparse observations (Warner 2015a). New observations of Warner (2015a) in 2015 give a period of 7.496 hours (the lightcurve amplitude of 0.63 mag at phase angle 39 deg) consistent with the Pravec et al. (2000).

We observed Magellan at Abastumani on September 7, 2015. The observations allow us to estimate the value of the period P = 7.47 ± 0.2 hours in a good agreement with the value previously defined by Pravec et al. (2000). The composite lightcurve showed in Fig. 3 covers a whole rotation period of Magellan. The maximum amplitude of the lightcurve is 0.41 mag at phase angle 3 deg, that close to the value 0.46 mag obtained by Pravec et al. (2000) in 2000.

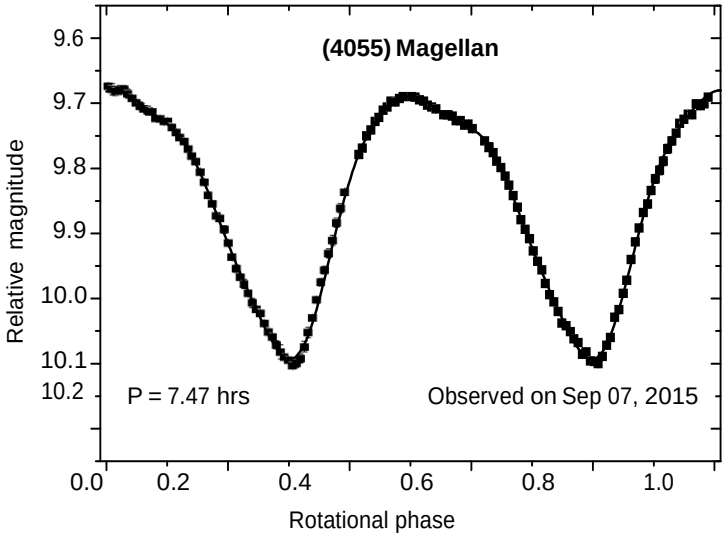

Fig. 3 Composite lightcurve of asteroid (4055) Magellan following observations on September 7, 2015. A solid line is an approximation with Fourier series of the asteroid's brightness variations with time using a period 7.47 hours.

We expect to estimate an infuence of the YORP effect on Magellan's rotation period in the future after carrying out observations in its next appearances in 2017, 2019, and 2020. During the former opposition the asteroid will be near its perihelion with a high brightness V = 15.8 mag. A good estimate of the YORP will be obained if a model of the asteroid's shape will be constrained as a result of radar observations carried out in that time.

(137925) 2000 BJ19 is Apollo asteroid with diameter 2-4 km which was discovered within the Catalina survey in January 2000 (MPC). The asteroid has highly elongated orbit (a = 1.292, e = 0.764, i = 31.1 deg) with an orbital period 1.47 years and crosses Mercury's orbit near the perihelion q = 0.305 AU. In 2015 opposition the asteroid was well visible on the Northern sky throughout a whole night in February-March. In this time the brightness of asteroid has reached maximal magnitude 16.7 mag that provides a good opportunity for photometry.

The CCD observations of 2000 BJ19 were carried out at Abastumani for four nights in the interval from 23 February up to 13 March 2015. The obtained data have allowed us to determine definitely the rotation period of 5.516 ± 0.003 hrs. The lightcurves of the asteroid composed of this period are shown in Fig. 4. The ordinates represent the relative magnitudes of the asteroid. There are two composite lightcurves for different dates of observations: from February 23 to March 3, and for the night on March 13. Shapes of the lightcurves differ significantly. February's lightcurve has smaller amplitude of 0.15 mag and asymmetrical minima with unusual shape. As opposed to February, the lightcurve on March 13 has a symmetrical shape with the maximum amplitude of 0.24 mag. The difference between amplitudes and shapes of the lightcurves may be related with an increase in phase angle from late February to mid-March from 26 to 43 deg, respectively. Also, the changing shape of the lightcurve may be connected with variation of aspect of the observations on more than 30 deg. We can say that the shape of the asteroid is irregular and markedly different from the equilibrium shape. An estimate of elongation of the body's shape can be made taking into account the correction of the amplitude of asteroid's variation to zero phase angle. If we assume that the growth of the amplitude with phase angle as m = 0.023 mag/deg (Zapalla et al. 1990), then the ratio of the largest semiaxes of the approximating ellipsoid is 1:0.9.

Warner (2015) observed this asteroid in mid-February 2015 and estimated the rotation period to be equal 48 or 24 hrs. This rough error in determining the period may be due to a poor accuracy of the observations. It could be caused by both the observations in the bad weather conditions (as was noted by the author) and a small aperture of the used telescope.

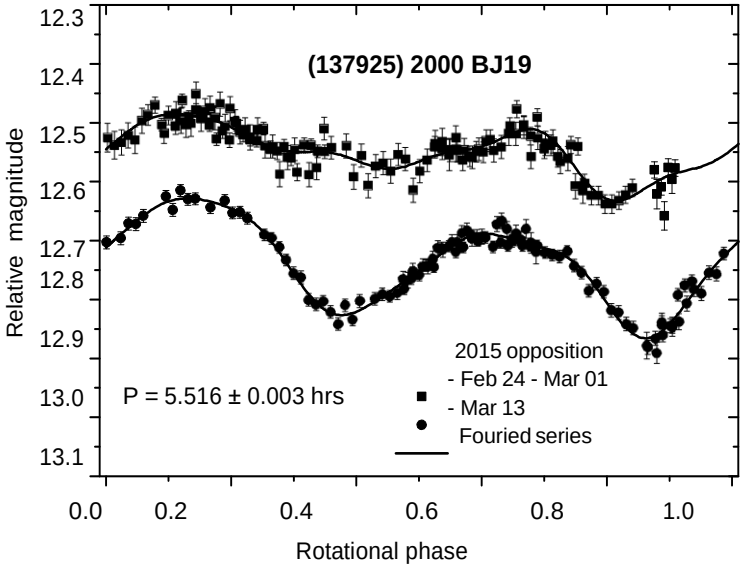

Fig. 4. The composite lightcurves of asteroid (137925) 2000 BJ19 following observations in February-March 2015. A solid line is an approximation with Fourier series of the asteroid's brightness variations with time using a period 5.516 hours.

(326290) Akhenaten is Aten asteroid with a small diameter about 100 m which was discovered in the private observatory Goodricke-Pigott in Tucson (USA) by R. A. Tucker in April 1998 (previously named 1998 HE3). The asteroid is listed at the MPC as Potentially Hazardous Asteroid due to the absolute magnitude H = 21.8 and Earth MOID = 0.0034 AU (EMOID is the minimum distance between the Earth and the minor planet). The asteroid orbit is highly eccentric (a = 0.879 AU, e = 0.440, i = 3.378) with aphelion Q =1.266 and perihelion q = 0.492. The asteroid positions were measured during 6 oppositions and now Akhenaten belongs to asteroids for which evidences of the Yarkovsky effect have been found (Farnocchia et al. 2013). Moderate albedo of the asteroid (SQ type) and its diameter of 0.1 km were assumed in Binzel et al. (2002).

In April-May 2012 the asteroid approached to the Earth. A close pass to the Earth at 12.4 lunar distances (0.032 AU) was on May 10, 2012. First photometric observations of the asteroid were made in April with the 2.6 m telescope of Crimean Astrophysical Observatory. They showed that the asteroid rotated very fast with a period of several minutes (Fig. 5A). Observations at Abastumani on May 9 confirmed very fast rotation of the asteroid with the period 3.921 min. There are some other published data on the value of the rotation period. The composite lightcurve constructed using the determined period is shown in Fig. 5B. The maximal amplitude of the brightness variations is as small as 0.06 mag. A small amplitude suggests either a nearly spheroidal shape of the asteroid or observations close to a polar aspect. Radar observations at Arecibo Observatory with 305 m radar in early May 2012 have confirmed a fast rotation of the asteroid (Nolan & Taylor 2012).

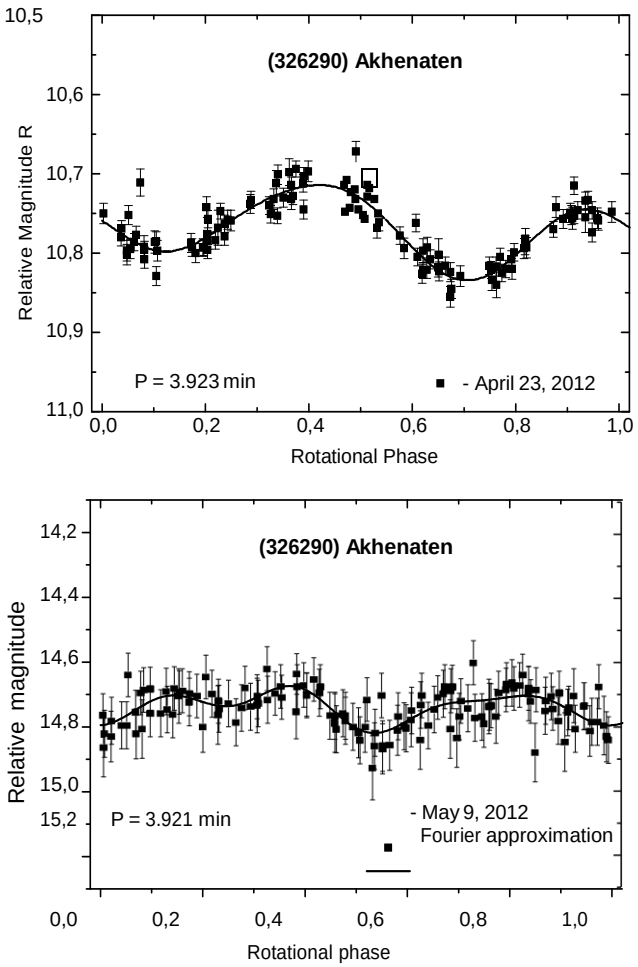

Fig. 5. The composite lightcurve of asteroid (326290) Akhenaten following observations at CrAO (A) on April 23, and at AbAO (B) on May 9 in 2012. A solid line is an approximation with Fourier series of the asteroid's brightness variations with time using periods (A) 3.923 and (B) 3.921 minutes.

Among NEAs with diameters larger the 200-300 m, almost all bodies rotate slower than about 11 revolutions per day (Pravec & Harris 2006). There is a rotation speed limit for these asteroids called "spin barrier". It is suggested that these bodies may composed of many individual parts, which held together only by the gravity. Such a composite body may be formed after catastrophic impact between asteroids and called "rubble-pile" asteroid (Richardson et al. 1998). In the same time a large number of NEAs with diameters less than 200 m show a very rapid rotation with periods less than 2.2 hours (Hergenrother & Whiteley 2011; Hetch & Wiegert 2015). A little of "rubble-pile" asteroids can spin faster than 2.2 hours, so it is assumed that the most rapidly rotating asteroids are monolithic bodies. Asteroid (326290) Akhenaten rotates very fast making about 367.25 revolutions per day, and its diameter about 100 m is close to the maximal diameter limit of fast-rotating asteroids. Therefore there are many reasons to assume that Akhenaten is a monolithic body.

2013 TV135 is Apollo asteroid discovered in the Crimean Astrophysical Observatory in October 2013. The asteroid is a small NEA with diameter of 400 m estimated from the absolute magnitude H = 19.5 (MPC) and essuming its albedo 0.18. The asteroid 2013 TV135 is located on an elongated orbit (a = 2.438 AU, e = 0.593, i = 6.75 deg, q = 0.987 AU). During the first weeks after its discovery the asteroid was assumed to be a potentially hazardous object.

Observations were carried out at Abastumani and Chuguev observatories immediately after its discovery in October 2013. The asteroid was observed at Abastumani with the 70-cm meniscus telescope AC-32 on Oct. 21-22 and 24-25, and Dec. 4, and at Chuguev with the 70-cm telescope AZT-8 on Oct. 23. The rotation period of the asteroid equals to 2.351 ± 0.001 hours was firstly found as a result of our observations. The maximum amplitude of the brightness variations of the asteroid is equal to 0.38 mag at phase angle of 55 deg. Lower estimate of the ratio of the largest semi-axes of an ellipsoid approximating the shape of the asteroid is a:b = 1:0.86 using m = 0.023 mag/deg (Zapalla et al. 1990). Figure 6 shows the lightcurve of the asteroid obtained at Abastumani on October 21.

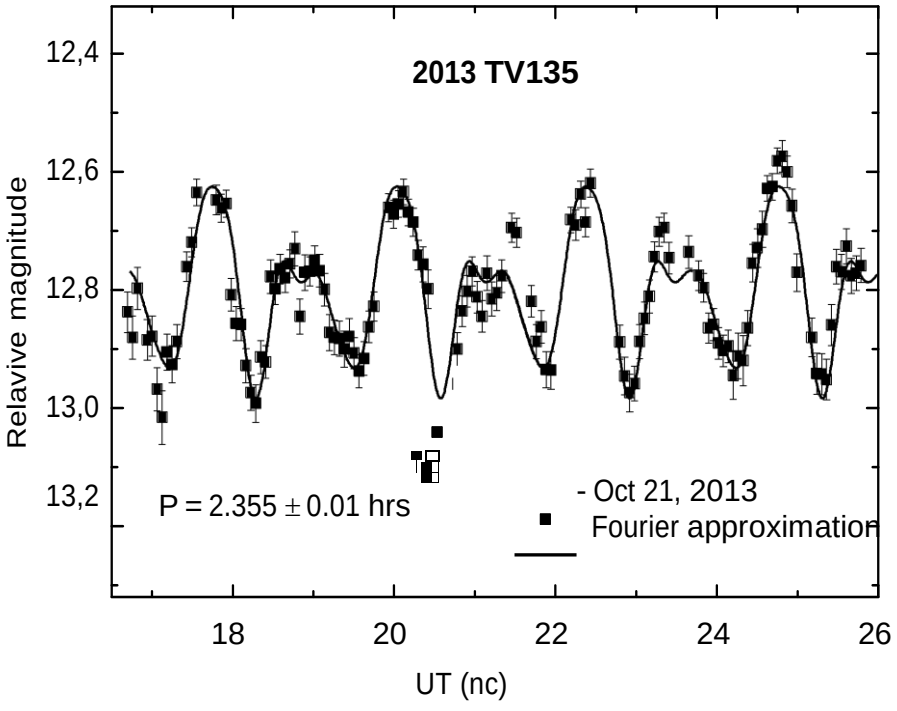

Fig. 6. Lightcurve of asteroid 2013 TV135 following observations on October 21, 2012. A solid line is an approximation with Fourier series of the asteroid's brightness variations with time using a period 2.355 hrs.

5. Observations in the Frame of the Optical Telescopes Network *Gaia*-FUN-SSO in Support of the *Gaia* Mission

The Abastumani Observatory joined the international optical network the *Gaia*-FUN-SSO in 2011 (Krugly et al. 2011, 2015). The network of observatories organized by the IMCCE - Paris Observatory and the Observatory of Nice (France) for astrometric and photometric observations of asteroids, which will be discovered or studied in details (UBVRI-photometry and spectrophotometry) during observations with the *Gaia*, a mission of the European Space Agency. The *Gaia* spacecraft has been placed in a special orbit near the Sun in the Lagrangian point L2 of the Sun-Earth system on December 2013. Throughout 2014, the equipment of the satellite was tested and observations of selected sky fields were made. In the spring of 2015 the mission has elaborated its main program to carry out the survey of the sky in order to obtain high-precision measurements of positions and magnitudes of the stars across the sky up to 20-21 mag. It is expected that the satellite will work at least 5 years. Currently, timely detection of asteroids in a flow of the *Gaia*'s observations is tested to start working on discovery of asteroids.

In 2011-2014 in order to prepare observatories participated in the *Gaia*-FUN-SSO network to follow-up observations of the asteroids, the organizers of the cooperation have been proposed several NEAs for test observations (Thuillot et al. 2015). The participation of the Abastumani Observatory in the test is reproduced in Table 1, which shows the observed asteroids and the dates of their observations. The observations were carried out at the 70 cm meniscus telescope with a CCD camera IMG-6303E. Accuracy of measured positions of asteroids is determined mostly by an accuracy of the used astrometric catalog (USNO-A20, UCAC3, UCAC4). On the average, accuracy is better than 0.5-0.7 arcsec.

In particular, one of the most dangerous (at that time) NEA (99942) Apophis was included in the program of observations. An astrometric observation campaign was launched during the latest period of observability of Apophis in 2012-2013 before its dangerous passing the Earth in 2029. Results of Apophis' observations show that the accuracy of astrometry obtained in Abastumani is high enough to be suitable for analysis of such a task (Thuillot et al. 2015).

Table 1. Asteroid observations, which were carried out at Abastumani in the framework of a test program to support the *Gaia* mission.

Asteroid	Interval of campaign	Dates of observations
(308635) 2005 YU55	Nov-Dec 2011	2011 Nov 17-19; Dec 17
(175706) 1996 FG3	Nov 2011 - Mar 2012	2011 Nov 22,25; Dec 1, 17-18, 30; 2012 Jan 21; Feb 24, 25
(99942) Apophis	Feb 2012	2012 Feb 24 – asteroid was not found
(99942) Apophis	Jan-Apr 2013	2013 Jan 28, 30, Feb 2-3, 11, 13- 14; Apr 1
2012 DA14	Feb 2013	2013 Feb 17
(163249) 2002 GT	Jun 2013	2013 Jun 19-20, 30
2013 TV135	Oct-Dec 2013	2013 Oct 21-22, 24-25; Dec 4
2014 HQ124	Jun 2014	2014 Jun 10

5. Conclusions

The program of investigation of physical properties of NEAs was launched in Kharadze Abastumani Astrophysical Observatory in the cooperation with the Institute of Astronomy of V. N. Karazin Kharkiv National University in 2011. The collaboration includes a participation in organizing observation projects, improving the instrumental base, and training highly qualified specialists. In the frame of this work the CCD photometric observations of NEAs are carried out at Abastumani on a regular base. More than hundred asteroids have been investigated during 2011-2015.

Our plans are aimed at the continuation of the study of asteroids in the following areas: characterization of potentially dangerous and newly discovered NEAs; detection of binary asteroids; study of the YORP effect; support of radar observations of NEAs. We are prepared to begin observations of the asteroids newly discovered by the *Gaia* mission.

We expect on technical improvements of the 70 cm telescope AC-32, which consist in using a more sensitive CCD camera, installing the camera in a primary focus, and modernization of the control system of the telescope. A significant contribution to the work would be made in case of upgrading of the 1.25 m telescope AZT-11. All these will improve the accuracy of photometric measurements and will provide an opportunity to observe more faint celestial objects.

Acknowledgments. The work at Kharadze Abastumani Astrophysical Observatory was supported by the Shota Rustaveli National Science Foundation, Grant FR/379/6-300/14.

References

Binzel, R. P., Lupishko, D. F., Di Martino, M., et al. 2002, in Asteroids III, eds. W.F. Bottke Jr. et al. (Univ. Ariz. Press, Tucson), 255

Chapman, C. R. 2004, EPSL, 222 (1), 1

Cruikshank, D. P., Tholen, D. J., Bell, J. F. et al. 1991, Icarus, 89, 1

Cuk M., & Burns, J. A. 2005, Icarus, 176, 418

Durech, J., Vokrouhlicky, D., Kaasalainen, M., 2008, A&A, 488, 345

Durech, J., Vokrouhlicky, D., Baransky, A. R. et al. 2012, A&A, 547, A10

Farnocchia, D., Chesley, S. R., Vokrouhlicky, D., et al. 2013, Icarus, 224, 1

Gladman, B., Michel, P., & Froeschle, C. 2000, Icarus, 146, 176

Harris, A. W., & Pravec, P. 2006, in IAUS229-ACM2005 conference proceedings held at Buzios, Rio de Janeiro, Brazil, August 7-12, 2005, eds. D. Lazzaro , S. Ferraz-Mello & J.A. Fernadez (Cambridge Univ. Press), 439

Hergenrother, C. W., & Whiteley, R. J. 2011, Icarus, 214, 194

Hetch, P., & Wiegert, P. A. 2015, P&SS, 111, 100

Kaasalainen, M., Durech, J., Warner, B. D., Krugly, Yu. N., & Gaftonyuk, N. M. 2007, Nature, 446, 420

Krugly, Yu. N. 2004, Solar Syst. Res., 38, 241

Krugly, Yu. N., Belskaya, I. N., Shevchenko, V. G., et al. 2002, Icarus, 158, 294

Krugly Yu.N., Maccone C., Gaftonyuk N.M., et al. 2007, P&SS, 55, 449

Krugly, Yu. N., Pravec, P., Behrend, R., et al. 2010, Abstracts of Binaries in the Solar System II workshop held at Poznan, Poland, July 13-15, 2010

Krugly, Yu. N., Molotov, I. E., Agapov, V. M., et al. 2011, in Gaia follow-up network for the solar system objects: Gaia FUN-SSO workshop proceedings, held at IMCCE - Paris Observatory, France, November 29 – December 1, 2010, eds. P. Tanga, & W. Thuillot, 101

Krugly, Yu., Molotov, I., Voropaev, V., et al. 2015, in Third Gaia follow-up network for the solar system objects: GAIA-FUN-SSO 2014 workshop proceedings, held at IMCCE/Paris Observatory, France, November 24 – 26, 2014, eds. P. Tanga, & W. Thuillot, 93

Molotov, I., Agapov, V., Khutorovsky, Z., et al. 2013, in 6th European Conference on Space Debris conference proceedings, ESA SP-723, ISBN 978-92-9221-287-2, 6 p.

Morbidelli, A., Bottke, Jr., W. F., Froeschlé, C., & Michel, P. 2002, in Asteroids III, eds. W.F. Bottke Jr. et al. (Univ. Ariz. Press, Tucson), 409

Mottola, S., De Angelis, G., Di Martino, M., et al. 1995, Icarus, 117, 62

MPC (the Minor Planet Center of IAU): http://www.minorplanetcenter.net

NEO-Report: Near-Earth Object Science Definition Team, Study to Determine the Feasibility of Extending the Search for Near-Earth Objects to Smaller Limiting Diameters, NASA Office of Space Science, Solar System Exploration Div., Washington, DC, 2003, 154 pp., http://neo.jpl.nasa.gov/neo/neoreport030825.pdf

Nolan, M., & Taylor, P. 2013, private communication

Pilcher F., Briggs, J. W., Franco, L., et al. 2012, Minor Planet Bul., 39, 148

Pravec, P., Wolf, M., Sarounova, L. (2000): http://www.asu.cas.cz/~ppravec/neo.htm

Pravec, P., Scheirich, P., Kusnirak, P., et al. 2016, Icarus, 267, 267
Richardson, D. C., Bottke, W. F., & Love, S. G. 1998, Icarus, 134, 47
Scheirich, P., Pravec, P., Jacobson, S. A., et al. 2015, Icarus, 245, 56
Shustov, B. M., Rykhlova, L. V., Kuleshov, Yu. P., et al. 2013, Solar Syst. Res., 47 (4), 302
Thomas, C. A., Trilling, D. E., Emery, J. P., et al. 2011, AJ, 142 (3), id 85
Thomas, C. A. , Emery, J. P., Trilling, D. E., et al. 2014, Icarus, 228, 217
Thuillot, W., Bancelin, D., Ivantsov A., et al. 2015, A&A, 583, A59
Warner, B. D. 2014, Minor Planet Bul., 41, 157
Warner, B. D. 2015, Minor Planet Bul., 42, 172
Warner, B.D. 2015a, Minor Planet Bul., 42, 256
Zappala, V., Cellino, A., Barucci, A. M., et al. 1990, A&A, 231, 548

Astronomy & Astrophysics (Caucasus) 1, (2016) 49-52

Spectropolarimetry of the Lunar Surface and Its Ground Samples

O. I. Kvaratskhelia[1], R. Z. Ivanidze[1,2], Sh. G. Gigolashvili[1]

[1]Kharadze Abastumani Astrophysical Observatory, Georgia
[2]Samtskhe-Javakheti State University

Email:kvara_otar@mail.ru

Received March 22, 2016; revised May 18, 2016

Abstract

Electropolarimetric observattions of 190 separete regions of the lunar surface were performed at Abastumani Astrophysical Observatory of the Georgian Academy of Scinces in 1976-2010. An automatic scanning electropolarimeter ASEP-74 (ASEP-78) attached to the Zeiss 40cm refractor (F=680mm) was used for observations. The instrument provided a high measurement accuracy of the linear polarization degree (<0.1%) and the angle of the plane ($<0.5^0$). More than 140 nights were observed under quite favourable seeing conditions.

In 1980 and 1982 during the two month's period altogether, laboratory polarimetric measurements of 21 lunar samples were done at the V. J. Vernadskij Institute of Geochemistry and Analytical Chemistry of the USSR Academy of Sciences. The samples were delivered to the Earth by the Soviet "Luna" and the American "Appolo" series spaceships.

Key words: Polarization degree, Positive polarization, Moon

1. Results of Telescopic Observations of the Moon.

1. Comprehensive spectropolarimetric observational data are obtained for 190 regions of the lunar surface in the visible spectral region. Most of objects including the landing sites of "Luna -16, 20, 24" and "Appollo – 11, 12, 14, 15, 16, 17" were measured for the first time.

2. Lunar details differing by morphological properties polarize the light in different ways. When a maximum polarization degree – P_{max} decreases the regions mainly arrange as follows: seas and gulfs (10-16%), certain craters of the marine surface and crater seas (8-12%), craters with central hills, mainlands and mainland craters with bright streamers (4-10%). The highest P_{max}=18% (in the integral light) is found between the craters of Flemstid D and K and the lowest one (3.6%) – near the crater Procle.

3. The curves of the phase angle dependent polarization degree for all measured objects at all wavelengths are absolutely systematic relative to a zero phase. The peak Piton, for which the phase curves of polarization before and after the opposition are of various shape, is an exception.

4. The degree of positive polarization for all objects at all phase angles depends on the wavelength. This dependence is of different character for different details. The seas, on the average, have a larger slope of the $P_{(\lambda)}$ curves than the mainlands and craters (Dollfus A., Geake J.E.1975).

A positive polarization attains its maximum value between the phase angles of $\pm 100^0 \div \pm 107^0$. For the marine surfaces in this interval there is shifts of P_{max} towards large phase angles by $3^0 \div 5^0$ compared with the continental formations.

For the object under study both in the integral light and at different wavelengths, P_{max} occurs at the same phase angles (Dzhapiashvili, V., Korol', A.,1978).

5. In the integral light the inversion angle for the lunar objects is found between the phase angles $\alpha = \pm(23^0 \div 24^0)$. The turning of the polarization plane at the inversion angle occurs abruptly.

For the lunar seas, gulfs and sea-like craters, it is proved that the inversion angle of the polarization curve really depends on the wavelength. For these surfaces the phase dependence of the inversion,

corresponding to the wavelength of λ=0.419 mkm and λ=704 mkm, reaches 2^0 (for λ=0.419 mkm, $\alpha_{inv} \approx \pm 22^0$ and for λ=0.704 mkm $\alpha_{inv} \approx \pm 24^0$). This mainly occurs in the short wavelength spectral region to λ=0.641 mkm.
For the mainlands and craters the spectral dependence of the inversion angle was not observed.
6. The minimum of the negative polarization for all the details measured is within the interval of the phase angle $\pm 11^0.5$ $\pm 0^0.5$.
The minimum of the negative polarization $/P_{min}/$, in separate regions of the lunar surface varies from object to object within 0.6%÷1.4%. It can be suggested that $/P_{min}/$=1.0%÷1.2%. This value is higher ($/P_{min}/$=1.2%÷1.4%) for the sea surfaces and mainlands in certain lunar regions. The craters with bright streamers and a few ones with the central hills are characterized by a low value of $/P_{min}/$=0.6%÷1.2%. For the sea surfaces and craters with a flat bed $/P_{min}/$ is higher by 0.2÷0.3% with increasing of the wavelength from 0.419 mkm up to 0.641 mkm. Afterwards this value is constant. When the phase angle α_{min} varies towards the inversion, the dependence $P_{min}(\lambda)$ keeps in the spectral interval and to the zero phases it reduces little by little and then disappears.
For the craters Aristarchus and Procle $/P_{min}/$ is found to decrease within λ=0.419mkm-0.641 mkm. After this it becomes constant. When the phase angle varies from α_{min} in both sides, $P(\lambda)$ diminishes gradually and then disappears.
7. The correlation dependence of $P_{max} - \rho$ constructed in the logarithmic scale, using the observational data of the present paper and those for the albedo ρ, borrowed from different charts, mainly show a linear relation (Kvaratskhelia O. I.1986).
8. The relation between P_{max} – h plotted for a blue region and integral light was checked for the first time, h is the slope of the polarization phase curve at the inversion point. A close correlation or any singnificant scatter on the logarithmic axis was not found. This points to a slight effect of a negative polarization on the slope h of the polarization curve at the inversion point. Therefore a close correlation between ρ – h is a consequence of Umov's effect.
9. Using different charts of the albedo ρ - P_{min} dependences are plotted for the Moon. A light tendency of decreasing / P_{min}/ with the albedo rise is observed. On the whole, these results confirm the data of laboratory measurements of the Earth samples and they may be of interest in constructing the models of the light negative polarization.

2. Laboratory Measurements of the Lunar Samples.

1. Some detailed spectropolarimetric data for 21 samples of the lunar ground delivered to the Earth by the Soviet "Luna – 16, 20, 24" and American "Apollo – 11, 15, 16, 17" spaceships are obtained.
2. For the measured samples P_{max} occurs at the same phase angles both in the integral light and at separate wavelengths. The positive polarization is of maximum value at different phase angles depending on the size of the fraction particles, sample soil extraction. For undivided samples and for those with the fraction size of < 83 mkm, P_{max} occurs between the phase angles of $100^0 \div 110^0$. For others $\alpha(P_{max}) > 110^0$. At the same time $\alpha(P_{max})$ increases up to 130^0 and more with the size of the fraction particles. According to the samples of the "Luna-24" there is an increase of P_{max}.
3. The negative polarization has a maximum value between the phase angles of $\alpha = 10^0 \div 12^0$ both in the integral light and at separate wavelengths. The samples N 2406 7-3 and 100017, for which $\alpha(P_{min}) = 6^0$, are exceptions.
$/P_{min}/$ is within 0.8÷1.2% in the integral light for all samples.
For the simples of the "Luna-20" and "Apollo-16" landing sites the negative polarization does not depend on the wavelength, i.e. in separate spectral regions this value is the same as in the integral light. For the samples of other long wavelength spectral regions the negative polarization
does not depend on the wavelength as well; in a short wavelength region, from λ=0.533 mkm to λ=0.419 mkm $/P_{min}/$ decreases gradually by 0.2÷0.3% (Kvaratskhelia O. I.1986).
For the samples measured by the authors the value of the inversion angle in the integral light is within the phase angles of $19^0 \div 24^0$, except for the sample N 1610, for which $\alpha_{inv} = 10^0$.
A detailed measurement of the samples N 1603 and 2409.4-4 the inversion angle shows that this angle is by $1.5^0 \div 2^0$ less in the blue than in the red. Such a dependence of $\alpha_{inv}(\lambda)$ is the case in the short

wavelength spectral region to λ=0.533 mkm. With $\lambda > 0.533$ mkm the inversion takes place simultaneously at all wavelengths. The spectral dependent inversion is also observed for other samples of the "Luna-16 and 24" as well as for those N 10005.35-6 and 75080-10 from "Apollo-11 and 17". There was no spectral dependence of $\alpha_{inv}(\lambda)$ for other samples.

5. Measurements of depolarizing properties of the lunar samples have been performed for the first time. The results show a great variety of these properties from the sample. Infortmation contained in these measurements certainly will be of value in interpreting the data obtained by the conventional methods.

So, the present monograph investigation contains a large observational data array on the polarization properties of separate areas of the lunar surface and of the lunar ground samples. At the same time a technique of observations, measurements and analysis is described. What kind of regions can the observed results applied in and what are the properties of a future development of investigations by the technique suggested?

As much as the Moon, for a long time, will be an object of astronomical investigations and for the terrestrials it will turn to the "seventh continent" only in a remote future, the methods of its observations must be improved and its distance probings must be enriched. Some information on a chemical-mineralogy content and physics-mechanical properties of the lunar mantle substance are being obtained by the selenologists analyzing the data on conventional astrophysical parameters: albedo, polarization degree, color index and spectrum.

In the optical region the albedo correlates well the element content of the lunar surface samples e.g. A1/S1, being the correlation order rather high (0.8). The spectral albedo in the absorption band zones is responsible for the information on the presence of certain minerals (or on probability of their presence) in the lunar ground.

The polarization degree has a clear-cut inverse dependence on the albedo; thus, its value depends on the concentration and variation of opaque minerals and dark-color oxides, such as FeO_2 and TiO_2 in the ground. All of these three optical parameters depend on the grading content of the matter, package density and other physics-mechanical properties of the samples.

As it was mentioned in Section 1.2, based on the analysis of the two component (Frenel and internal ones) model of the lunar reflecting layer, as well as on the investigation of interrelation of a normal albedo with the polarization degree, a new optical parameter $\varrho * P_{max}$, which has turned out to be very informative, is found. It enables to separate the effects connected, on the one hand, with mineralogy paculiarities and with physical characteristics of the lunar ground, on the other hand.

These investigations will develop later on if, based on a large body of experimental data, one successively studies first the interrelation of the albedo, polarization degree as well as of the color index in the optical spectral region, with the chemical content, then with the mineralogy abundance and finally with the structure properties of well studied samples of the terrestrial magma rocks, those similar to the lunar ground and to the lunar samples themselves.

Such works are under way and the first results will be published shortly. They will permit to compile a data bank on the optical characteristics of the terrestrial magma changeful and changeless rocks as well as of the lunar samples. The bank will enable one to interpret the optical parameters of the lunar regions besides other nonatmosphere celestial bodies as to the mineralogy content and physical properties of the surface matter; it will also serve as the basis for optical classification of the lunar surface regions.

The optical classification itself can be done only due to a multiparametric zoning of the visible side by the telescopic data. At present there exist rather accurate charts and atlases of the albedo, polarization degree and color. Using these data two or three – parameter zoning can be done manually, but reliability of such classifications will not be high. At the same time the charts of new optical parameters – a relative porosity and species of the lunar rocks – are missing at all. There are only separate fragments, but without allowance for the action of the phase functions on the result.

A new step in this direction is a digital facilities for the telescopic images to be treated. In this respect the works are in progress in some institutions of our country.

After the capabilities of the photographic method are exhausted a step, leading to an increased accuracy of observational data, must follow. The application of new sensitive and high-precision receivers – CCD matrices will favor this matter.
Thus, the measurement technique of the polarization properties of the lunar samples and observational results presented in the monograph will be used for creation of the data bank of the magma rock optical characteristics of the Earth and Moon. The degree of a maximum polarization (P_{max}) will be applied as the most informative parameter; then other polarization parameters will do. The catalog of maximum polarization for a hundred of the lunar regions will be used as a basic one for calibration of the high-accuracy polarimetric charts in constructing the classification of the lunar regions. But subsequent observations of the lunar regions will allow to reveal the relation of the relative porosity parameter to a known photometric function of Hapke (H). This makes it possible to distinguish regolith density inhomogeneities on the lunar surface.
The data, on a detailed investigation of the parameters P_{min}, $P_{min}(\lambda)$, $P(\alpha_{inv})$, h obtained in bulk in the present work for the lunar regions and samples, are essential in studying other objects of the solar system. The same results are also extremely important for the astronomers – theoreticians elaborating the theory of diffusion reflection of the light by rough surfaces.
The experimental material of the present work enables to establish reliably that P_{min} and α_{inv} undergo regional variations over the lunar surface. So, planetologists can classify the lunar formations according to two more physical characteristics. In the future, based on this fact, it will be possible to make the charts of the lunar surface regions for P_{min} and α_{inv}. This will enrich a subject chart making of the Moon markedly. A successful construction of a theoretical model of a negative polarization will help to connect the parameters P_{min} and α_{inv} with the characteristics of the lunar ground microstructure, such as the size of particles, porosity, homogeneity and others.(Kvaratskhelia O. I,2006,2015).

References

Dollfus A., Geake J.E. Polarimetric Properties of the Lunar Surface and Its Iterpretation. Part VII: Other Solar System Objects. – Proc. Lunar. Sci.Conf.6-th 1975, 3.
Dzhapiashvili, V., Korol', A., "Polarimetricheskii atlas luny", "Tbilisi : Izd-vo "Metsniereba", 1978.
Kvaratskhelia O. I. "Spectropolarimetria otdelnikh uchastkov lunnoi povekhnosti i obrazci lunnovo grunta" – Avtoreferat kan. diss. Kiev. 1986.
Kvaratskhelia O. I, Dissertation. Abastumani,2006. , 219.
Kvaratskhelia O. I, International Scientific Conference ,,Problems of Modern Astrophysics" report**,,**Spectropolarimetry of the Moon". Akhaltsikhe.2015.

Astronomy & Astrophysics (Caucasus) 1, (2016) 53-57

On Some Aspects of Stellar System's Gravitational Field with Steckel Potential

G. A. Malasidze, R. A. Chigladze

Samtskhe-Javakheti State University, E. Kharadze Abastumani Astrophysical Observatory

Email: **revazchigladze@ yahoo.com**

Received March 24, 2016; revised May 18, 2016

Abstract

On the basis of Steckel's form of gravitational potential on the context of theory of the third quadratic relating to velocity components of isolating integral of motion are studied some basic characterustics of stellar orbits. In particular is constructed interesting two-component model of stationary rotationally symmetrical Galaxy for that the problem of star's spatial orbits definition is solved in elliptic integrals.

Key words: gravitation; potential; star; Galaxy; model; integral of motion; period; frequency; canonical variables, function, diagram

1. INTRODUCTION

The problem of the third isolating integral of motion in the stellar systems with axial and planar symmetries recently takes on special significance due to the regular as well as stochastic properties of stellar orbits in phase space. This fact indicates the monographs of Arnold (Arnold 1979), A. Lichtenberg and Liberman (Liberman 1984), as well as Zaslavski (Zaslavski 1984) that makes invaluable contribution to the search for solutions. They descriptively indicate that this problem has already gone far beyond the dynamics of stellar systems, becoming as one of the major problems of the general theory of dynamical chaos.

On the basis of Stäckel potential with taking into account the classical works of Kuzmin (Kuzmin 1953,1956,1987), as well as works of the author of the present work (Malasidze 1973,1982) and works of other authors (Dejonge 1988), within the scope of theory of third quadratic regarding of velocity's components, the isolating integral of motion we are preparing for consider the some significant characteristics of stellar orbits. In particular let's consider one of the interesting two-component models with Stäckel's form of potential that assumes the solution of orbit's determination task in elliptical integrals.

2. Canonic Variables

Let's select as generalized coordinates the system of confocal ellipsoidal coordinates:

$$q_1 = \xi_1, \quad q_2 = \xi_2, \quad q_3 = \theta, \tag{1}$$

where θ – is the azimuth angle located in the stellar system's simmetry plane and q_1 and q_2 (or ξ_1 and ξ_2) are connected with remained cylindrical coordinates R and z in the following way:

$$R = z_0\sqrt{(q_1^2-1)(1-q_2^2)}, \qquad z=z_0 q_1 q_2 . \tag{2}$$

For generalized impulses we found that

$$P_1 = x_0\frac{w_1}{q_1^2-1}, \quad P_2 = z_0\frac{w_2}{1-q_2^2}, \quad P_3 = z_0 I_2. \tag{3}$$

There z_0 - is the parameter having the length dimension and the $w_1 = w(q_1)$ and $w_2 = w(q_2)$ functions are given by expression:

$$w(q) = \sqrt{2[1_1\, q^2 - I_3 + \varphi(q)](q^2-1) - I_2^2 q^2} \tag{4}$$

In the given case we mean that the motion is described in the field of Stäckel's gravitational potential

$$\Phi = \frac{\varphi(q_1)-\varphi(q_2)}{q_1^2-q_2^2}\ , \tag{5}$$

which assumes three isolating integrals of motion:

energy integral

$$I_1 = v_1^2 + v_2^2 + v_3^2 - 2\Phi\,, \tag{6}$$

kinetical moment's integral relating to symmetry axis (R=0)

$$I_2 = z_0\sqrt{(q_1^2-1)(1-q_2^2)}v_3\,, \tag{7}$$

and third qaudratic relating to velocity's components of integral of motion

$$I_3 = q_2^2v_1^2 + q_1^2v_2^2 + q_1^2q_1^2v_3^2 - 2\Phi^*. \tag{8}$$

The $\varphi(q_1)$ and $\varphi(q_2)$ functions are the arbitrary function of their arguments that satisfies the conditions

$$q_1 \geq 1, \quad |q_1| \leq 1, \tag{9}$$

and for the Φ* function we accordingly will have

$$\Phi^* = \frac{q_2^2\varphi(q_1)-q_1^2\varphi(q_2)}{q_1^2-q_2^2}. \tag{10}$$

It is clear that as generelized velocities would be

$$v_1 = \frac{dq_1}{dt}, \quad v_2 = \frac{dq_2}{dt}, \quad v_3 = \frac{d\theta}{dt} = \frac{dq_3}{dt}. \tag{11}$$

The canonic variables (1) would be transformed for action variables

$$P_j = \frac{1}{2\pi}\oint p_j dq_j, \quad \text{(j=1, 2, 3)} \tag{12}$$

(where integral is taken on one cycle of variable q_j changing) and accordingly canonic conjucted cyclic variables Q_j :

$$z_0^{-1}Q_j = \frac{1}{2}(I_6+t)\frac{\partial I_1}{\partial P_j} - \frac{1}{2}I_4\frac{\partial I_3}{\partial P_j} - I_5\frac{\partial I_2}{\partial P_j}. \qquad \text{(j=1, 2, 3)} \tag{13}$$

For the non-isolating integrals I_4 , I_5 and I_6 of motion it is necessary to take the expressions:

$$I_4 = U_1 - U_2, \quad I_5 = S_1 - S_2 - q_3, \quad I_6 = T_1 - T_2 - t, \tag{14}$$

where t – is the arbitrary instant time. Simultaneously U_1, U_2, S_1, S_2, T_1, T_2 represent the functions from isolating integrals of motion I_1, I_2, I_3 and variables q_1, q_2 that are defined due the following formulae:

$$U_i = \int_{x_i}^{q_i}\frac{dq_i}{w_i}, \quad S_i = I_2\int_{x_i}^{q_i}\frac{dq_i}{(q_i^2-1)w_i}, \quad U_i = z_0\int_{x_i}^{q_i}\frac{q_i^2dq_i}{w_i}, \quad (i=1,2) \tag{15}$$

where x_1 and x_2 are the roots of equation:

$$2[I_1q^2 - I_3 + \varphi(q)](q^2-1) - I_2^2q^2 = 0, \tag{16}$$

that satisfies conditions: $x_1>1$, $0<x_2<1$.

The patrial derivatives of isolating integrals I_1, I_2, I_3 on P_j are necessary to espress through reciprocal derivatives: $\frac{\partial P_j}{\partial I_1}$

and so on. The variable $P_3 = P_\theta$ is exactly equal to z_0I_2 and therefore

$$\frac{\partial I_2}{\partial P_\theta} = z_0^{-1}, \quad \frac{\partial I_1}{\partial P_1} = \frac{\partial I_2}{\partial P_2} = 0. \tag{17}$$

The remaimig derivatives would be expressed through cyclic integrals:

$$U^0 = \oint\frac{dq}{w}, \quad S^0 = \oint\frac{|q|dq}{(q^2-1)w}, \quad T^0 = z_0\oint\frac{q^2dq}{w}. \tag{18}$$

The variables P_j being the functions of I_1, I_2, I_3 are the isolating integrals of motion. At the same time they are adiabatic invariants, i.e. if the function $\varphi(q)$, describing the gravity field of stellar system, would be slowly changing on time then values P_j would be remained.

As main freqiencies of oscillations of stars at its motion would be

$$\omega_j = \frac{2\pi}{\tau_j} = \frac{1}{2}\frac{\partial I_1}{\partial p_j}, \tag{19}$$

where τ_j - are the periods interconnected by the relations:

$$\tau_1 U_2^0 = \tau_2 U_1^0 = \tau_\theta \frac{S_1^0 U_2^0 - S_2^0 U_1^0}{2\pi} = T_1^0 U_2^0 - T_2^0 U_1^0 \ . \tag{20}$$

The formulae for τ_1 and τ_2 in due time were received also by Van de Hulst [13].

Similarly with distortion of Keplerian motion these periods would be called as anomalistic, nodical and sidereal periods accordingly.In the case of Keplerian ellipse such expressions are obtained:

$$P_1 = I\left(\frac{1}{\sqrt{1-e^2}} - 1\right), \quad P_2 = I - |I_2|, \quad P_\theta = I_2 = I\cos\alpha \tag{21}$$

where e – is the eccentricity of orbit, α – is the angle of its inclination angle and I – is the total kinetical moment. Hence we found that

$$\frac{1}{\sqrt{1-e^2}} - 1 = \frac{P_1}{|P_\theta| + P_2}, \tag{22}$$

$$\cos\alpha = \frac{P_\theta}{|P_\theta| + P_2}. \tag{23}$$

If we apply these formulae for galaxy orbits of stars we obtain the defiitions of "quasykeplerian" elements. Tge definition of e eccentricity due formula (22) for the first time was offered by Lynden-Bell (Lynden-Bell 1962).

3. Two-Component Model for Steckel's Potential

For the arbitrary function φ (q) in the expresasaion (4) it would be interesting to take the specific form:

$$\varphi(\xi) = (1-\eta)\varphi_d + \eta\varphi_h, \tag{24}$$

as the result of two elementary models superposition from the series of lens-shaped models that were found earlier by us jointly with Kuzmin (Kuzmin1987). Accordingly this is the Kuzmin-Toomre disc with the espression:

$$\varphi_d = \Phi_0 |q|, \tag{25}$$

and so-called quasi isochronous model

$$\varphi_h = \Phi_0 \frac{2q^2}{1+|q|}. \tag{26}$$

The parameter η∈[0,1] defined the relatively contribution of quasi isochronous lens-shaped model in value of potential in the center of offered two-component model. By taking into account the (24) form function $w^2(q)$ according to formula (4) becomes the fourth power polinom relating the variable $|q|$. Thus for the offered two-component model as well as for its composed each simple model the problem of stellar orbits definition is solved analytically in the elliptic integrals.

For the potential in the plane of symmetry (z=0) we will had

$$\Phi(R,0) = \Phi_0\left(\frac{1-\eta}{\zeta} + \frac{2\eta}{1+\zeta}\right), \tag{27}$$

$$\zeta = \sqrt{1 + \frac{R^2}{z_0^2}}. \tag{28}$$

The surface density and equivalent half-thickness of flat disc are defined due the expressions:

$$\delta_d = \frac{\Phi_0}{2\pi G z_0}\zeta^{-3}, \quad \overline{|z|}_d = 0, \tag{29}$$

whereas in the case of quasi isochronous model as the same characteristics would be

$$\delta_h = \frac{\Phi_0}{\pi G z_0}\zeta^{-1}(1+\zeta)^2, \quad \overline{|z|}_h = \frac{1}{2}z_0\zeta. \tag{30}$$

For the two-component model the surface density is expressed in such a way:

$$\delta = \frac{\Phi_0}{2\pi G z_0}\left[\frac{1-\eta}{\zeta^3} + \frac{4\eta}{\zeta(1+\zeta)^2}\right], \tag{31}$$

and equivalent half-thickness of model takes the following form:

$$\overline{|z|} = \frac{2\eta z_0 \delta_0}{\delta(1+\zeta)^2}, \tag{32}$$

where

$$\delta_0 = \frac{\Phi_0}{2\pi D z_0}, \tag{33}$$

is the surface density in the center of model.

It should be noted that for our Galaxy roughly $\eta \approx 0.1$. Proceedings from circumsolar observational data for the remaining parameters of model the following evaluations were obtained:

z_0=6kps, Φ_0 =144552 km^2·sec^2.

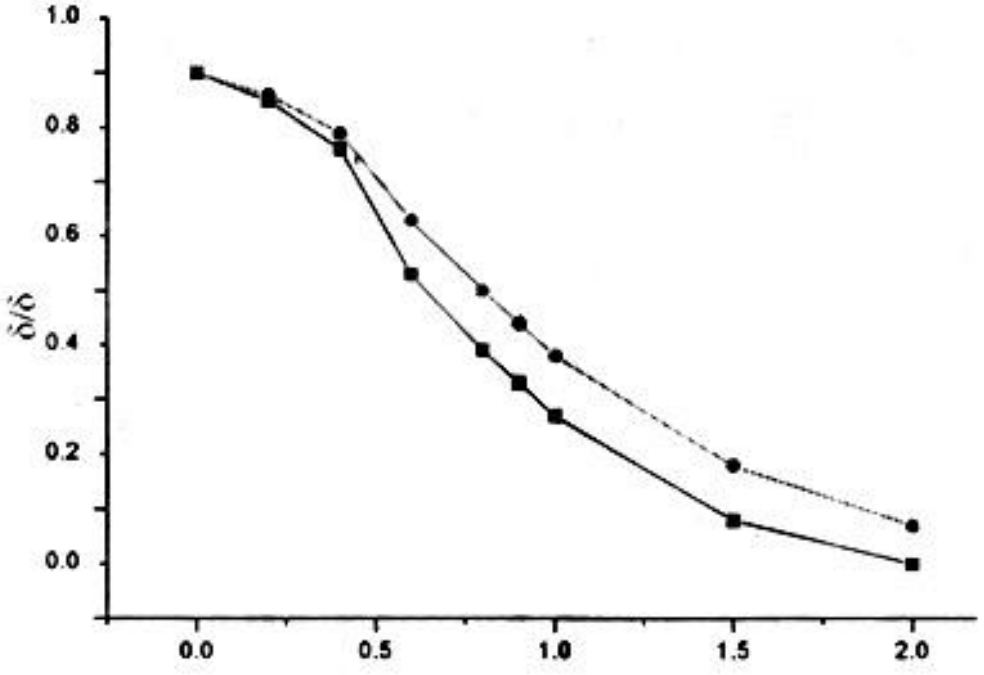

Fig. 1.

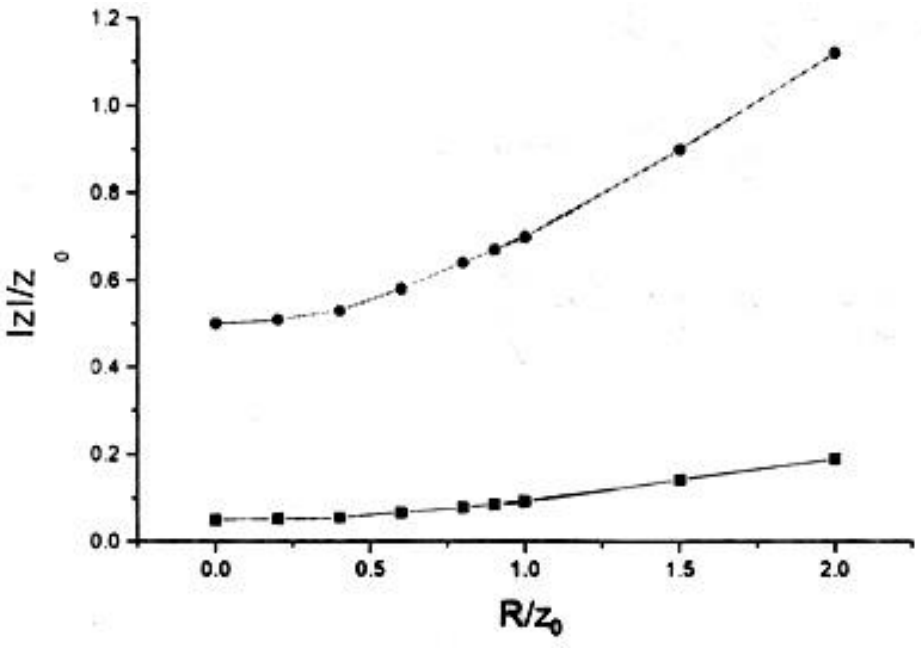

Fig.2.

In Fig. 1 it is shown that the rate of model's surface density drops depending on R(Fig.2) .

REFERENCES

Arnold V.I. Mathematical methods of classic mechanics. Moscow: Nayka, 1979. 432 p. (In Russian).
Dejonge H., de Zeeuw P.T. Astrophys. J., 329, 1988, pp. 720-728.
Dejonge H., de Zeeuw P.T. Astrophys. J., 333, 1988, pp. 90-129.
Kuzmin G.G. Astron. Journ., 33, 27, 1956. -45 p. (In Russian).
Kuzmin G.G. Publ. of Tartu Astron. Observ., 33, 1953, pp. 332-368. (In Russian).
Kuzmin G.G., Malasidze G.A. Publ. of Tartu Astron. Observ., 52, 1987, pp. 48-63. (In Russian).
Likhtenberg A., Liberman M. Regular and stohastic dynamics. Moscow: Mir, 1984. -528 p. (In Russian).
Lynden-Bell D. Observatory, 83, 1962, pp. 23-25.
Malasidze G.A. Dynamics of Galaxy and clusters. Alma-Ata: Hayka, 1973. (In Russian).
Malasidze G.A. Bull. of Abastumani Astrophys. Observ., 55, 1982, pp. 197-202. (In Russian).
Malasidze G.A. Bull. of Abastumani Astrophys. Observ., 55, 1982, pp. 203-208. (In Russian).
van de Hulst C. B.A.N., 16, 1962, pp. 235-240.
Zaslavski G.M. Stochasticity of dynamic systems. Moscow: Nayka, 1984. -272 p. (In Russian).

Astronomy & Astrophysics(Caucasus) 1, (2016) 58-67

Observations of Gamma-ray Bursts in Abastumany Observatory

A. Pozanenko [1,2], A. Volnova[1] E. Mazaeva[1], R. Inasaridze[3], V. Ayvazyan[3], G. Inasaridze[3], V. Zhuzhunadze[3], I. Reva[4], O. Burkhonov[5], V. Rumyantsev[6], Y. Krugly[7], and I. Molotov[8]

[1] Space Research Institute of the Russian Academy of Sciences, Moscow, Russia
[2] National Research Nuclear University MEPhI (Moscow Engineering Physics Institute), Moscow, Russia
[3] Kharadze Abastumani Astrophysical observatory, Georgia
[4] Fesenkov Astrophysical Institute, Almaty, Kazakhstan
[5] Ulugh Beg Astronomical Institute of the Uzbek Academy of Sciences, Tashkent, Usbekistan
[6] Crimean Astrophysical Observatory, Nauchniy, Crimea
[7] Institute of Astronomy of Kharkiv National University, Ukraine
[8] Keldysh Institute of Applied Mathematics, Russian Academy of Sciences, Russia

Email: apozanen@iki.rssi.ru

Received March 26, 2016; revised May 18, 2016

ABSTRACT
Phenomenological properties of gamma-ray bursts (GRB) are briefly reviewed and observations of GRB optical afterglow and other transients in Abastumani astrophysical observatory are discussed. In particular, the catalog of observations in 2012-2015, and some results including the final photometry of the optical afterglow of GRB 140801A are presented.

Key words: gamma-ray bursts, transients, afterglow, cosmology

1. Basic GRB Properties

Gamma-ray bursts (GRB) are among the most energetic events in the Universe and brightest on the gamma-sky and yet among the most enigmatic phenomena. GRBs are commonly defined as cosmological nonrepetitive violent flashes of gamma-rays with photon energy about several tens of keV registering from un-predictable directions in the sky. Duration of GRB active phase (prompt emission) in gamma-rays are ranging from~0.01 s to ~1000 s. They were discovered for the first time in 1969 (but published only in 1973, Klebesadel 1973). Gamma-ray spectrum of these events is mostly non-thermal, with the bulk energy emitted in 0.1 to 1 MeV range. Light curves of GRBs are highly variable, with significant variability down to a few milliseconds, consisting of non-symmetrical mostly overlapping pulses with Fast Rise and Exponential Decay (FRED pulse type).

1.1. Results of BATSE/CGRO

An important result obtained by Burst and Transient Experiment (BATSE) on-board the *Compton Gamma Ray Observatory* (operated in 1991-2000) which recorded over 2700 GRBs, is an isotropy of the error box localization across the sky (Fishman 1995). The absence of concentration of the events to the Galactic plane suggested a cosmological origin of the GRB sources, but the distance to the sources were still undefined.

Another result from *BATSE* was a confirmation of two classes of bursts initially pointed out by (Mazetz, 1981). The parameter of T_{90}, which is defined as the duration of the time interval comprising 90% of GRB flux, showed a bimodal distribution for all GRBs detected by *BATSE* with separation point between two modes at 2 seconds. All GRBs with T_{90} <2 s were referred as short duration and with T_{90} >2 as long duration gamma-ray bursts (Kouveliotou 1993). Now it became clear that most of long GRBs are associated with the core collapse of massive

stars and a progenitor of short GRBs are likely merging compact binaries, e.g. neutron star - neutron star or neutron star - black hole (e.g., Zhang 2012).

1.2. GRB Afterglow

In 1997 the era of BATSE changed into the era of the afterglow starting with the BeppoSAX space observatory, equipped with X-ray detectors (Boella 1997). It is supposed that the after-glow is a passive phase of GRB phenomenon when relativistic jet accelerated in the active phase expanding in circumburst media. In 1997 the first X-ray and optical transient accompanying the GRB was discovered e.g.,GRB 970228, and after the afterglow faded away, the deep follow-up optical observations showed that the after-glow coincided with a distant small galaxy (e.g., Bloom 2001). This galaxy was suggested to be a host galaxy of the GRB and confirmed the extragalactic origin of these events. Today the nearest GRB is GRB 980425 with a red shift z =0.0085 Fynbo (2000), the most distant is GRB 090429B with z=9.4. Cucchiara(2011).

GRBs are being discovered by several space-born experiments, but only three space observatories can localize GRB in near real-time: Swift (Gehrels 2004), INTEGRAL (Courvoisier 2003), and Fermi (Michelson 2007; Meegan 2007), of triggers from the orbit to a ground-based the Gamma-ray Coordinates Network[1] system and numerous ground based optical and radio telescopes around the world allowed to effectively discover optical and radio afterglow. Since the first afterglow detection in 1997 till the end of 2015 the space missions discovered about 1550 well localized GRBs[2] , and of them have X-ray afterglow. Optical afterglows are detected for∼60 % of GRBs with X-ray afterglow, and radio transients are discovered for only∼11 % of the bursts from the same sample. Gamma-ray bursts were also detected in high energy domain up to 100 GeV by LAT/Fermi detector (Ackermann 2014). The nature of GeV emission seems to be different from both prompt and afterglow emission.

1.3. Afterglow and Its Properties

The standard model of GRB afterglow formation states (Sari 1998, 1999), that the afterglow radiation is originated from relativistic bulk motion of electrons in the collimated ejecta (jet) from the dying massive star (long duration GRB) and from merging a compact binary system (short duration GRB). It is supposed that synchrotron radiation is a main origin of the afterglow in different energy bands.

The model of a long GRB states that during the collapse of a massive star the relativistic jet with high gamma-factor $\boldsymbol{\Gamma}$ is formed. It has a narrow opening angle $\theta\sim 7$ degrees and is oriented toward the observer. In initial stage of the afterglow $\boldsymbol{\Gamma}$ is high, the cone emission of relativistic electrons is much smaller than the jet opening angle. While expanding the ejecta loses energy and $\boldsymbol{\Gamma}$ decreases. At the moment when the emission cone of relativistic electrons is equal to the opening angle of the ejecta cone, i.e. when$\sim \mathbf{1/\Gamma}$ becomes more than θ, the decay of the afterglow flux becomes steeper, and the observer registers a break in the light curve, which is called a jet-break. The time t_b corresponding to the jet-break allows to estimate the jet opening angle. This phenomenon was predicted theoretically (see, e.g., Rhoads 1997) and is observed for many GRB afterglows. This effect is based only on the outflow geometry and thus is achromatic, i.e. seen in all energy bands at the same time.

The "zoo" of afterglow light curves displays a diversity of forms and flux, but there are common properties (see, e.g., Kann 2010). The light curve of typical optical afterglow of a GRB may be generally approximated by simple power law$\sim t^{\alpha}$, where $t = T - T_0$ is the time from GRB trigger, and $\alpha = -(0.5-2)$. In many cases the light curve has a jet break.

In general case the light curve of an GRB counterpart in optic or X-rays can be divided into phases of different emission origin. The first one is an active phase also called a prompt emission; the emission is generating when central engine of the GRB is still active. Sometimes the prompt optic emission could be registered simultaneously with gamma-radiation (see e.g. Zheng 2012). The prompt emission light curve is complex and highly variable. This phase is rarely observable in optics because of unpredictable location of a GRB source in the sky. The most effective way to register the prompt

[1] http://gcn.gsfc.nasa.gov/

[2] http://www.mpe.mpg.de/~jcg/grbgen.html

emission is simultaneous observations of the same field of view in optic and in gamma-rays by space-born telescopes (see e.g. Pozanenko 2013). Sometimes prompt emission in optics can be caught by a chance (see e.g. Racusin 2008) or if the prompt emission is sufficiently long it could be registered with fast slewing robotic telescopes (see e.g. Rykoff 2009).
The second phase is a passive pase, i.e. the afterglow itself with power law decay of a light curve. In case of X-ray after-glow the slope of the light curve decay may become shallower or even temporally come out to a plateau (see e.g. Xin 2012). Typical optical or X-ray afterglow lasts for a few days, but bright one may be observable for months (e.g., GRB 030329, Lipkin 2004), (e.g., GRB 130427A, Perley 2014). The X-ray afterglows are usually monitored by X-ray Telescope (XRT) on-board Swift cpace observatory, and the light curve may be very detailed. But in most cases the only information obtained about the optical afterglow is a few broad-band photometric observations. Some afterglows may be accompanied with flares and bumps, which are not described by a standard model.
In some cases the GRB afterglow may be accompanied with a supernova feature. Hjorth (2012). On the light curve it appears as a significant flux increase in the late phases of the afterglow and a subsequent decay which can not be fitted with a power law model (see Fig.3). Spectroscopic observations made at the time of the brightening maximum and decay demonstrate broad lines which are typical for Ib/c type supernova. But current observations allow to register the supernova feature only for nearby GRBs, with redshift less than ∼0.5. Today there are about 30 GRB associated supernovae with spectroscopic confirmation (e.g., Cano 2014) and a few dozens of photometrically detected supernova.
The first GRB supernova was discovered in 1998 during observations of GRB 980425, which is the closest discovered burst till now. The SN 1998bw associated with this GRB has an extremely low redshift (z =0.0085) and it allows to obtain detailed multicolor light curve, and multiple spectroscopic observations. Galama 1998; Iwamoto 1998; Kulkarni 1998. This fact allows to use photometric and spectroscopic data of the SN 1998bw as templates for empirical estimations of main parameters of other GRB connected supernovae (e.g. Cano 2013).
For ∼35% of GRBs the optical afterglow is not registered down to a deep limit. These bursts are called optically dark bursts (e.g. Greiner 2011). Dark bursts usually may have bright X-ray afterglow. A model suggests that the absence of an optical counterpart or its unusual faintness result from a high optical extinction in a line of sight to the burst source. However in ∼10% cases the darkness of the optical counterpart is related to a high redshift of GRB sources, because of at $z \geq 4$ flux in optical bandpass is highly absorbed by Ly_{α} at the line of sight to the observer. In some cases the optical darkness can be explained by absorption in circumburst medium of d GRB (e.g. Volnova 2014).
Often observations of the GRB host galaxy may be the only way for estimating the distance to the burst source. The host galaxy may be observed at the location of the GRB after the afterglow fading away. The search for GRB host galaxies is an important problem and require deep photometric and spectroscopic observations. Usually long GRBs follow young blue galaxies with a high star formation rate, but there is a less numerous population of GRBs formed in dusty and red galaxies (e.g. Rossi 2012)

2. Abastumani Astrophysical Observatory

Abastumani Astrophysical Observatory (former Georgian National Astrophysical Observatory) was founded in 1932 by Academician Eugene Kharadze on Mount Kanobili (1600 m above sea level), near the resort Abastumani (in Samtskhe-Javakheti, southeastern part of Georgia). Its location is $41^{o}45'15"$ N and 42^{o} 49'10" E, i.e. 200 km to the west from Tbilisi. A study of the astroclimate conducted in 1960 – 1980 in the observatory confirmed excellent parameters (Kharadze 1983). Due to difficult access to the original paper about astroclimate investigation we report some parameters from (Kharadze 1983) below.

2.1. Astroclimate

The mean, maximal mean and minimal mean temperature in the Observatory is 6.3,12.6 and 2.2 C., The mean ground wind-speed is 2.1 m/s and mean speed measured only in clear nights is only 0.6 m/s, the number of calm nights is 68 % of the total ones. The mean number of clear night hours is 972,

while minimal (maximal) hours measured in 1960 – 1977 is 772 (1153) hours per year. Maximal number of clear nights is in July – October season. (It was 220 observational nights (full or partial) in 2015.) Sky background in filters close to bandpass B and V is 21.82m and 20.81m per arcsec^2. Seeing was measured by a visual method with two-beams telescope in 1976 – 1977. The mean seeing is 0.63 arcsec.
Our observations in Abastumani observatory (see below) are random in seasons, part of night, elevation etc. The sample of FWHM measurements in the images obtained for GRB observations with AS-32 telescope (Figure 1) may be a good practical estimating for planning observations. Since we have not mea-sured FWHM less than 2 arcsec the distribution is biased by telescope optical system CCD detector and a dome. The median of the FWHM distribution is 2.7 arcsec. Indeed, the FWHM is an upper limit of the seeing parameter.

2.2. Telescopes

Abastumani observatory has a dozen of optical telescopes and a few solar instruments. The main instrument used for GRB afterglow observations is the Maksutov telescope AS-32 equipped with CCD-camera. It was constructed in 1955, the meniscus diameter is 0.7 meter, the main mirror is 975 mm in diameter, the focal length is 210 mm, so the whole system has a field of view about 5 degrees in diameter. Since 2005 Abastumani observatory collaborates with the ISON project (Molotov 2008) for space debris observations. In 2007 a new telescope ORI-22 was installed in the framework of the collaboration. Space debris observations were stopped in 2009. Since 2011 observation of potentially hazardous near-Earth asteroids started with AS-32 telescope, and in 2014 the asteroid survey started with ORI-22 telescope. The telescope is not operational since 2011 due to failure of telescope control system.

3. GRB Observations

The first observations of a GRB afterglow was carried out at the end of 2012. Since then Abastumani observatory provides observations for GRBs operating in an alert mode (Pozanenko 2013). The results of quick data reduction are published via GCN: The Gamma-ray Coordinates Network in the form of Circulars[3].

3.1. Catalog of GRB Observations

Table 1 contains the information about all GRB fields observed in Abastumani till the end of 2015. In the first column there is a name of the GRB, the second one is a time delay between the GRB trigger onboard a space observatory and the start of observations, the third column contains the brightest magnitude observed during the set, and the last one contains references for the publications.
Some of the bursts observed are of a particular interest. GRB 130427A (redshift z=0.34) is one of the brightest GRBs in optics (Perley 2014) was observed in AbAO in the first 3 days (April 27-29) and in May 1-4. In all observations the optical afterglow of GRB 130427A detected. The image of fading afterglow of GRB 130427A observed in AbAO is presented in Figure 2.
GRB 130702A was detected initially by GBM/Fermi experiment with a poor localization error box. However optical scanning of the error box of 71 square degrees with Palomar Transient Factory discovered the bright optical afterglow candidate (iPTF13bxl, see also (Singer 2013) which was observed in AbAO observatory within three days. A light curve of GRB 130702A afterglow reconstructed from observations in AbAO and IKI follow up network is presented in Figure 3. The light curve clearly exhibits the initial afterglow phase, supernova bump at~12 days and the host galaxy with brightness of about 22.5m. A redshift of the burst source is confirmed as z=0.145
Also in 2015 Abastumani observatory participated in a worldwide observational campaign of the V404 Cyg flash activity – the black hole binary the last activity of which was detected in 1989 (Kimura 2015). The log of V404 Cyg observations is presented in Table 2.

[3] http://gcn.gsfc.nasa.gov/gcn3_archive.html

3.2. GRB 140801A

GRB 1400801A was detected by GBM/Fermi with poor localization error-box of about 1.2 degrees (radius, statistical only) on August, 1, 2014 (UT) 18:59:53. MASTER robotic telescope in Tunka valley discovered a bright optical source 98 seconds after GBM/Fermi trigger (Lipunov 2016). Our observations started on the same day at (UT) 22:13:30 in Maidanak observatory with AZT-22 telescope and continued up to 23 rd days after GRB trigger with AbAO AS-32 telescope, Tien Shan Zeiss-1000 (East), and Crimean Astrophysical Observatory ZTSh (2.6m) telescopes. A log of our observations as well as the photometry of the afterglow of GRB 140801A are pre-sented in Table 3. For calibration we use following stars of USNO-B1.0 catalog (USNO-B1.0 id, R2): 1209-0038209, 18.02; 1209-0038197, 17.35; 1209-0038227, 15.88. The calibration stars were chosen with automatic pipeline for identification candidates into secondary photometric standards in the field of GRB (Skvortsov 2016). Using our data from Table 3 and data from the paper (Lipunov 2016) we constructed the light curve (Fig. 4). The light curve consists of afterglow phase, and a host galaxy with brightness of about 24.6 m. It is evident that the light curve is non-monotonous, and at least three bumpy episodes are evident, on∼0.1 days,∼1 days, and∼6 days after trigger. The last bump on ∼6 days cannot be a supernova feature since it is to early in comparison with known GRB supernova (see section above), especially taking into account the redshift of the GRB 1400801A source of z =1.32. The bumpy light curve is not a rare in GRB afterglows, see e.g. well sampled GRB 030329, GRB 100901A, GRB 151027A etc. A nature of bumpy (non-monotonous) behavior of afterglow light curves is not yet established.

4. Conclusions

Fast and world wide observations of GRB optical counterparts are crucial for a detailed light curve construction. Well sampled multicolor light curves provide experimental support for modeling of GRB physics including central engine activity, afterglow emission mechanism and its evolution, properties of the medium around the burst source. Abastumani observatory provides fast observational data of a good quality and successfully participates in the world wide GRB follow-up campaign.

Table 1.GRBs observed in Abastumani astrophysical observatory

[1]- of the first observation
[2]- of the set
[3]- in the first frame or stacked frames

GRB name	Date & time	Delay	Exposure, s[2]	FWHM, ¨	Mag.[3]	Reference
121123A	2012-11-23 15:18:28	5.3 h	180×24	2.5	19.0	GCN #14200
121128A	2012-11-28 15:27:50	10.7 h	300×42	2.9	20.2	GCN #14201
130427A	2014-04-27 17:00:56	9.2 h	180×71	2.7	16.4	-
130603BS	2013-06-03 22:19:06	44 m	300×22	3.2	18.8	GCN #14806, Pandey (2016)
130606A	2013-06-06 21:47:43	16.2 h	180×8	3.4	20.3	GCN #14813
130702A	2013-07-03 17:40:00	1.7 d	120×34	2.7	18.7	Volnova (2016)
130822A	2013-08-22 20:56:42	8.8 h	30×144	3.2	>21.9	GCN #15137
130829A	2013-08-29 18:55:48	13.2 h	120×9	2.7	>20.6	GCN #15136
130912A	2013-09-13 00:18:46	15.7 h	120×31	2.6	>22.3	GCN #15239
131011A	2013-10-11 22:32:33	5.3 h	120×26	2.8	21.3	GCN #15341

131024B	2013-10-25 00:26:12	3.9 h	120×46	2.9	>22.6	GCN #15392
131026A	2013-10-26 21:06:35	14.5 h	180×32	3.2	>22.6	GCN #15394
131108A	2013-11-11 00:44:00	2.2 d	120×36	2.9	21.2	GCN #15484
131231A	2014-01-03 17:08:16	3.5 d	120×33	2.7	20.3	GCN #15711
140102A	2014-01-05 00:48:24	2.1 d	120×38	2.6	>22.5	GCN #15730
140103A	2014-01-03 01:21:18	0.9 h	120×15	2.7	21.1	GCN #15735
140114A	2014-01-15 00:07:23	0.5 d	120×40	2.6	>20.6	GCN #15756
140129B	2014-01-29 12:23:49	2.6 h	120×4	3.2	>18.7	GCN #16055
140423A	2014-04-24 00:29:23	16.4 h	120×16	2.9	.20.3	GCN #16264
140521A	2014-05-21 18:12:00	1.4 h	120×28	2.7	>21.2	GCN #16317,16372
140606AS	2014-06-06 18:16:50	7.9 h	120×30	2.7	>21.7	GCN #16371, Pandey (2016)
140606B	2014-06-07 21:40:06	1.8 d	120×46	2.7	21.9	GCN #16398
140703A	2014-07-03 23:27:06	1.0 d	120×23	2.1	21.3	GCN #16536
140801A	2014-08-02 21:54:52	1.1 d	60×26	2.2	22.1	GCN #16667
141020A	2014-10-20 15:41:01	8.7 h	120×38		>21.4	GCN #16948
141109A	2014-11-10 01:05:04	20.0 h	120×37	2.4	21.7	GCN #17062
141109B	2014-11-09 15:26:30	9.2 h	120×71	2.3	>22.0	GCN #17067
141121A	2014-11-21 20:01:35	17.6 h	120×54	3.6	20.1	GCN #17089
Swift #625898 (SZ Psc)	2015-01-18 15:31:24	3.3 d	2×30	3.8	7.2	-
150213B	2015-02-13 23:22:23	0.9 h	120×39	2.5	19.0	GCN #17468,17478
150222A	2015-02-23 01:21:55	4.6 h	120×37	3.2	>22.9	-
150309A	2015-03-10 01:40:55	3.0 h	120×19	3.1	>21.2	GCN #17570
150314A	2015-03-14 22:06:54	18.2 h	120×24	2.7	>19.8	-
150323A	2015-03-23 22:47:06	20.4 h	180×15	2.4	>21.2	GCN #17647
150407A	2015-04-07 22:11:07	22.1 h	120×20	3.5	>21.1	-
150428A	2015-04-28 17:33:59	16.8 h	120×31	2.2	>21.9	-
150428B	2015-04-28 23:39:49	21.2 h	120×31	2.2	>21.3	-
150607A	2015-06-07 17:54:22	11.0 h	120×44	2.1	21.2	GCN #17915

150728A	2015-07-28 19:32:14	7.3 h	120×28	2.1	20.6	GCN #18094
150811A	2015-08-11 19:07:37	15.7 h	120×31	2.2	19.8	-
150817A	2015-08-17 17:00:31	15.5 h	120×24	2.2	21.6	GCN #18160
150910A	2015-09-10 18:53:55	11.0 h	120×52	2.0	20.2	GCN #18289,18327
150911A	2015-09-12 00:04:59	-	120×31	-	-	-
151022A	2015-10-22 15:59:07	-	120×42	-	-	-
SGR1819-1600	2015-11-22 14:54:30	-	60×18	-	-	-
151118A	2015-11-18 18:08:10	15.8 h	120×35	2.1	>22.1	GCN #18627
151215A	2015-12-15 20:08:51	18.6 h	120×35	2.4	>21.8	-
151228B	2015-12-29 14:38:28	16.6 h	120×34	2.1	>22.1	GCN #18891

Table 2.Observations of V404 Cyg outburst of 2015 in Abastumani

Date & time, UT	Exposure, s	FWHM, "	Mag.	Reference
2015-06-15 22:44:54	120×1 (25)	2.3	14.9	Kimura (2015)
2015-06-17 22:21:54	60×1 (74)	2.2	13.0	"–"
2015-07-18 21:44:14	20×1 (160)	2.2	16.6	"–"
2015-07-01 19:09:26	30×1 (100)	2.3	15.9	"–"
2015-12-29 16:34:45	60×8	-	-	-
2015-12-28 16:19:10	60×1 (39)	2.7	15.5	GCN #18767

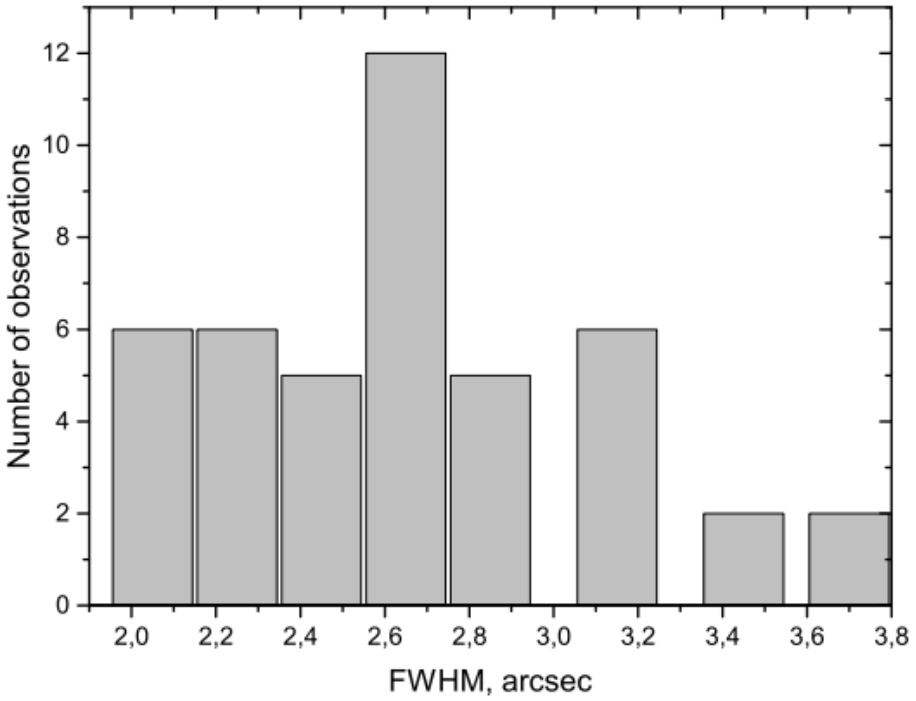

Fig. 1.FWHM distribution of point-like objects in a combined images of GRB afterglow observations presented in Table 1.

Table 3. Observations of GRB 140801A. Photometric magnitudes are not corrected for Galactic extinction in the direction of GRB.Abbreviations:

MAO is a Maidanak astrophysical observatory, TSHAO is Tien. Shan astrophysical observatory.

Date	Time UT	t-T0, days	Filte	Exposure, s	Mag & err	Observatory/telesco
2014-08-01	22:13:30	0.13550	R	180	20.14 0.06	MAO/AZT-22
2014-08-01	22:16:55	0.13787	R	180	20.24 0.04	MAO/AZT-22
2014-08-01	22:20:20	0.14024	R	180	20.13 0.04	MAO/AZT-22
2014-08-01	22:23:46	0.14263	R	180	20.17 0.04	MAO/AZT-22
2014-08-01	22:27:12	0.14501	R	180	20.22 0.04	MAO/AZT-22
2014-08-01	22:30:38	0.14739	R	180	20.24 0.05	MAO/AZT-22
2014-08-01	22:34:04	0.14978	R	180	20.23 0.04	MAO/AZT-22
2014-08-01	22:37:29	0.15215	R	180	20.17 0.04	MAO/AZT-22
2014-08-01	22:40:55	0.15454	R	180	20.09 0.03	MAO/AZT-22
2014-08-01	22:44:21	0.15692	R	180	20.19 0.04	MAO/AZT-22
2014-08-02	21:54:52	1.14962	Non	26×60	22.13 0.18	AbAO/AS-32
2014-08-02	22:02:04	1.14422	R	15×180	21.96 0.05	MAO/AZT-22
2014-08-04	20:44:49	3.11106	R	11×600	>22.9	TSHAO/Z-1000
2014-08-07	22:48:48	6.17073	R	10×180	23.40 0.20	MAO/AZT-22
2014-08-24	00:31:46	23.0511	R	39×120	>24.3	CrAO/ZTSh

Acknowledgements. R.Ya.I. is grateful to the grant RUSTAVELI FR/379/6-300/14 for a partial support.

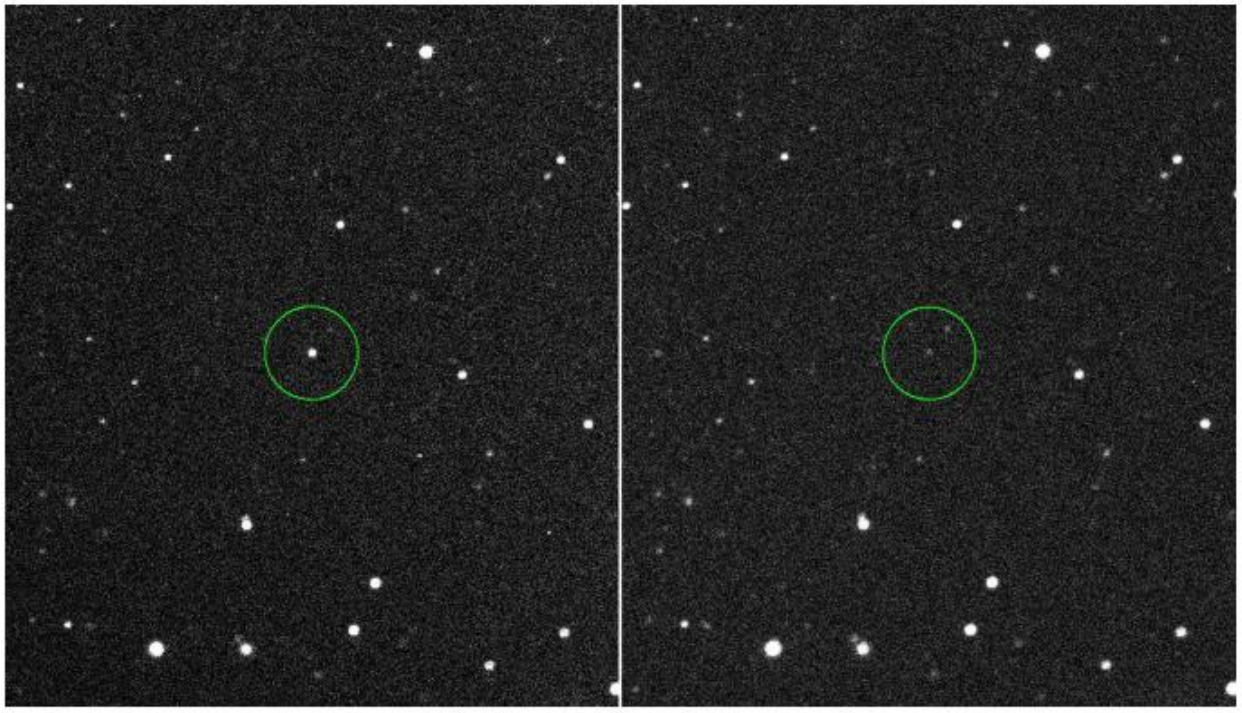

Fig. 2. Observation of the GRB 130427A afterglow with AS-32 telescope on the first day starting 2013-04-27T17:00:57 (left) and on the 3rd days (2013-04-29T16:59:56) after GRB trigger.

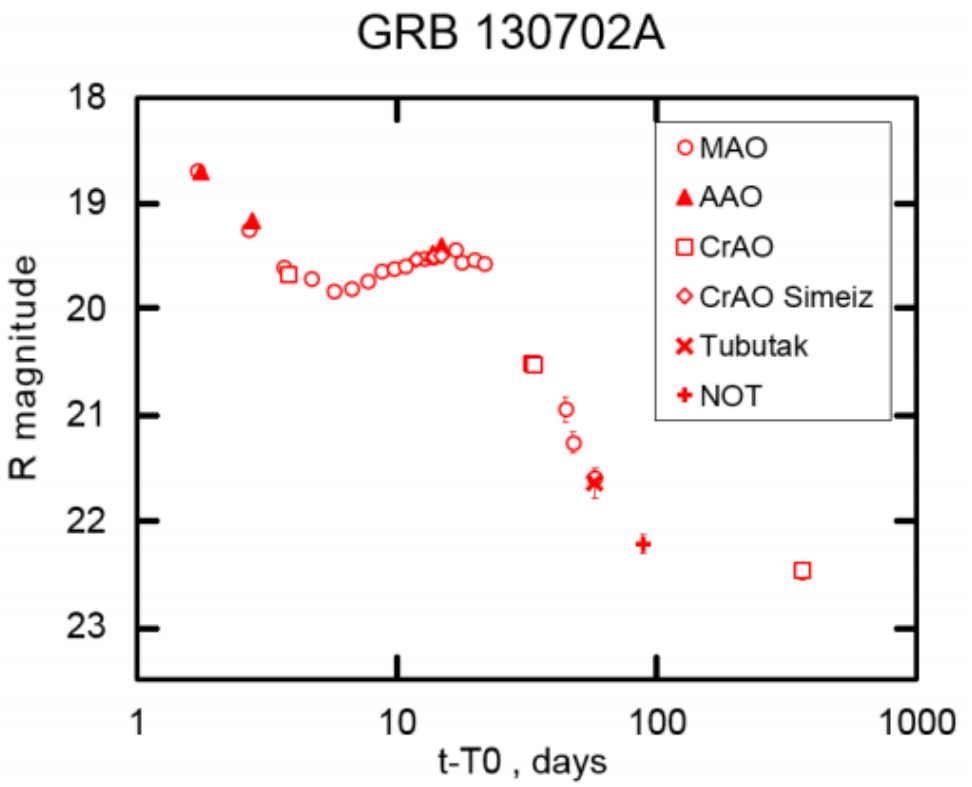

Fig. 3. The optical light curve of the GRB 130702A. After the opticalafterglow with power law decay the supernova feature is observed(SN 2013dx). The observations of Abastumani observatory are shown with filled triangles.

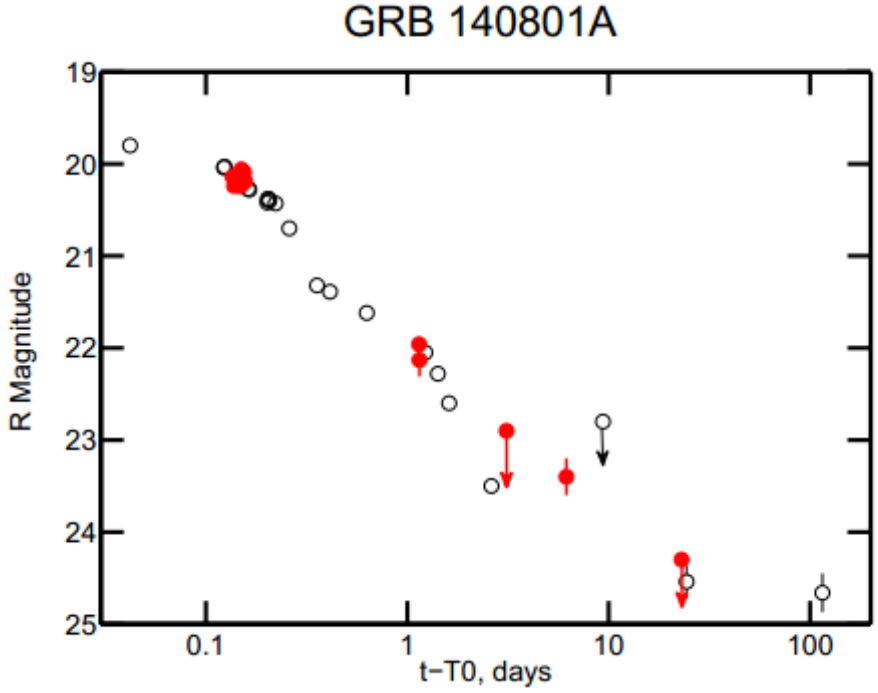

Fig. 4.The optical light curve of the GRB 140801A. Filled red circles depict the observations presented in the Table 3, open circles are the data taken from Lipunov (2016). The photometry of the first observation from Lipunov (2016) is not shown.

References

Ackermann, M.; Ajello, M.; Asano, K.; et al., 2014, Science,343, 6166, 42
Bloom, J. S.; Djorgovski, S. G.; Kulkarni, S. R. et al., 2001,ApJ, 554 (2): 678
Boella G., Butler R.C., Perola G.C.; et al., 1997, A&A Supplement series, 122, 299
Cano Z., 2013, MNRAS, 434, 1098.
Cano, Z.; de Ugarte Postigo, A.; Pozanenko, A., et al., 2014,A&A, 568, 19
Caste, et al., 1997, Nature 387,783. Panday (2016) - submitted in A&A
Cucchiara, A.; Levan, A. J.; Fox, D. B.; et al., 2011, ApJ, 736, article id. 7, 12
Fishman G.J. & Meegan C.A., 1995, Annu. Rev. Astron. Astrophys., 33, 415
Fu-Wen Zhang, Lang Shao, Jing-Zhi Yan, Da-Ming Wei. 2012, ApJ, 750, 88
Fynbo, J. U.; Holland, S.; Andersen, M. I.; et al., 2000, ApJ,542, L89
Galama, T. J., Vreeswijk, P. M., van Paradijs, J., et al. 1998, Nature, 395, 670
Gehrels, N.; Chincarini, G.; Giommi, P.; et al. 2004, ApJ, 611, 1005
Greiner J., Krühler T., Klose S., et al., 2011, A&A, 526, A30
Hjorth, J., & Bloom, J. S. 2012, The Gamma-Ray Burst - Supernova Connection (Cambridge University Press: Cambridge), 169
Iwamoto, K., Mazzali, P. A., Nomoto, K., et al. 1998, Nature, 395, 672
Kann, D. A.; Klose, S.; Zhang, B. et al., 2010, ApJ, 720, 1513
Kharadze E.K, Salukvadze G.N. - "Astroclimate of Abastumany Observatory"(in Russian), 1983, New technique in Astronomy, 136
Kimura, Mariko; Isogai, Keisuke; Kato, Taichi; et al., 2015, Nature, 529, 54
Klebesadel, Ray W.; Strong, Ian B.; Olson, Roy A. 1973, ApJ, 182, L85
Kouveliotou, Chryssa; Meegan, Charles A.; Fishman, GeraldJ.; et al. 1993, ApJ, 413, L101
Kulkarni, S. R., Frail, D. A., Wieringa, M. H., et al. 1998, Nature, 395, 663
Lipkin, Y. M.; Ofek, E. O.; Gal-Yam, A.; et al., 2003, ApJ, 606, 381
Lipunov V.M., Gorosabel J., Pruzhinskaya M. V. et al., 2016,MNRAS, 455, 712
Mazets, E. P.; Golenetskii, S. V.; Ilinskii, V. N.; et al. 1981, Astrophysics and Space Science, 80, 3
Meegan C. et al, 2007, AIP Conf. Proc., 921, 13
Michelson P. F. (GLAST-LAT Collaboration), 2007, AIP Conf.Proc., 921, 8
Molotov, I., Agapov, V., Titenko, V., et al., 2008, Advancesin Space Research, 41, 1022
Perley D. A., Cenko S. B., Corsi A., et al., 2014, ApJ, 781, 37
Pozanenko, A.; Chernenko, A.; Beskin, G.; et al., 2003, Astronomical Data Analysis Software and Systems XII ASP Conference Series, Vol. 295, H. E. Payne,
Pozanenko, A.; Elenin, L.; Litvinenko, E.; et al., 2013, Gamma-ray Bursts: 15
Racusin, J. L.; Karpov, S. V.; Sokolowski, M.; et al., 2008, Nature, 455, 7210, 183
Rhoads J., 1997, ApJ Letters 487, 1
Rossi A. et al., 2012, A&A, 545, A77
Rykoff, E. S.; Aharonian, F.; Akerlof, C. W.; et al., ApJ, 702, 1, 489
Sari R., Piran T., and Halpern J.P., 1998, ApJ Letters, 519, L17
Sari R., Piran T., and Narayan R., 1998, ApJ Letters, 497, L17
Singer, Leo P.; Cenko, S. Bradley; et al., ApJ Letters, 776, 2, L34
Skvortsov N. A., Avvakumova E. A., Bryukhov D. O., et al., 2016, Astrophysical Bulletin, 71, 122
van Paradijs, J.; Groot, P. J.; Galama, T.; et al. 1997, Nature, 386, 686
Volnova, A. A.; Pozanenko, A. S.; Gorosabel, J. et al., 2014,MNRAS, 442, 2586
Winkler, C.; Courvoisier, T. J.-L.; Di Cocco, G.; et al., 2003, Astronomy and Astrophysics, 411, L1
Xin, L. P.; Pozanenko, A.; Kann, D. A., et al., 2012, MNRAS, 422, 2044
Zheng, W.; Shen, R. F.; Sakamoto, T. et al., 2012, ApJ, 751, id. 90

Astronomy & Astrophysics (Caucasus) 1, (2016) 68-80

Some New Directions of Development of the Radiative Transfer Theory

A. G. Nikoghossian
Byurakan Astrophysical Observatory, Aragatsotn Region, 378433, Armenia

Email: nikoghoss@yahoo.com

Received March 30, 2016 ; revised May 18, 2016

Abstract

It is shown that the problems of radiation transfer in homogeneous plane-parallel atmospheres admit a variational formulation, the equation of transfer then being the Euler-Lagrange equation and the known quadratic and bilinear relations being the conservation law due to form-invariance of the suitable Lagrangian. The group of transfer problems is revealed which are reducible to the source-free problem. We present a group-theoretical description of radiation transfer in inhomogeneous and multi-component atmospheres with plane-parallel geometry. The concept of composition groups is introduced for the media with different optical and physical properties. The group representations are derived for two possible cases of illumination of a composite finite atmosphere from outside. An algorithm for determining of the global optical characteristics (reflectance and transmittance) of inhomogeneous and multi-component atmospheres is given. The group theory approach is also applied to determine the field of radiation inside the inhomogeneous atmosphere. The concept of a group of optical depth translations is introduced. The developed theory is illustrated with the problem of radiation diffusion with partial frequency distribution for the case where the inhomogeneity of the medium is due to the depth-variation of the scattering coefficient. It is shown that once reflectance and transmittance of a medium are determined, the internal field of radiation in the source-free atmosphere is found without solving any new equations.

Key words: **line formation; groups; groups representations; methods analytical; methods numerical**

1.Introduction

The research on the theory of radiative transfer carried out in recent two decades in Byurakan observatory develops Ambartsumian's ideas concerning the laws of addition of layers (Ambartsumian V.A 1943,1944) and the principle of invariance (Ambartsumian V.A 1944,1960,1980). Being of importance for analytical theory itself, new results allow elaborating of efficient computational schemes for various astrophysical applications involving radiation transfer in inhomogeneous absorbing and scattering atmospheres. In this context there is a need to define their place and importance in the modern transfer theory.

The report considers results obtained in two directions, the first of which concerns the variational formulation of radiation transfer problems in a plane-parallel homogeneous atmosphere.

2.Lagrangian formalism

Before turning to immediate description of the variational or Lagrangian approach to radiative transfer problems we will briefly dwell on premises of this research. The fact is that although Ambartsumian's principle of invariance has been known for a long time, but its physical meaning remained obscure. In particular, it was unclear what are the limits of applicability and efficiency of the principle. The second point concerns Rybicki's work (Rybicky G.B,1977) , where some quadratic integrals of the transfer equation were derived referred by him to as Q - and R - integrals. He supposed that these integrals are

possibly related with the principle of invariance. In some problems they lead to non-linear relations linking to each other some characteristics of the radiation field in the atmosphere. Further generalization of Rybicki's results for monochromatic and isotropic scattering in a plane-parallel medium was given in (Ivanov V.V,1978, Nikoghossian A.G,1977),where new sorts of relations were obtained referred to as bilinear and two-point bilinear relations, which couple the radiation fields in different atmospheres.

In frameworks of variational formalism we developed the equations of transfer are proved to be none the other than the Euler - Lagrange equations and the non-linear *Q* - relations are the conservation laws due to form-invariance of the suitable Lagrangian. In fact, a single functional dependence comprises all the information on features of the problem and allows a systematic connection between symmetries and conservation laws. Being the first integrals of the Euler - Lagrange equation, these laws may facilitate the solution of the problem under consideration and assist in its interpretation.

To demonstrate the approach we write the transfer equations in terms of the function Y having the following probabilistic meaning: it characterizes the probability of the photon exit from atmosphere in the direction μ, if originally it was moving at depth τ with the directional cosine η We have

$$\pm\eta\frac{dY(\tau,\pm\eta,\mu)}{d\tau}=-Y(\tau,\pm\eta,\mu)+\frac{\lambda}{2}\int_{-1}^{1}Y(\tau,\eta',\mu)\mathrm{d}\eta', \tag{1}$$

where λ is the scattering coefficient.

The Lagrangian density L corresponding to Eq (1) was obtained in (Anderson D., J, 1973)

$$L(\Phi,\Phi',\tau,\eta,\mu)=\Phi^2+(\eta\Phi')^2-2\Phi U, \tag{2}$$

where we introduced notations

$$\Phi(\tau,\eta,\mu)=Y(\tau,+\eta,\mu)+Y(\tau,-\eta,\mu),\qquad U(\tau,\mu)=\frac{\lambda}{2}\int_{0}^{1}\Phi(\tau,\eta',\mu)\mathrm{d}\eta'. \tag{3}$$

In accordance with the results of (Anderson D., J, 1973), the Euler-Lagrange equation has a form

$$\frac{\partial L}{\partial\Phi}-\frac{\mathrm{d}}{\mathrm{d}\tau}\frac{\partial L}{\partial\Phi'}+\lambda\int_{0}^{1}\frac{\partial L}{\partial U}\mathrm{d}\eta'=0. \tag{4}$$

One will make sure that insertion of the Lagrangian (2) into (4) yields the transfer equation (1). It is important that both the transfer equation (1) and the Lagrangian density (2) do not depend explicitly on τ, or stated differently, they are form-invariant under infinitesimal transformation of the optical depth. This implies that the transformation (or translation) of the optical depth, is the symmetry transformation for the system (1). The derivation of conservation laws from direct study of the variational integral is based on Noether's theorem (see, for instance, (Gelfand I.M., Fomin S.V,1965)), which was generalized in (Tavel M,1971) to encompass the integro-differential equations. For the problem under consideration it suggests a conservation law as follows

$$\int_{0}^{1}\left[L-\frac{\partial L}{\partial\Phi}\Phi'\right]\mathrm{d}\eta=\mathrm{const}, \tag{5}$$

which, in view of (2), takes a form

$$\int_0^1 Y(\tau,\varsigma,\mu)Y(\tau,-\varsigma,\mu)\,\mathrm{d}\varsigma = \frac{\lambda}{4}\left(\int_{-1}^{+1} Y(\tau,\varsigma,\mu)\,\mathrm{d}\varsigma\right)^2 + \text{const}. \qquad (6)$$

This relation is, in essence, a prototype of the Q – integral obtained by Rybicki (Rybicky G.B,1977). The above considerations imply that by its content the integral (6) is an analog of the momentum conservation law in mechanics and is due to the axes translaton . It holds everywhere where λ does not vary with depth.

The variational formalism allows not only to elucidate the physical meaning of invariance principle but enables one to derive along with many known results a great number of new relations of great importance for the theory and applications. It also allows to find out some statistical characteristics of the diffusion process in the atmosphere (Nikoghossian A.G,1977 Nikoghossian A.G,2000)

Some of the known non-linear relations possess a fairly obvious physical or/and probabilistic meaning and can be written immediately on the base of simple arguments.

We showed that there exists a group of different frequently occurring radiation transfer problems of astrophysical interest which admit quadratic and bilinear integrals. All of them can be reduced to the source-free problem. This group of problems referred to as RSF – problems includes the Milne's problem, the problem of diffuse reflection (and transmission in the case of the atmosphere of finite optical thickness) as well as problems with exponential and polynomial laws for the distribution of internal energy sources. The group problems are characterized at least by three features. First of all, the invariance principle implies bilinear relations connecting the solutions of the listed problems. It was shown in (Nikoghossian A.G,2013)that the group of the RSF - problems admits a class of integrals involving quadratic and bilinear moments of the intensity of arbitrarily high orders. Secondly, if the problem can be formulated for finite atmosphere then the principle allows connecting its solution with that of the proper problem for a semi-infinite atmosphere. Finally, knowledge of the Ambartsumian φ-function reduces their solutions to the Volterra-type equations for the source function with the kernel-function

$$L(\tau) = \frac{\lambda}{2}\int_0^1 \varphi(\varsigma)e^{-\frac{\tau}{\varsigma}}\frac{d\varsigma}{\varsigma}. \qquad (7)$$

While the variational approach is widely used in various branches of theoretical physics, it was not the case in the field of the radiative transfer theory, with the only exception being the paper of Anderson (Anderson D., J, 1973) who establishes the conservation law suitable for the case of non-isotropic scattering. We used the results of the rigorous mathematical theory in applying the Lagrangian formalism to the one-dimensional transfer problem (Krikorian R.A, 1996)

3. Group-theoretical description of radiative transfer in inhomogeneous atmospheres

The next topic of the report concerns the application of the group theory to solve the radiative transfer problems under general assumptions on the frequency-angle distribution of the radiation field, the elementary event of scattering and properties of the medium, As we shall see, the theory we put forward can be regarded as a further extension of the layers adding the method proposed first by Ambartsumian (Ambartsumian V.A , 1944, Ambartsumian V.A, 1960) for one-dimensional homogeneous media and generalized by Nikoghossian (Nikoghossian A.G, 2004-a Nikoghossian A.G,2004-b) over the case of inhomogeneous media, We remind that the method establishes summation laws for global optical properties of absorbing and scattering media (reflectance and transmittance), which express these properties of the combined medium through similar properties of

its components. Of special interest is the particular limiting case of this method when optical thickness of one of the added components tends to zero. This allows one to find the global optical characteristics of a medium simultaneously for a family of the media of different thicknesses. This branch of the theory was developed by Bellman and his co-authors (see e.g., (Bellman R., & Wing G.M,1973, Casti J., & Kalaba R., 1973)) and is known as 'invariant imbedding',

3.1 Composition groups

We start with considering the amalgamation procedure of the plane-parallel absorbing and scattering inhomogeneous media. It is assumed that the added components do not contain primary energy sources and are allowed to differ one from the other not only by optical thicknesses, but also by the nature of inhomogeneity. By inhomogeneity we mean that each of the physical parameters specifying the elementary event of scattering or physical state of the medium may vary with depth. Of them we note the profile of the absorption coefficient, the quantum scattering (or destruction) coefficient, Voigt's parameter, indicatrix, the frequency redistribution function, the Stokes parameters in the case of polarized radiation, the correlation length for turbulent media, and so on. However, in illustrating the approach, we restrict ourselves by treating the 1D transfer problem for the case of partial redistribution over frequencies by assuming that the only variable parameter is the scattering coefficient.
Now we introduce the concept of composition or transformation of scattering and absorbing inhomogeneous media, which refers to the addition of a new medium to the initial one. The transformations induced in this way form a group if under the group product (binary operation) one takes the resultant of two successive transformations. It is remarkable that this definition does not specify the nature of inhomogeneity of added media. It is easily seen that all the required conditions for forming a group are satisfied. In particular, the role of the unit element is played by the identity transformation, which leaves the initial medium unchanged, and the inverse element is the transformation which reverses the effect of the already performed transformation. The associativity of the group product is obvious. We refer to this group of transformations as the GN(2,) group, which, evidently, is not commutative. As a result of the described compositions, one can construct different atmospheres composed of inhomogeneous components.
Of special interest is one of subgroups of the introduced group which describes the case when the added media are homogeneous. The components of such a composite atmosphere may differ from each other not only by optical thicknesses but also by any characteristics of the radiation diffusion in them. Such groups, referred nominally to as GNH(2,), are two-, three- and multi-parameter dependent on the number of parameters changing in passing from one component to another. The groups of these types are infinite and non-commutative. They can serve as archetypes for a number of real radiating media of astrophysical importance. Finally, of independent interest is the narrower subgroup of the introduced two groups which involves compositions of homogeneous media with identical physical properties but, in general, of different optical thicknesses. These compositions obviously yield homogeneous medium. This one-parameter group, we call it GH(2,), is infinite and commutative, i.e., Abelian (Wigner E, 1959).It becomes continuous when the only parameter, optical thickness, varies continuously.

3.2 The group representations

In order to find the representations of introduced groups, consider a composite atmosphere consisted of two layers, which generally differ in both the optical thickness and functional behavior of parameters specifying the elementary event of scattering (Fig.1). This means that both components are inhomogeneous and possess the property of polarity (Nikoghossian A.G, 2004-a).The scattering in the media is supposed occurring with redistribution over directions and frequencies so that the optical characteristics of media may be presented in the operator-matrix form with the matrix elements possessing probabilistic meaning (as above, we use the probability language). They describe the angle and/or frequency dependent probabilities of a single event of reflection and transmission. Having in mind the polarity property of inhomogeneous media, we introduce the notations, $\mathbf{R}_i$, $\mathbf{Q}_i$ and $\bar{\mathbf{R}}_i$, $\bar{\mathbf{Q}}_i$

$(i=1,2)$ for the reflection and transmission coefficients of the components of a composite medium illuminated correspondingly from the right and left. In accordance with the principle of reversibility of optical phenomena, $\bar{\mathbf{Q}}_i = \mathbf{Q}_i^*$, where the transposed matrix is supplied by asterisk. Everywhere below we follow the designation $\mathbf{Q}_i^*$. An important role in this research belongs to the inverse of the transmittance matrix $\mathbf{P} = \mathbf{Q}^{-1}$ and the other three combined matrices, $\mathbf{S} = \mathbf{RP}$, $\bar{\mathbf{S}} = \mathbf{P}\bar{\mathbf{R}}$, $\mathbf{M} = \mathbf{Q}^* - \mathbf{S}\bar{\mathbf{R}}$. These four matrices provide a complete description of the optical properties of an inhomogeneous absorbing and scattering medium independent of how are its boundaries illuminated from outside.

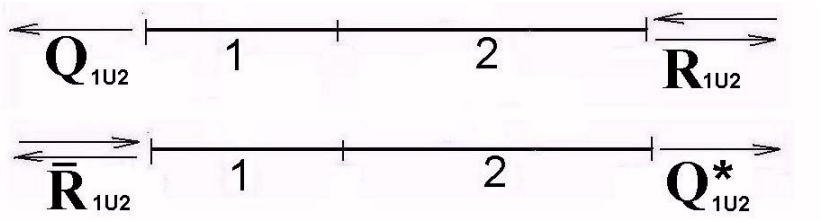

Fig.1. Reflection and transmission by inhomogeneous atmosphere

Let us treat now the transfer of radiation through composite medium when a photon falls on its right boundary (top drawing in Fig.1). Taking account of possibility of multiple reflections between the components of the medium, we can write .

$$\mathbf{Q}_{1\cup 2} = \mathbf{Q}_1\mathbf{T}\mathbf{Q}_2, \tag{8}$$

where

$$\mathbf{T} = \mathbf{I} + \sum_{k=1}^{\infty}\left(\bar{\mathbf{R}}_2\mathbf{R}_1\right)^k. \tag{9}$$

From (9) we have $\mathbf{T} = \mathbf{I} + \bar{\mathbf{R}}_2\mathbf{R}_1\mathbf{T}$, or

$$\mathbf{T}^{-1} = \mathbf{I} - \bar{\mathbf{R}}_2\mathbf{R}_1. \tag{10}$$

Now the relation (8) can be rewritten in the form $\mathbf{P}_{1\cup 2} = \mathbf{P}_2\mathbf{T}^{-1}\mathbf{P}_1$, or in view of (10)

$$\mathbf{P}_{1\cup 2} = \mathbf{P}_2\mathbf{P}_1 - \bar{\mathbf{S}}_2\mathbf{S}_1. \tag{11}$$

This is the first of the requisite relations which expresses one of the optical parameters of the composite atmosphere in terms of parameters of its components.

Let us turn now to the reflectance of the composite medium. Simple physical arguments allow one to write

$$\mathbf{R}_{1\cup 2} = \mathbf{R}_2 + \mathbf{Q}_2^*\mathbf{R}_1\mathbf{T}\mathbf{Q}_2. \tag{12}$$

By virtue of (10) and (11) we obtain

$$\mathbf{S}_{1\cup 2} = \mathbf{R}_{1\cup 2}\mathbf{P}_{1\cup 2} = \mathbf{S}_2\mathbf{T}^{-1}\mathbf{P}_1 + \mathbf{Q}_2^*\mathbf{S}_1, \tag{13}$$

which leads to the second of the required relations

$$\mathbf{S}_{1\cup 2} = \mathbf{S}_2\mathbf{P}_1 + \mathbf{M}_2\mathbf{S}_1. \tag{14}$$

Taking together, relations (11) and (13) can be presented in the more convenient compact form

$$\begin{pmatrix} \mathbf{P}_{1\cup 2} \\ \mathbf{S}_{1\cup 2} \end{pmatrix} = \begin{pmatrix} \mathbf{P}_2 & -\bar{\mathbf{S}}_2 \\ \mathbf{S}_2 & \mathbf{M}_2 \end{pmatrix} \begin{pmatrix} \mathbf{P}_1 \\ \mathbf{S}_1 \end{pmatrix}. \qquad (15)$$

where we used the concepts of supervector and supermatrix (Wigner E, 1959, Chen J.-Q., Ping J & Wang F,2002)

The supermatrix entering in (15) is denoted by $\tilde{\mathbf{A}}$ (hereafter the supermatrices are supplied by a tilde). The set of matrices $\tilde{\mathbf{A}}$ is the first of representations of the group of compositions GN(2,□) which also is a group (we denote it by g) and provides a one-to-one mapping of GN(2,□) to supervector space, i.e., the group product of two transformations $g_1 \otimes g_2$, corresponds to $\tilde{\mathbf{A}}_{1\cup 2} = \tilde{\mathbf{A}}_1 \tilde{\mathbf{A}}_2$, or $\Im(g_1 \otimes g_2) = \Im(g_1)\Im(g_2)$ (isomorphism). On the other hand, supermatrix $\tilde{\mathbf{A}}$ can be regarded as an operator of the mapping one supervector space to another one. It is natural to refer nominally to this supermatrix as 'composer'. As we shall see, it plays an important role in the developed theory

$$\tilde{\mathbf{A}} = \begin{pmatrix} \mathbf{P} & -\bar{\mathbf{S}} \\ \mathbf{S} & \mathbf{M} \end{pmatrix}. \qquad (16)$$

It is noteworthy that both the group of compositions and the obtained rules of transformations of the reflectance and transmittance do not depend on the nature of inhomogeneity of the added layers, i.e., the variable parameters in different layer cannot be necessarily the same.

It is easy to see that the transformation realizing by $\tilde{\mathbf{A}}$ provides determination of the optical properties of the composed medium partially, namely, only for the case when it is illuminated from the right side. In order to find the missing relations we must derive the transformation laws for the quantities $\mathbf{S}$ and $\mathbf{M}$. The easiest way to derive these laws is performing of two successive compositions which corresponds to the product of two elements of the group $\Im(g)$.

The net result is

$$\bar{\mathbf{S}}_{1\cup 2} = \mathbf{P}_2 \bar{\mathbf{S}}_1 + \bar{\mathbf{S}}_2 \mathbf{M}_1, \quad \mathbf{M}_{1\cup 2} = \mathbf{M}_2 \mathbf{M}_1 - \mathbf{S}_2 \bar{\mathbf{S}}_1. \qquad (17)$$

Note that these relations could be derived directly. In the matrix-operator form they read as:

$$\begin{pmatrix} \mathbf{M}_{1\cup 2} \\ \bar{\mathbf{S}}_{1\cup 2} \end{pmatrix} = \begin{pmatrix} \mathbf{M}_2 & -\mathbf{S}_2 \\ \bar{\mathbf{S}}_2 & \mathbf{P}_2 \end{pmatrix} \begin{pmatrix} \mathbf{M}_1 \\ \bar{\mathbf{S}}_1 \end{pmatrix}. \qquad (18)$$

Thus, we are led to an alternative group of representations given by the supermatrix

$$\tilde{\mathbf{B}} = \begin{pmatrix} \mathbf{M} & -\mathbf{S} \\ \bar{\mathbf{S}} & \mathbf{P} \end{pmatrix}, \qquad (19)$$

which we denote by $\tilde{\Im}(g)$. It is evident that this group also is isomorphic to the group of compositions GN(2,□) and together with $\Im(g)$ gives a complete description of optical properties of the composite atmosphere illuminated from the right. In both cases the identity transformation is given by the supermatrix

$$\tilde{\mathbf{E}} = \begin{pmatrix} \mathbf{I} & \mathbf{0} \\ \mathbf{0} & \mathbf{I} \end{pmatrix}, \qquad (20)$$

where $\mathbf{I}$ is the unit matrix.
Now we shall note some properties of introduced supermatrices. It is easy to show that the supermatrices $\tilde{\mathbf{A}}$, $\tilde{\mathbf{B}}$ are not degenerate and the two-sided inverse matrices exist.(Nikoghossian A.G,2014)

$$\tilde{\mathbf{A}}^{-1} = \begin{pmatrix} \mathbf{M}^* & \bar{\mathbf{S}}^* \\ -\mathbf{S}^* & \mathbf{P}^* \end{pmatrix}, \qquad \tilde{\mathbf{B}}^{-1} = \begin{pmatrix} \mathbf{P}^* & \mathbf{S}^* \\ -\bar{\mathbf{S}}^* & \mathbf{M}^* \end{pmatrix}. \qquad (21)$$

We notice that both the inverse matrices differ from the corresponding supertransposed supermatrices. The supermatrices $\tilde{\mathbf{A}}$, $\tilde{\mathbf{B}}$ as well as $\tilde{\mathbf{A}}^{-1}$, $\tilde{\mathbf{B}}^{-1}$ are non-degenerate with the superdeterminant equaled to 1 (Berezin F.A,1965, Nikoghossian A.G,2014)

By introducing the four-dimensional supervector $\tilde{\mathbf{Y}}$ with components $\left(\mathbf{P},\mathbf{S},\mathbf{M},\bar{\mathbf{S}}\right)$, the group representations $\Im(g)$, $\bar{\Im}(g)$ can be joined and presented as a reducible representation

$$\tilde{\mathbf{Y}}_{1\cup 2} = \tilde{\Psi}_2 \tilde{\mathbf{Y}}_1, \qquad (22)$$

where

$$\tilde{\Psi} = \begin{pmatrix} \mathbf{P}_2 & \mathbf{-\bar{S}}_2 & \mathbf{0} & \mathbf{0} \\ \mathbf{S}_2 & \mathbf{M}_2 & \mathbf{0} & \mathbf{0} \\ \mathbf{0} & \mathbf{0} & \mathbf{M}_2 & \mathbf{-S}_2 \\ \mathbf{0} & \mathbf{0} & \bar{\mathbf{S}}_2 & \mathbf{P}_2 \end{pmatrix}. \qquad (23)$$

We conclude that, given the optical properties of the component layers, the common matrix multiplications allow one to determine these properties for the compound atmosphere. If the atmospheres are homogeneous one can restrict oneself by transformation (15).

In the case when the composite atmosphere is illuminated from the side of the left boundary (bottom drawing in Fig.1) in place of (22) and (23) we have (Nikoghossian A.G,2014)

$$\tilde{\mathbf{Y}}^+_{1\cup 2} = \tilde{\Psi}^+_1 \tilde{\mathbf{Y}}^+_2, \qquad (24)$$

where

$$\tilde{\Psi}^+ = \begin{pmatrix} \mathbf{P}^* & \mathbf{-S}^* & \mathbf{0} & \mathbf{0} \\ \bar{\mathbf{S}}^* & \mathbf{M}^* & \mathbf{0} & \mathbf{0} \\ \mathbf{0} & \mathbf{0} & \mathbf{M}^* & \mathbf{-\bar{S}}^* \\ \mathbf{0} & \mathbf{0} & \mathbf{S}^* & \mathbf{P}^* \end{pmatrix}. \qquad (25)$$

3.3 The 1D source-free problem for partial redistribution over frequencies

Consider a subgroup of the composition group GNH(2,□) subjected to the only condition that the optical thickness of the medium obtained as a result of compositions must not exceed some presetting value of τ_0. When the optical thickness varies continuously, this infinite group is obviously

continuous. Then this group together with its representation $T(g)$ are one-dimensional Lie groups (Berezin F.A,1965, Chen J.-Q., Ping J & Wang F,2002, Heine V.1960). With the help of compositions of this groups one can construct a multi-component atmosphere with components which generally can differ one from the other by their physical characteristics.

As an example, let us treat the matrix problem of radiation diffusion in a one-dimensional inhomogeneous atmosphere illuminated from the boundary $\tau = \tau_0$ when the scattering obeys the angle averaged law of partial redistribution over frequencies. Suppose that the atmosphere consists of components of equal and sufficiently small thickness characterized by some constant values of the scattering coefficient λ, so that in the limit of the components thicknesses tending to zero it might be regarded as a continuous function of the optical depth.

The infinitesimal operator of this group of compositions at τ_0 can be represented in the form

$$\tilde{\Xi}(\tau_0) = \lim_{\Delta\tau_0 \to 0} \frac{\tilde{\mathbf{A}}(\tau_0 + \Delta\tau_0) - \tilde{\mathbf{A}}(\tau_0)}{\Delta\tau_0} = \begin{pmatrix} \mathbf{m}(\tau_0) & -\mathbf{n}(\tau_0) \\ \mathbf{n}(\tau_0) & -\mathbf{m}(\tau_0) \end{pmatrix}, \tag{26}$$

where

$$\mathbf{m}(\tau_0) = \boldsymbol{\alpha} - \mathbf{n}(\tau_0), \quad \mathbf{n}(\tau_0) = \frac{\lambda(\tau_0)}{2}\boldsymbol{\Gamma}. \tag{27}$$

Here $\boldsymbol{\alpha}$ and $\boldsymbol{\Gamma}$ are the discrete analogs correspondingly of the profile of the absorption coefficient and the law of the frequency redistribution (Mihalas D,1970)

For the sake of simplicity, they are supposed to be independent of the depth. Evidently, $\boldsymbol{\Gamma}$ is a symmetric matrix and $\boldsymbol{\alpha}$ is a diagonal matrix with the elements $\alpha_i = \alpha(x_i)$.

Transformation (15) implies (Nikoghossian A.G,2011)

$$\frac{d\mathbf{P}}{d\tau_0} = \mathbf{m}(\tau_0)\mathbf{P}(\tau_0) - \mathbf{n}(\tau_0)\mathbf{S}(\tau_0), \tag{28}$$

$$\frac{d\mathbf{S}}{d\tau_0} = \mathbf{n}(\tau_0)\mathbf{P}(\tau_0) - \mathbf{m}(\tau_0)\mathbf{S}(\tau_0) \tag{29}$$

with the initial conditions $\mathbf{P}(0) = \mathbf{I}$, $\mathbf{S}(0) = \mathbf{0}$, where $\mathbf{0}$ is the null matrix.

Inversion of the matrix $\mathbf{P}(\tau_0)$ found from the set of equations (28), (29) allows one to determine the requisite values of the medium reflectance and transmittance. Analogously, by using the infinitesimal operator of the supermatrix $\tilde{\mathbf{B}}$ and (23) we are led to a new set of the matrix differential equations

$$\frac{d\mathbf{M}}{d\tau_0} = -\mathbf{m}(\tau_0)\mathbf{M}(\tau_0) - \mathbf{n}(\tau_0)\bar{\mathbf{S}}(\tau_0), \tag{30}$$

$$\frac{d\bar{\mathbf{S}}}{d\tau_0} = \mathbf{n}(\tau_0)\mathbf{M}(\tau_0) + \mathbf{m}(\tau_0)\bar{\mathbf{S}}(\tau_0), \tag{31}$$

with the initial conditions $\mathbf{M}(0) = \mathbf{I}$, $\bar{\mathbf{S}}(0) = \mathbf{0}$. Taking together, equations (28), (29), (30), (31) can be presented in the form as follows:

$$\frac{d\tilde{\mathbf{Y}}}{d\tau_0} = \tilde{\mathrm{M}}(\tau_0)\tilde{\mathbf{Y}}(\tau_0), \tag{32}$$

where

$$\tilde{\mathrm{M}}\left(\tau_0\right)=\begin{pmatrix}\mathbf{m}\left(\tau_0\right) & -\mathbf{n}\left(\tau_0\right) & \mathbf{0} & \mathbf{0}\\ \mathbf{n}\left(\tau_0\right) & -\mathbf{m}\left(\tau_0\right) & \mathbf{0} & \mathbf{0}\\ \mathbf{0} & \mathbf{0} & -\mathbf{m}\left(\tau_0\right) & -\mathbf{n}\left(\tau_0\right)\\ \mathbf{0} & \mathbf{0} & \mathbf{n}\left(\tau_0\right) & \mathbf{m}\left(\tau_0\right)\end{pmatrix}. \qquad (33)$$

In the case of homogeneous atmosphere one can restrict oneself to solving the set of equations (28), (29). Its solution can be presented in the form of the matrix exponential (Nikoghossian A.G,2011)

$$\tilde{\mathbf{Y}}\left(\tau_0\right)=\exp\left(\tilde{\Xi}\tau_0\right)\tilde{\mathbf{Y}}\left(0\right),$$

(34)

where

$$\tilde{\mathbf{Y}}\left(\tau_0\right)=\begin{pmatrix}\mathbf{P}\left(\tau_0\right)\\ \mathbf{S}\left(\tau_0\right)\end{pmatrix},\quad \tilde{\mathbf{Y}}\left(0\right)=\begin{pmatrix}\mathbf{I}\\ \mathbf{0}\end{pmatrix}. \qquad (35)$$

Being expanded into series, the matrix exponential reads

$$\mathbf{P}\left(\tau_0\right)=\mathbf{I}+\left(\boldsymbol{\alpha}-\frac{\lambda}{2}\boldsymbol{\Gamma}\right)\frac{\tau_0}{1!}+\left[\boldsymbol{\alpha}^2-\frac{\lambda}{2}\left(\boldsymbol{\Gamma}\boldsymbol{\alpha}-\boldsymbol{\alpha}\boldsymbol{\Gamma}\right)\right]\frac{\tau_0^2}{2!}+\ldots, \qquad (36)$$

$$\mathbf{S}\left(\tau_0\right)=\mathbf{R}\left(\tau_0\right)\mathbf{P}\left(\tau_0\right)=\frac{\lambda}{2}\boldsymbol{\Gamma}\frac{\tau_0}{1!}+\frac{\lambda}{2}\left(\boldsymbol{\Gamma}\boldsymbol{\alpha}-\boldsymbol{\alpha}\boldsymbol{\Gamma}\right)\frac{\tau_0^2}{2!}+\ldots \qquad (37)$$

The obtained expansions give a highly accurate solution of the problem of radiative transfer through the inhomogeneous atmosphere.

Similar reasoning for the atmosphere illuminated from the boundary $\tau=0$, leads to the new pair of the matrix differential equations which being joined can be written as follows

$$\frac{d}{d\tau_0}\begin{pmatrix}\mathbf{P}^*\\ \bar{\mathbf{S}}^*\\ \mathbf{M}^*\\ \mathbf{S}^*\end{pmatrix}=\begin{pmatrix}\mathbf{P}^* & -\mathbf{S}^* & \mathbf{0} & \mathbf{0}\\ \bar{\mathbf{S}}^* & \mathbf{M}^* & \mathbf{0} & \mathbf{0}\\ \mathbf{0} & \mathbf{0} & \mathbf{M}^* & -\bar{\mathbf{S}}^*\\ \mathbf{0} & \mathbf{0} & \mathbf{S}^* & \mathbf{P}^*\end{pmatrix}\begin{pmatrix}\mathbf{m}\left(\tau_0\right)\\ \mathbf{n}\left(\tau_0\right)\\ -\mathbf{m}\left(\tau_0\right)\\ \mathbf{n}\left(\tau_0\right)\end{pmatrix}. \qquad (38)$$

In writing (38), we took into account the symmetry of the matrices $\boldsymbol{\alpha}$ and $\boldsymbol{\Gamma}$. Note that from the sets of equations (28), (29), (30), (31) one can derive separate matrix differential equations of the second order for unknown matrix-functions, as it is the case in the scalar case (Nikoghossian A.G,2011)

Equations obtained with the group approach exhibit the intimate connection between the group approach and the method of invariant imbedding (Bellman R., & Wing G.M,1973, Casti J., & Kalaba R., 1973).

As a matter of fact, the invariant imbedding technique is equivalent to action of infinitesimal operators of the proper group representations introduced in the paper.

For homogeneous atmosphere the obtained equations admit invariants or conservation laws, the continual analogs of which were obtained in the mentioned papers (Nikoghossian A.G,1977 , Anderson D., J, 1973 ,Nikoghossian A.G,2011, Nikoghossian A.G,1999)

3.4 Multi-component atmospheres

The efficiency of the developed theory becomes especially discernible when solving radiative transfer problems for the atmospheres with a complex multi-layer structure. In applying any of the introduced composers, one needs to predetermine the global optical properties of each of the layers added to the boundary $\tau = \tau_0$, namely, the matrices $\mathbf{P}$, $\mathbf{S} = \mathbf{RP}$, $\bar{\mathbf{S}} = \mathbf{P}\bar{\mathbf{R}}$ and $\mathbf{M} = \mathbf{Q}^* - \mathbf{S}\bar{\mathbf{R}} = \mathbf{Q}^* - \mathbf{R}\bar{\mathbf{S}}$, i.e., the triad of matrices $\mathbf{R}$, $\bar{\mathbf{R}}$, $\mathbf{Q}$. The problem is simpler when the components are homogeneous. Particularly, in the scalar problems these quantities are determined analytically. In the general case of inhomogeneous components, we can turn to solutions of the systems of equations (28), (29), (30), (31) or (38) with subsequent inversion of the matrix $\mathbf{P}$. The advantages of this route will be discussed later on. However, it is expedient to mention here an alternative way and write down the basic differential equations obtained in (Nikoghossian A.G,2013, Nikoghossian A.G, 2012), which make it possible to find the required optical properties by solving easily realizable initial-value problems:

$$\frac{d\mathbf{R}}{d\tau_0} = -\left[\mathbf{Rm} + \mathbf{mR}\right] + \mathbf{n} + \mathbf{RnR}, \qquad (39)$$

$$\frac{d\mathbf{Q}}{d\tau_0} = -\mathbf{Q}\left(\mathbf{m} - \boldsymbol{\alpha}\mathbf{R}\right), \qquad (40)$$

$$\frac{d\bar{\mathbf{R}}}{d\tau_0} = \mathbf{QnQ}^*, \qquad (41)$$

where, for brevity, dependence on the optical thickness is not indicated explicitly. Equations (39) - (41) satisfy initial conditions $\mathbf{R}(0) = \bar{\mathbf{R}}(0) = \mathbf{0}$, $\mathbf{Q}(0) = \mathbf{I}$. As for $\mathbf{P}$, in place of the time-consuming inversion of this matrix at each stage, it is convenient to use the equation (28), which in view of that $\mathbf{S} = \mathbf{RP}$ acquires a form similar to (40)

$$\frac{d\mathbf{P}}{d\tau_0} = -\left(\mathbf{m} - \boldsymbol{\alpha}\mathbf{R}\right)\mathbf{P} \qquad (42)$$

with the initial condition $\mathbf{P}(0) = \mathbf{I}$.

Thus, algorithm of solution of the transfer problem in the most general case of the multi-component atmosphere is as follows. One starts with finding the reflectance and transmittance of the layers to be added by using one of the routes described above. Further, transformations of the compositions are continued until the optical thickness of the composite atmosphere specified by the problem formulation is attained. Inversion of the matrix $\mathbf{P}(\tau_0)$ allows one to find $\mathbf{Q}(\tau_0)$ what, in its turn, determines other properties of the composite atmosphere. In the special case when the supplemented layers are homogeneous and possess similar properties, we deal with the cyclic group and the composition process reduces to the action of powers of corresponding operators ($\tilde{\mathbf{A}}^n$, for instance). This naturally reduces the volume of computations to a great extent.

3.5 Radiation field inside the medium

The goal we pursue in this section is to extend the group theory approach over the field of radiation inside inhomogeneous media. Consider a plane-parallel inhomogeneous atmosphere of the optical thickness τ_0, the boundary $\tau = \tau_0$ of which is illuminated from outside (Fig.2). Light scattering is generally assumed to occurr with the angle and frequency redistribution. The internal field of radiation we assign by the matrices $\mathbf{U}(\tau, \tau_0)$ and $\mathbf{V}(\tau, \tau_0)$, which specify the probabilities that the quantum with the angle-frequency characteristics (η, x) falling on the boundary $\tau = \tau_0$, will be found, as a

result of diffusion in the medium, at the depth τ moving correspondingly to the boundaries $\tau = 0$, and $\tau = \tau_0$, generally with some other characteristics (η', x').

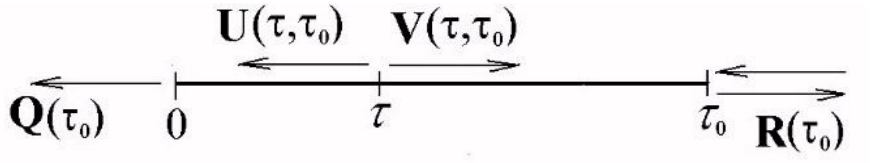

Fig 2. Description of the radiation field inside the inhomogeneous atmosphere

Let us treat now the procedure of transition from one optical depth to another one by supplementing a new layer. The infinite set of such transitions obviously composes a group if the group product is defined as the result of two subsequent transitions. One can easily check that all the group postulates are satisfied. In accordance with the physics of the problem, the resulting value of the optical depth should not exceed the optical thickness of the medium $\tau \le \tau_0$. This group is a subgroup of the group GN(2, □) and is equivalent to the similar subgroup considered in the preceding sections for composition of different media.

Taking into account the probability meaning of matrices $\mathbf{U}(\tau, \tau_0)$ and $\mathbf{V}(\tau, \tau_0)$, one can write

$$\mathbf{Q}(\tau_0) = \mathbf{Q}(\tau)\mathbf{U}(\tau, \tau_0), \qquad \mathbf{V}(\tau, \tau_0) = \mathbf{R}(\tau)\mathbf{U}(\tau, \tau_0), \tag{43}$$

hence

$$\mathbf{U}(\tau, \tau_0) = \mathbf{P}(\tau)\mathbf{Q}(\tau_0), \qquad \mathbf{V}(\tau, \tau_0) = \mathbf{S}(\tau)\mathbf{Q}(\tau_0). \tag{44}$$

The fact of separation of arguments in $\mathbf{U}(\tau, \tau_0)$ and $\mathbf{V}(\tau, \tau_0)$ is one of advantages of the applied approach. Equations (44) imply that the subgroup of representation $T(g)$ relevant to the media compositions group may be now regarded as representation of the depth-translation group.

Indeed, on the base of (15), one may write

$$\begin{pmatrix} \mathbf{P}(\tau + \delta\tau) \\ \mathbf{S}(\tau + \delta\tau) \end{pmatrix} = \begin{pmatrix} \mathbf{P}_\tau(\delta\tau) & \bar{\mathbf{S}}_\tau(\delta\tau) \\ \mathbf{S}_\tau(\delta\tau) & \mathbf{M}_\tau(\delta\tau) \end{pmatrix} \begin{pmatrix} \mathbf{P}(\tau) \\ \mathbf{S}(\tau) \end{pmatrix}, \tag{45}$$

and

$$\begin{pmatrix} \mathbf{U}(\tau + \delta\tau, \tau_0) \\ \mathbf{V}(\tau + \delta\tau, \tau_0) \end{pmatrix} = \begin{pmatrix} \mathbf{P}_\tau(\delta\tau) & \bar{\mathbf{S}}_\tau(\delta\tau) \\ \mathbf{S}_\tau(\delta\tau) & \mathbf{M}_\tau(\delta\tau) \end{pmatrix} \begin{pmatrix} \mathbf{U}(\tau, \tau_0) \\ \mathbf{V}(\tau, \tau_0) \end{pmatrix}, \tag{46}$$

where $\delta\tau$ is an increment to the optical depth τ. The subscript τ indicates that the internal physical properties of supplemented layer are relevant to (or vary in) the interval $(\tau, \tau + \delta\tau)$.

Thus, the supermatrix $\tilde{\mathbf{A}}$ plays an important role not only in adding the media of different optical thicknesses but also in translating optical depths inside inhomogeneous atmosphere. Stating differently, at the same time it serves as a 'composer' of inhomogeneous atmospheres and as a 'translator' in transitions between optical depths within the atmosphere. It is noteworthy that in the latter case only the global optical properties of the incremented layer provide the transformations. The internal physical characteristics do not take an immediate part in these transformations, so that the nature of inhomogeneity in different media or layers are allowed to be different.

To illustrate the obtained results, let us return to the matrix case of the transfer problem treated in Section 4, where we confined ourselves to the global optical characteristics of the medium. Our

immediate objective now is to find the field of radiation inside the medium, where, again, the only parameter varying with depth is the scattering coefficient λ. In light of that said in Section 4, we conclude that the depth-translation group together with its representation are one-dimensional Lie groups.

Given the supermatrix (26), the transformation (46) leads to the customary differential equations of radiation transfer for the operator-functions $\mathbf{U}$ and $\mathbf{V}$.

$$\frac{d\mathbf{U}}{d\tau} = \mathbf{m}(\tau)\mathbf{U}(\tau,\tau_0) - \mathbf{n}(\tau)\mathbf{V}(\tau,\tau_0), \tag{47}$$

$$\frac{d\mathbf{V}}{d\tau} = \mathbf{n}(\tau)\mathbf{U}(\tau,\tau_0) - \mathbf{m}(\tau)\mathbf{V}(\tau,\tau_0). \tag{48}$$

In place of the usual boundary conditions, one can now adopt those at $\tau = \tau_0$, $\mathbf{U}(0,\tau_0) = \mathbf{Q}(\tau_0)$, $\mathbf{V}(0,\tau_0) = \mathbf{0}$, then reduce the problem to that with initial conditions. Derivation of the transfer equations (47), (48) on the base of physical reasoning is straightforward, what is usually done in the classical astrophysical literature. As it was shown, the operator-functions $\mathbf{P}(\tau)$ and $\mathbf{S}(\tau)$ satisfy the same set of equations (28),(29) with the initial conditions $\mathbf{P}(0) = \mathbf{I}$, $\mathbf{S}(0) = \mathbf{0}$. By comparing the initial conditions of these two sets of equations we are led to relations (46) written above on the base of probabilistic reasoning (Nikoghossian A.G,1999)

Bearing in mind the computations described in Section 3.3 for the composite inhomogeneous atmosphere, as well as the equivalence of the medium-composition and the depth-translation subgroups of GNH(2, □), we arrive at an important conclusion that the internal field of radiation now can be found without solving any new equations. Indeed, it is sufficient to this end to multiply the obtained value of $\mathbf{Q}(\tau_0)$ by $\mathbf{P}$ and $\mathbf{S}$ found above in intermediate calculations in constructing the atmosphere under study. Similar derivations are easy to perform if the opposite boundary of the medium is illuminated (Nikoghossian A.G,2014)

4. Conclusions

We applied the group theory to solve the problems of radiative transfer in inhomogeneous absorbing and scattering atmospheres. The media composition groups and their representations introduced in the paper generalize the layers adding approach, which now covers inhomogeneous, particularly multi-component, atmospheres with allowance for the angle and frequency distribution of the radiation field. The group representations being expressed in terms of some combined discrete quantities allow to find the most general summation laws for reflectance and transmittance of the plane-parallel media. We adhere to an idea developed in our recent papers, according to which one preliminarily determines the global optical characteristics of the atmosphere and only after that finds the field of radiation inside the medium. This contrasted with the approach adopted in the classical transfer theory. Usage of composers facilitates solution of a rather broad class of the line-formation problems by reducing the most part of computations to the simple algebraic operations with matrices. The efficacy of the approach becomes more discernable in the case of multi-component atmospheres often encountered in astrophysical applications.

Employment of infinitesimal operators of the introduced groups makes it possible to establish the close connection of the introduced groups with the classical transfer equations and those ensuing from invariant imbedding. In fact, the first of them are connected with the depth translation groups, while the second - with composition groups for media of different optical thicknesses.

An important result in considering the internal field of radiation is the separation of variables of the optical depth and thickness in the expression of quantities describing the optical properties. This implies that the introduced group of the optical depths translations is a subgroup of the group of the

media compositions. In its turn, this means that after finding the reflectance and transmittance of the atmosphere, there is no need to solve any new equations to determine the internal field of radiation in the source-free atmosphere. Moreover, such approach facilitates solution of some other standard transfer problems of astrophysical importance as, for instance, the problem of multiple scattering in inhomogeneous atmosphere with internal energy sources or in a semi-infinite atmosphere (Nikoghossian A.G,2014)The theory we put forward is of sufficiently great generality since it does not depend on the nature of inhomogeneity of the media, as well as on the angle and frequency distribution of the radiation field.

REFERENCES

Ambartsumian V.A., Izvestija Academii Nauk Arm-SSR, 1944, No.1-2, 31
Ambartsumian V.A., Scientific Papers, Vol.1, Izd AN ArmSSR Yerevan (in Russian), 1960
Ambartsumian V.A., Dokl.Acad. Nauk SSSR, 1943, 38, 257
Ambartsumian V.A., Ann. Rev. Astron. Astrophys., 1980, 18, 1
Rybicky G.B., Astrophys.J., 1977, 213, 165
Ivanov V.V., Astron. J., 1978, 23, 612
Nikoghossian A.G., Astrophys.J., 1977, 483, 849
Anderson D., J. Inst. Math. Applic., 1973, 12, 551
Gelfand I.M., Fomin S.V., Calculus of Variations, Prentice-Hall,Englewood Cliffs, Nj, 1965
Tavel M., Transport Theory Statist. Phys., 1971, 1, 271
Nikoghossian A.G., Astrophysics, 2000, 43, 337
Nikoghossian A.G., Light Scattering Reviews, 2013, 8, 377.
Krikorian R.A., Nikoghossian A.G., 1996, 56, 465
Nikoghossian A.G., Astron. Astrophys., 2004-a, 422, 1059
Nikoghossian A.G., Astrophysics, 2004-b, 47, 248
Bellman R., & Wing G.M., An Introduction to Invariant Imbedding, Wiley, NY, 1973
Casti J., & Kalaba R., 1973, Imbedding Methods in Applied Mathematics, Addison-Wesley Publ. Co., Mass.
Wigner E., Group Theory, Acad. Press, New York, Mass., Toronto, London, 1959
Bellman R., Introduction to Matrix Analysis, Mcgraw-Hill Book Co. Inc., NY 1960
Berezin F.A., The Method of Second Quantization, Acad. Press, Boston, 1965
Chen J.-Q., Ping J & Wang F., Representation Theory for Physicists, World Sci. Publ. Co., Mass., 2002
Nikoghossian A.G., Astrophysics, 2014, 57, 272
Heine V., Group Theory in Quantum Mechanics, Pergamon press, 1960
Mihalas D., Stellar Atmospheres, Freeman and Co, San Francisco, 1970
Nikoghossian A.G., Astrophysics, 2011, 54, 553
Nikoghossian A.G., J. Quantit. Spectrosc. Radiat. Transfer, 1999, 61, 345
Nikoghossian A.G., Astrophysics, 2012, 55, 261
Nikoghossian A.G., Astrophysics, 2014, 57, 375

Astronomy & Astrophysics (Caucasus) 1, (2016) 81-91

Modern Problems of Asteroid Photometry

V. G. Shevchenko[1,2], Yu. N. Krugly[1], I. N. Belskaya[1], I. E. Molotov[3]

[1]Institute of Astronomy of V. N. Karazin Kharkiv National University, Kharkiv, Ukraine
[2]Department of Astronomy and Space Informatics of V. N. Karazin Kharkiv National University, Kharkiv, Ukraine
[3]Keldysh Institute of Applied Mathematics, RAS, Moscow, Russia

Email:shevchenko@astron.kharkov.ua

Received March 31, 2016; revised May 18, 2016

Abstract

Photometry is one of the main techniques for studying the physical properties of asteroids. The large bulk of valuable information on rotation and shapes, sizes and albedos, structural and optical properties of asteroids is provided by photometry, especially during the last decade. We review the progress and some problems in asteroid photometry focusing on the most important areas, which include shape modeling and determination of rotation parameters, detection and study of the binary systems and that of the optical properties of asteroid surfaces.

Key words: Photometry, asteroid, albedo, computer techniques

1. Introduction

Photometry is one of the most productive techniques of investigations of physical properties of small Solar system bodies. This technique is successfully used for asteroids for a long time. A big massive of various data for many thousand asteroids has been obtained with this method and the correctness of these data is confirmed by space missions for some of asteroids. The primary information obtained from a single photometric observation of an asteroid is the absolute magnitude that allows to make an estimation of the object's size. This is widely applied first of all to the newly discovered asteroids, particularly for potentially hazardous ones that may come into collision with the Earth. Long-term photometric observations allow obtaining of a lightcurve of an asteroid to determine its rotational period, direction of rotational axis in the space, shape of the body, and the sufrace optical properties .At present the rotational periods for about fifteen thousand asteroids were determined (Warner et al., 2009; Waszczak et al., 2015) and about two hundred of binary asteroid systems were found for the last ten years (Warner et al., 2009; Pravec et al., 2016). More than eight hundred positions of rotational axes and reconstruction of shapes were obtained from an analysis of the lightcurves (Warner et al., 2009; Durech et al., 2010, 2015). Also new effects in the light scattering by asteroid surfaces were discovered (Shevchenko et al., 2012). In this paper recent data on rotational properties, shapes and sizes, parameters of binary systems and optical properties of the asteroid surfaces are briefly reviewed.

2. Rotation and Shape

Photometric observations of asteroids are generally carried out for obtaining their lightcurves. The lightcurve is a periodic function that describes a dependence of asteroid brightness variations on time. These variations can be caused by several factors, such as a) the irregular shape of an asteroid; b) photometric heterogeneity of its surface; c) the multiplicity of asteroid system. Analysis of many lightcurves, laboratory and modeling experiments allowed to conclude that in the most cases the brightness variations are basically formed by changing cross section of an irregular shape body during the asteroid rotation. From observations in different spectral bands of standard *UBVRI*- system it was found that variations in color indices *U-B*, *B-V*, *V-R* and *V-I* on the asteroid surfaces do not exceed 0.05 mag, while the amplitudes of the lightcurves reach up to 2 mag. This suggests that the asteroid lightcurves are formed primarily by its shapes, and the contribution of the albedo variation can be ignored.

The asteroid lightcurve is characterized by *amplitude* and *period* of the brightness variations. The amplitude is defined as a difference between minimal and maximal brightness of the asteroid. It characterizes an elongation of the body. Amplitudes of asteroid lightcurves are enclosed within wide range, from values not exceeding the observational errors to about 2 mag (e.g. asteroids (1620) Geographos and (1865) Cerberus). The asteroids with amplitudes greater than 1 mag are rare, most of the amplitude values do not exceed 0.3-0.4 mag and on the average equal to ~0.2 mag.

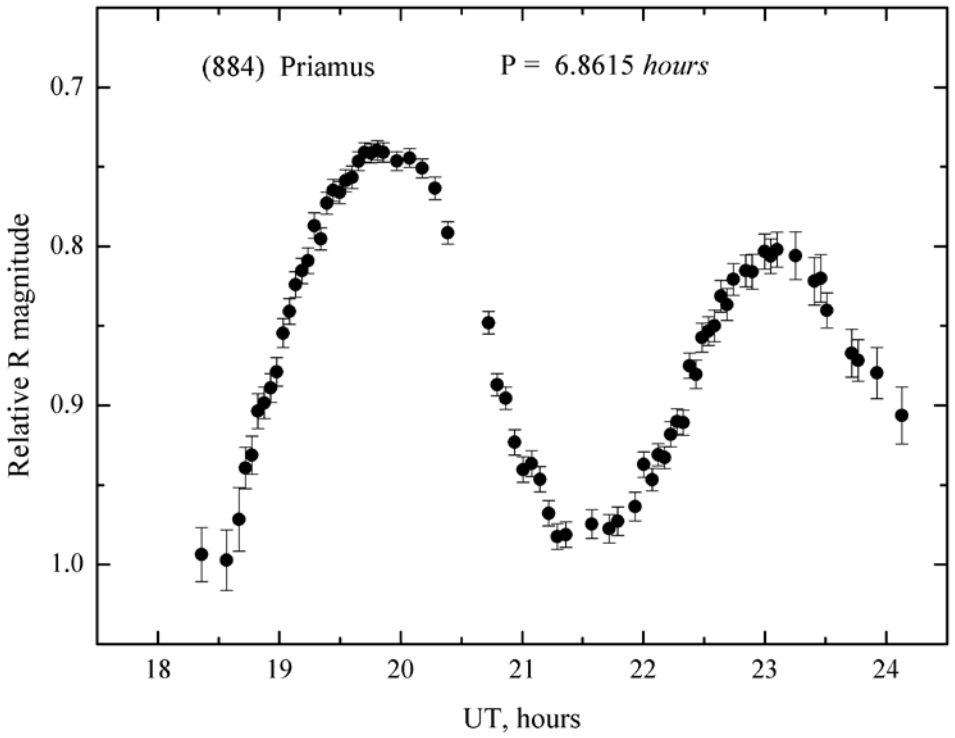

Fig. 1. Lightcurve of Jupiter Trojan asteroid (884) Priamus (Shevchenko et al., 2012)

There are also complex, unusual lightcurves, for example, having more than two pairs of extrema on the rotational period, with a different degree of symmetry, humps, depressions, flat areas etc. These phenomena can be explained by the extremely complex shape of surface, the multiplicity of systems, tumbling rotation and so on. Rotation periods of asteroids are quite diverse and for asteroids with diameter $D > 1$ km lie in the range from 2.2 hours to several days. One of the fastest rotating asteroids is the near-Earth asteroid (1566) Icarus with period 2.273 hrs, and the most slowly rotating asteroid is (1235) Shorria with P= 1265 hrs. There are also asteroids that have rotation periods of a few minutes (for example, (54509) YORP, $P = 0.20288$ hrs). These fast- rotating bodies belong to the near-Earth asteroids (NEA) having a size of less than 200 meters (Kwiatkowski et al. 2010). At present there are no observational data available for main-belt asteroids of such small sizes because of their faintness.

In Fig. 2 the diagram of "rotation period – diameter" is shown for about fifteen thousand asteroids (data are taken from Warner et al., (2009) and updated according to the latest known data). It indicates an existence of the rotational limit or "barrier" at a speed which is higher than about 12 rev/day corresponding to the period $P = 2.2$ hr for bodies with $D \geq 200$ m. This barrier can be reached for almost spherical body such as "rubble piles" for the expected density of 2 - 3 g/cm^3 when the centrifugal force at the equator of the body becomes equal to the force of the gravity. The existence of this barrier suggests that even small asteroids with sizes in the range from several tenth kilometers up to 200 m can have a rubble-pile structure of gravitationally connected stones. On the

other hand, some bodies with D < 200 m can keep very rapid rotation, that is, they can be monolithic bodies with the large forces of internal cohesion. Thus, the region on the diagram "rotation period - diameter" of poorly consolidated bodies with a structure of "rubble piles" lies in the range of P > 2.2 hrs and D > 200 m. These interesting results were initially obtained for about 1700 objects with known rotation periods (Harris and Pravec, 2006). Now these results are confirmed for larger statistics.

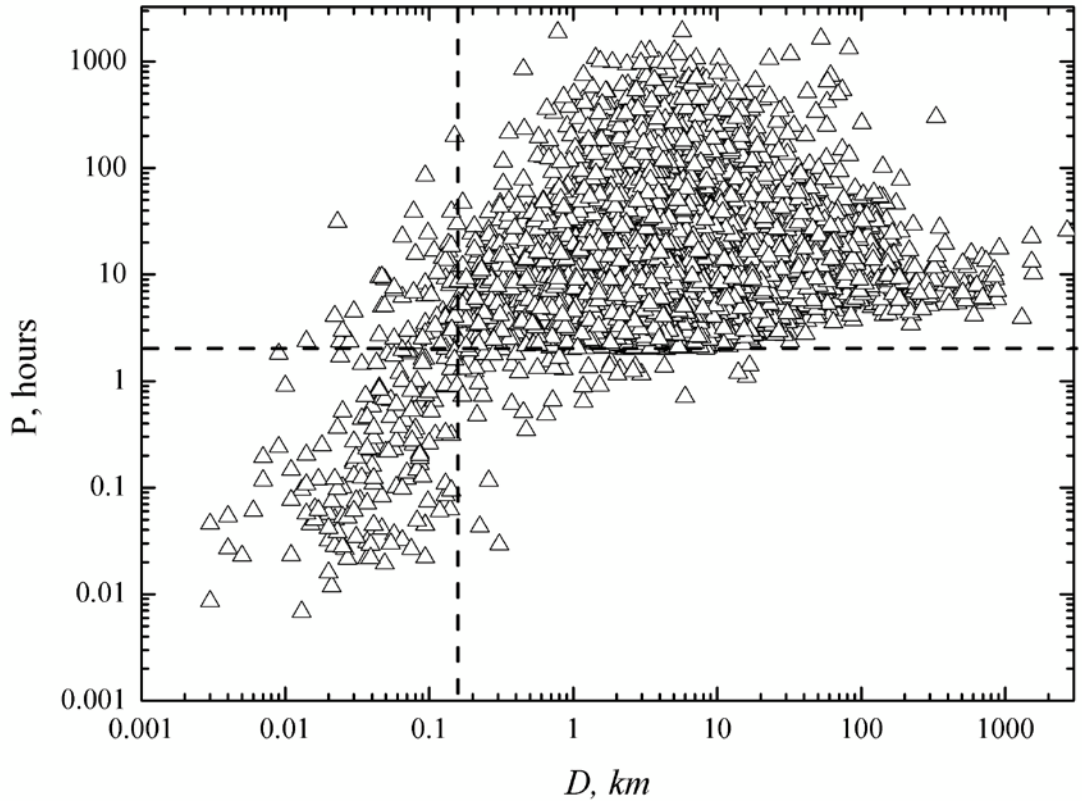

Fig. 2. Diagram of "rotation period – diameter" (data are taken from Warner et al., 2009)

One of the possible effects which contributes to spinning up and destroying small asteroids is the so-called "YORP-effect" (Yarkovsky-O'Keeffe-Radzievskii-Paddack, Kaasalainen et al., 2007). It is connected with the uniform heating of a surface of the rotating asteroid of an asymmetrical shape by the Sun. Since the asteroid morning side is the colder than the evening one, therefore a thermal radiation from the evening side of the asteroid is much stronger than from the morning one. This leads to an appearance of the reactive forces generated by the emission of thermal photons from the evening surface of the asteroid, which are practically not balanced on the morning side, because this part of the surface had time to cool overnight.

One of the first direct observational detection of the YORP effect was obtained for NEA (1862) Apollo in 2007 (Kaasalainen et al., 2007). New observations of the asteroid in April 2008 (see Fig. 3) confirmed the influence of the YORP effect on Apollo's rotation period (Durech et al., 2008). It was found that a behaviour of Apollo's spin can not be explained with a simple assumption of a constant sidereal rotational period P. To achieve a data fit down to the noise level, the standard lightcurve inversion model had been extended by a linear increase of rotational speed $w=2\pi/P$ in time t: $w = w(t_0) + t \cdot dw/dt$. Using Apollo's model: λ_p = 48 deg, β_p = -72 deg, sidereal period P (JD 2444557.0) = 3.065448 ± 0.000003 h, acceleration of the rotational speed dw/dt = (5.5 ± 1.2) x 10^{-8} rad/day^2, this gives variation of the rotational period dP/dt = -4.5 - 10^{-3} sec/year.

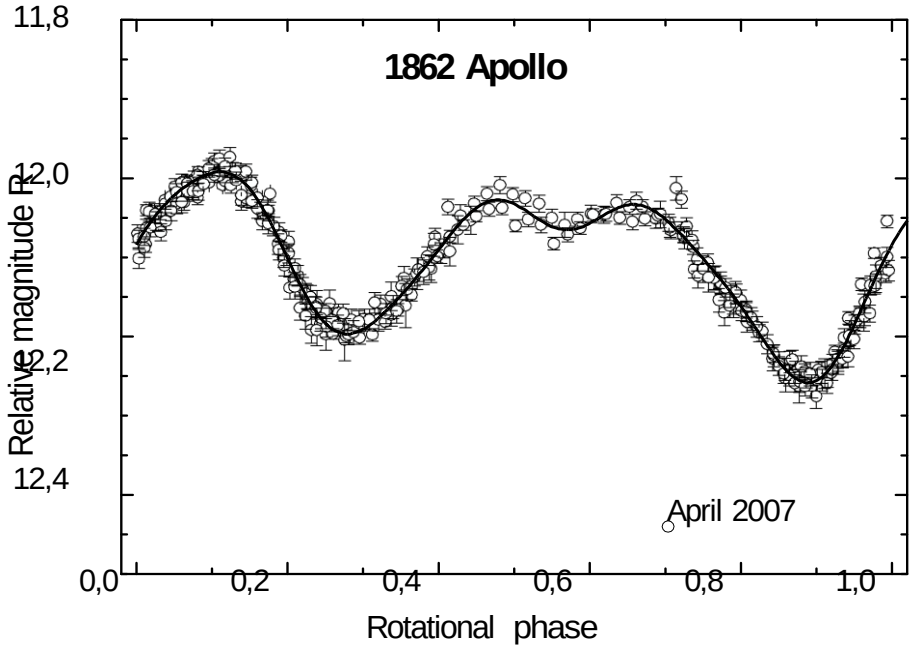

Fig. 3. Lightcurve of (1862) Apollo (open circles) and modeling fit (solid line) (Durech et al., 2008)

On the other hand, the thermal model of Apollo with parameters: density ρ = 2.7 g/cm^3, diameter D = 1.45 km, Bond albedo p_v = 0.1, thermal conductivity K = 0.02 W/mK have predicted the value of YORP acceleration of dw/dt = 8.0 - 10^{-8} rad/day^2, which is in a good agreement with the lightcurve modeling.

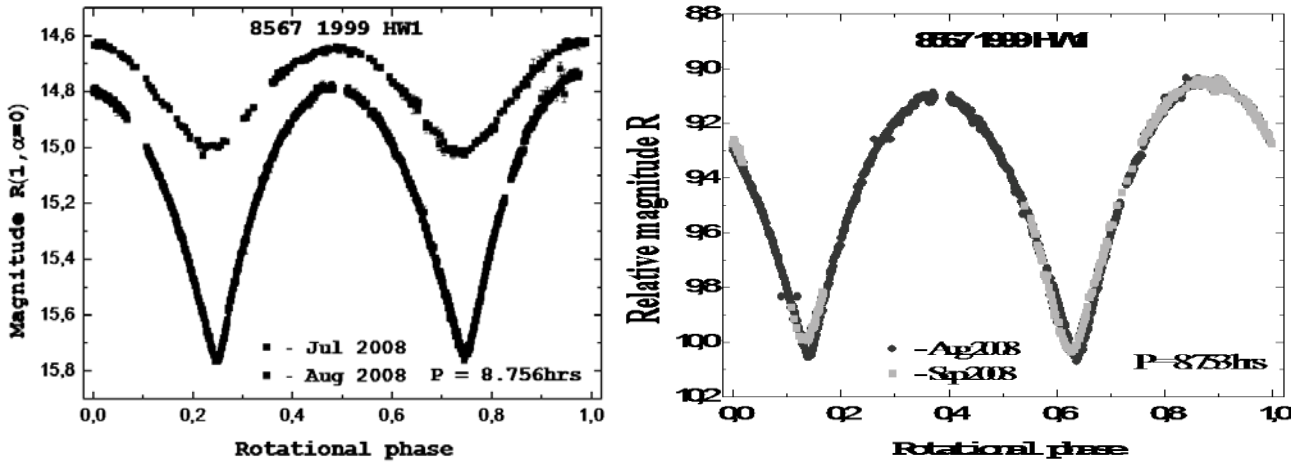

Fig. 4. Lightcurve of (8567) 1996 HW1 (Magri et al., 2011).

Up to now the YORP-effect has been investigated only for five asteroids, though it plays an essential role in evolution of rotational states of asteroids. As it was shown by Pravec et al., (2008), the small main belt and Mars crossing asteroids of 3-15 km in diameters have uniform distribution of the spin rates with an excess of slow rotators that can be controlled by the YORP-effect.

Active observations of main-belt asteroids and NEAs for determination of their rotational properties are carried out at the Institute of Astronomy of V. N. Karazin Kharkiv National University (Ukraine) in collaboration with other observatories, including Abastumani Astrophysical Observatory (Georgia). During the lastest years the work performed within ISON network (e.g., Molotov et

al., 2013; Shevchenko et al., 2014b; Krugly et al., 2015), and the hundred lightcurves and several tens of new rotational periods have been obtained every year.
The essential increase of the rotational data (about three times) has been occurred during only the last two years as a result of wide-field surveys (Waszczak et al., 2015). This massive is needed in more detailed investigation especially on rotation properties of asteroid families, groups, and some peculiar rotating asteroids.
A big progress was reached in the determination of spin vector directions and reconstruction of shapes of the asteroids from the lightcurves obtained in different oppositions. Using old methods (astrometrical photometry and magnitude-amplitude methods (Taylor 1979; Zappala 1981; Shevchenko et al., 2009; Cellino et al., 2015) and new inversion methods (Kaasalainen et al. 2001; Durech et al., 2010, 2015; Hanus et al., 2013; Viikinkoski et al., 2015) the pole coordinates were obtained for about eight hundred asteroids (Warner et al., 2009; Marciniak et al., 2015) and the isotropy in position of the poles was detected. Using the data from integral photometry and those from other sources including radar data, occultation profiles, images of asteroids and thermal data, and applying inversion methods a reconstruction of shape models becomes very close to real shapes of asteroids (Kaasalainen et al. 2001; Hanus et al., 2013; Viikinkoski et al., 2015; Benner et al., 2015). As an example of such complex investigation, the lightcurves of NEA (8567) 1996 HW1 and their shape reconstruction obtained by combining photometric and radar data are presented in Figs. 4 and 5 (Magri et al., 2011).

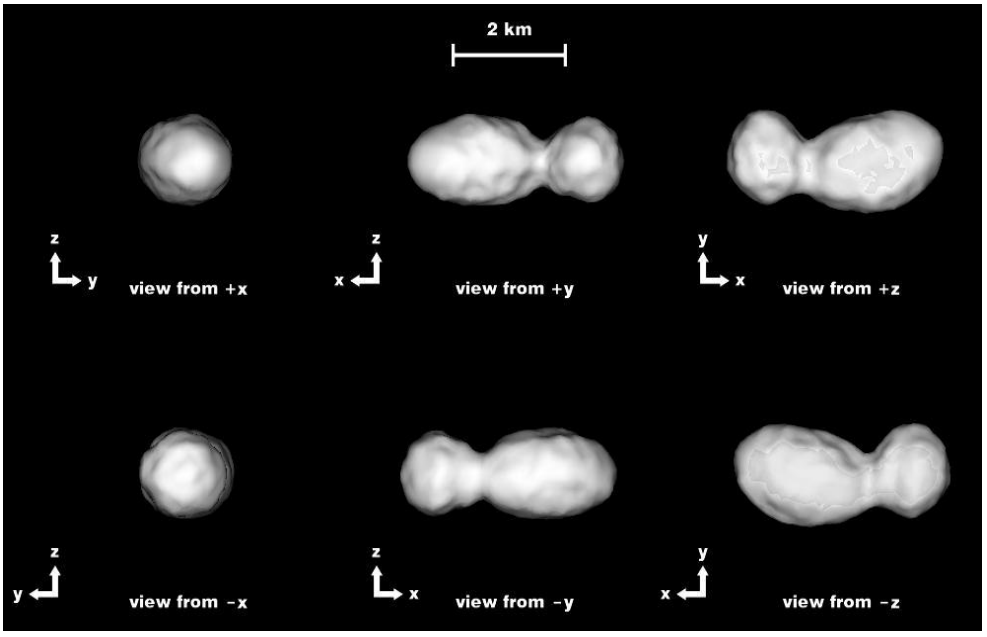

Fig. 5. Reconstructed shape of (8567) 1996 HW1 (Magri et al., 2011).

At present more lightcurve observations are needed in different aspects to obtain more data for asteroids suitable for their shape reconstructions and determination of the direction of spin vectors, including support for radar observations and space missions. The information about opportunities for lightcurve photometry of asteroids (for shape/spin modeling, magnitude-phase relations, etc.) is regularly published in the Minor Planet Bulletin (see, as example, Warner et al., 2016).

3. Binary and Multiple Systems

Binary systems are the main source for estimation of the masses and densities of asteroids. Regular discoveries of binary systems by the photometrical method have been started since 1997 (Pravec et al., 1998). Up to now about two hundred of the binary or triple asteroid systems have

been discovered (Warner et al., 2009; Margot et al., 2015; Pravec et al., 2016). As an example, the lightcurves of the binary asteroid (11264) Claudiomaccone observed for two nights are presented in Fig. 6 (Krugly et al., 2007). The form of lightcurves is caused both by the rotation of the main body and by mutual shadowing in the binary system. Analysis of all obtained observational data of the asteroid allowed us to determine the rotational period of the main body and to obtain the composite lightcurve of the binary system (Fig. 7). Later these data were used for the determination of the mass of the main body and the size ratio of the system components. The lower limit of the body diameter ratio is found to be D_2:D_1 = 1:3.2 for the binary asteroid (11264) Claudiomaccone (Krugly et al., 2007).

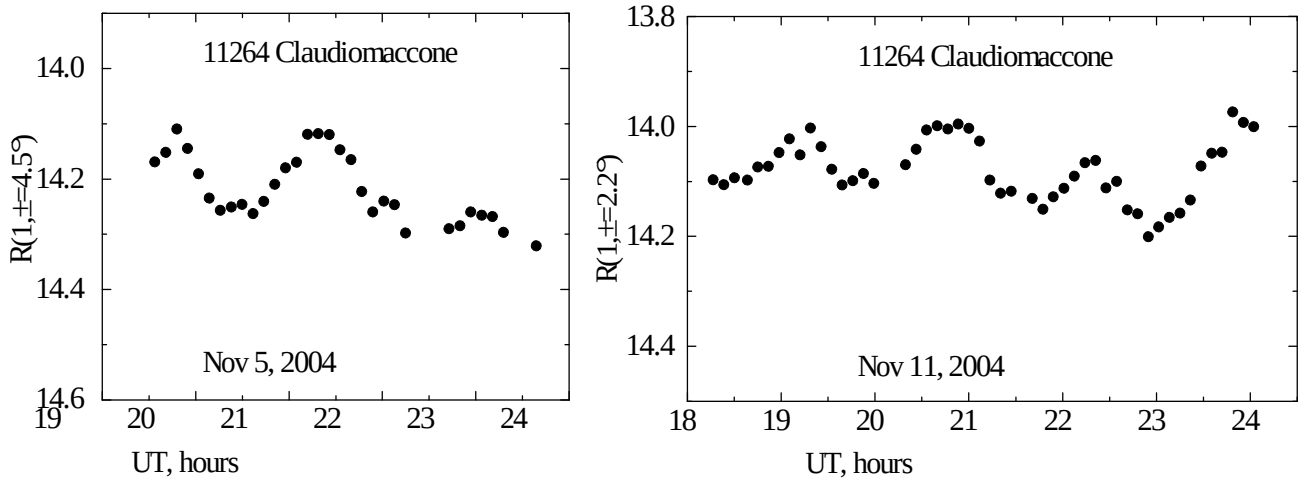

Fig. 6. Observed lightcurves of (11264) Claudiomaccone (Krugly et al., 2007)

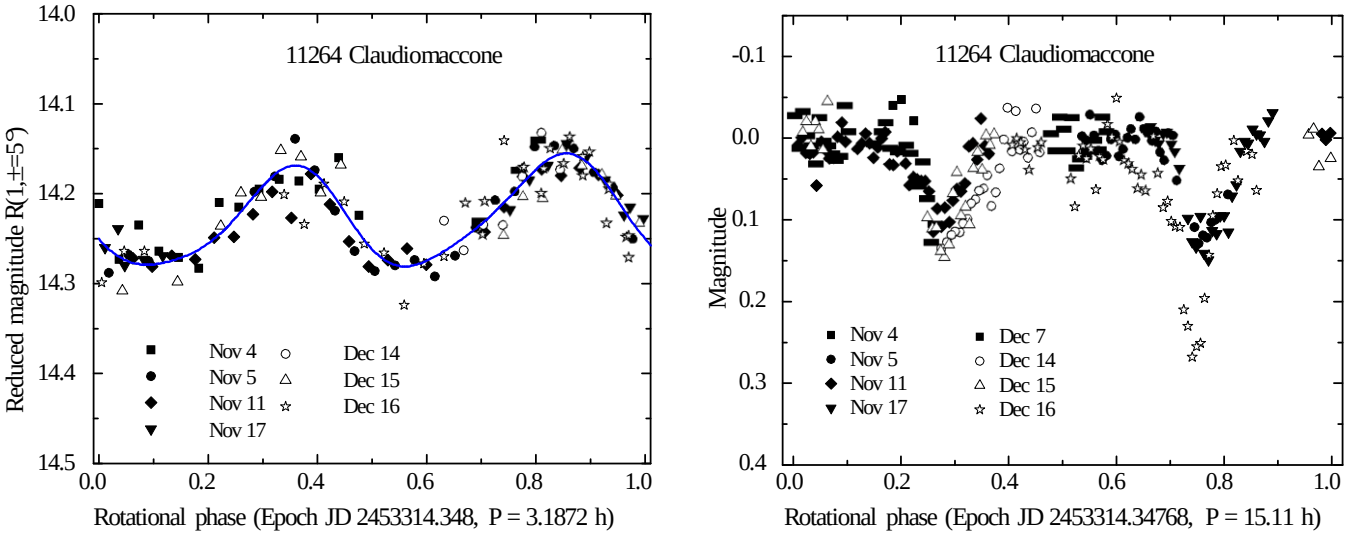

Fig. 7. Composite lightcurves of the main body (left) and the binary system (right) (Krugly et al., 2007)

Components of the known binary systems have very different sizes: from similar values, as in case of (90) Antiope, up to very small satellites, as in case of (45) Eugenia (the satellite Petit-Prince is about 6 mag fainter than the main body). There is some limitation for discovery of a binary asteroid from photometric observations. The main feature of a binary object is two- or three-periodic lightcurve. The photometric precision puts a limit for maximum diameter ratio of the bodies, which can be distinguishable from their lightcurves. The accuracy of photometry should be about 0.01

mag to detect a binary system with a diameter ratio down to D_2:D_1 = 1:5. Searching for the binary systems by photometric method demands both a high photometric accuracy and a long-term observations that are possible only in the frame of cooperative program (e.g., the long-term project of photometric observations of binary systems among small mainbelt asteroids "Photometric Survey for Asynchronous Binary Asteroids" coordinated by P. Pravec (Pravec et al., 2012a)).

4. Optical Properties

The optical properties measured by the photometry are, first of all, the absolute magnitude, the color indices, the magnitude-phase dependence, and the albedo of an object. The absolute magnitude gives information about a size of asteroid. Observed color indices allow to perform a preliminary taxonomical classification of the asteroids. Now the data on the *U-B*, *B-V*, *V-R* and *V-I* color indices are available for several hundred asteroids. Average values of the color indices for the main composition types are given in Shevchenko & Lupishko (1998) and Lupishko et al., (2007) which can be used for classification of newly observed asteroids. The magnitude-phase dependence allows obtaining the absolute magnitude and contains also information about the texture of the surface reflective layer (the degree of roughness and porosity) and the scattering properties of particles or aggregates (refractive index of material). For the main belt asteroids, whose phase angles are typically less than 25-30 deg, the magnitude-phase dependences are linear up to 5-7 deg and can be described by a phase coefficient ″ (mag/deg). At the smaller phase angles the so-called opposition effect (OE) is observed, that is nonlinear increase in brightness close to opposition. The opposition effect of asteroids usually starts at the phase angles less than 5-7 deg. Asteroids of low, moderate and high albedos show distinct differences both in the linear slopes and in the values of the opposition effect (Fig. 8).

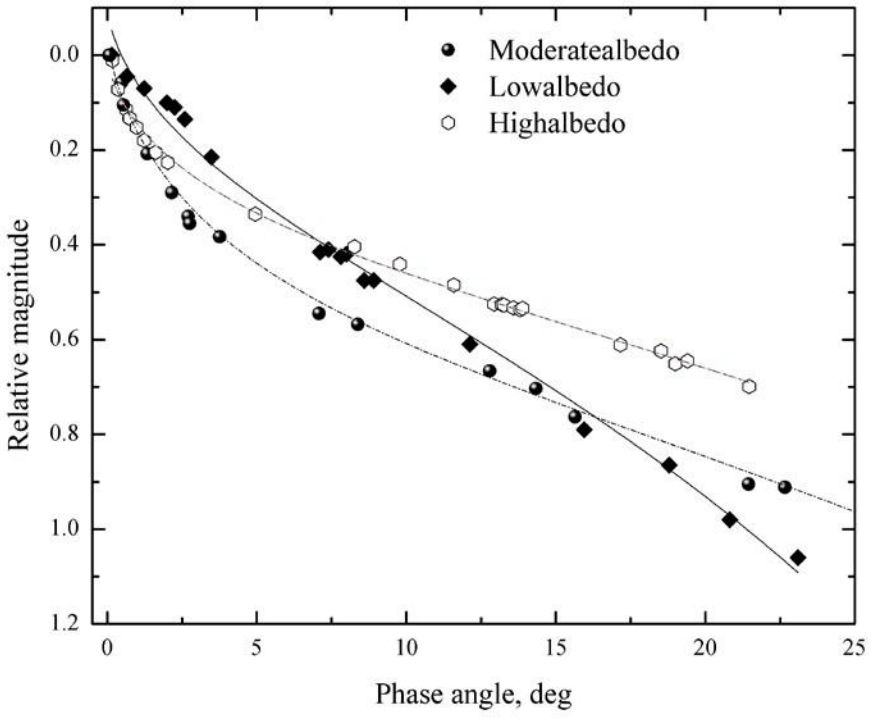

Fig. 8. Relative magnitude-phase relations for high, moderate and low albedo asteroids (Belskaya & Shevchenko 2000)

High quality data on magnitude-phase relations in the wide phase angle range were obtained for less than hundred asteroids. Most of the asteroids show noticeable opposition effect, while there are some low albedo asteroids which do not show the OE (Shevchenko et al., 2012).

As it was shown by Belskaya & Shevchenko (2000) and Shevchenko et al. (2012) asteroid taxonomical classification can be also made using their magnitude-phase dependences. The main asteroid compositional types are well-distinguished in the relationship of the OE amplitude and the linear slope (Fig. 9). As it was demonstrated by Shevchenko et al. (2015) two main-belt asteroids (723) Hammonia and (16551) 1991 RT14 which lie inside the region of S and M taxonomic types (see Fig. 9), can be classified as belonging to these moderate albedo types.

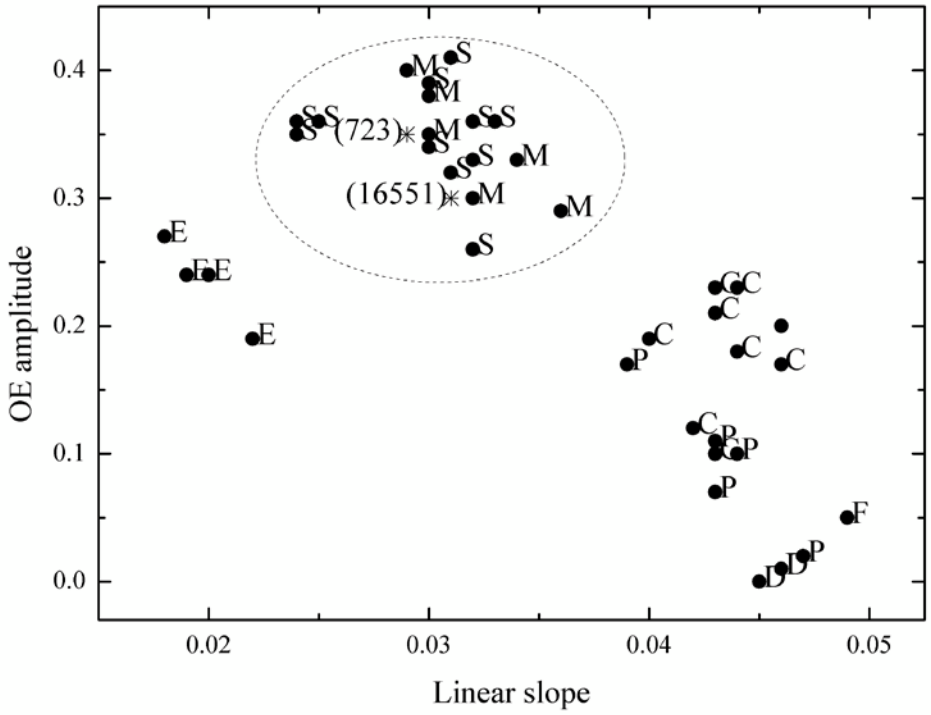

Fig. 9. The relationship of the OE amplitude and the linear slope for asteroids of different types (defined by letters) (Shevchenko et al., 2015)

Fig. 10 shows the dependence of the linear phase coefficient on the geometric albedo obtained by Belskaya & Shevchenko (2000). If the albedo is represented in a logarithmic scale, this relationship takes the linear form: $'' = -0.026 \lg p_v + 0.011$.

This relationship is very important because it gives a possibility to estimate the asteroid albedo using photometric measurements only. By measuring the linear slope of magnitude-phase dependence it is possible to distinguish between low, moderate and high albedo surfaces.

The determination of asteroid albedos by radiometric methods requires knowledge of asteroid absolute magnitudes. Since asteroids are observed at nonzero phase angles, absolute magnitudes are calculated using special function for reducing observed magnitudes to zero phase angle. Incorrect values of absolute magnitudes result in wrong values of albedos obtained from data of infrared surveys (WISE, AKARI, IRAS, etc.), that were demonstrated by Pravec et al., (2012b) and Shevchenko et al., (2014a). Up to now the two parameter HG-function was used for determination of an asteroid absolute magnitude (Bowell et al, 1989). But this function fits poorly the magnitude-phase relations of high and low albedo asteroids (Belskaya & Shevchenko, 2000; Shevchenko et al., 2008, 2012, 2014a). Recently new three parameter HG_1G_2-function has been proposed and actively used (Muinonen et al., 2010; Oszkiewicz D. A., et al. 2012). New high quality magnitude-phase relations for a large number of asteroids of different taxonomic classes are needed to perform a thorough check of this function.

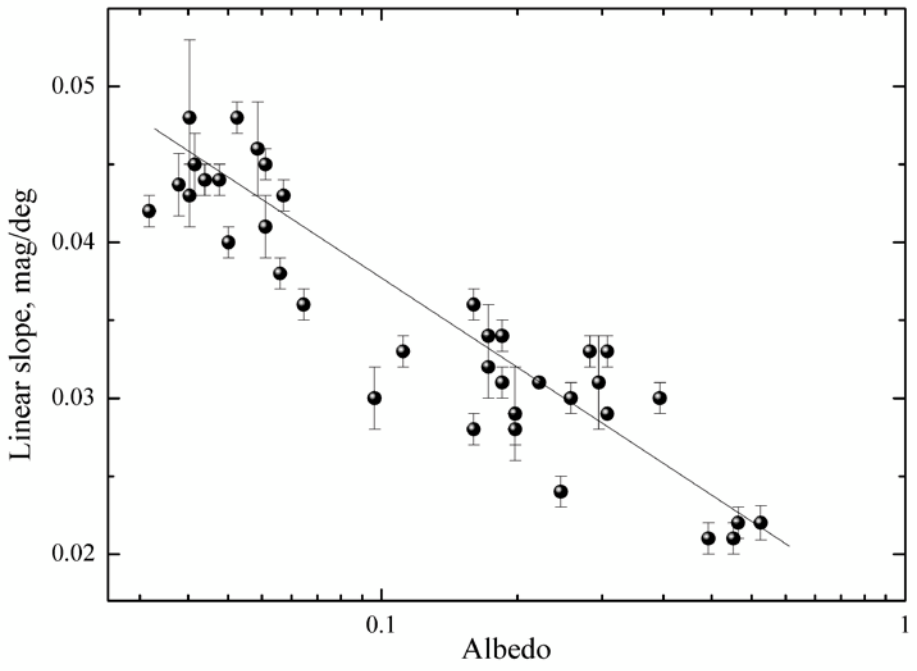

Fig. 10. The relationship of the linear slope and albedo (Belskaya & Shevchenko 2000)

The study of the magnitude-phase dependences and the opposition effect of asteroids is of a great value to understand the processes of lightscattering from regolith of atmosphereless bodies. In addition, knowledge of the magnitude-phase behavior at small phase angles is necessary to calculate the absolute magnitudes of these objects. Absolute magnitude of an asteroid is its basic characteristic for determination of its albedo and diameter, and for the ephemerid computation of apparent magnitudes.

5. Conclusions

Photometry is one of the most important techniques used to study physical properties of asteroids. It has provided a large amount of data on rotation periods, shapes, albedos, surface properties, densities etc. The main directions of asteroid photometry for the nearest years can be summarized as following:

- Study of the rotational characteristics of the asteroid groups and families (rotation periods, coordinates of poles, YORP-effect, etc.).
- Observations of the lightcurves for the selected asteroids for modeling their shape.
- Ground-base photometric observations in support of radar research and space missions.
- Search for binary and multiple systems, especially in the outer part of the main-belt.
- Obtaining high-precision magnitude-phase dependencies of mainbelt asteroids and NEAs to study the optical properties of their surfaces and to verify approximation functions used for determination of absolute magnitude.

Acknowledgments

Shevchenko V. G. and Belskaya I.N. are grateful to the Samtskhe-Javakheti State University for the support allowing them to participate at the International Scientific Conference “Problems of modern astrophysics”. This research was partly supported by the Ukrainian Ministry of Education and Science.

References

Belskaya, I. N., & Shevchenko, V. G. 2000, Icarus, 146, 490.
Benner, L. A. M., Busch, M. W., Giogini, J. D., et al. 2015, In Asteroids IV (Tuscon: Univ. Ariz. Press), 165.
Bowell, E., Hapke, B., Domingue, D., et al. 1989, In Asteroids II (Tucson: Univ. Ariz. Press), 524.
Cellino, A., Muinonen, K., Hestroffer, D., Carbognani, A. 2015, PSS, 118, 221.
Durech, J., Vokrouhlický, D., Kaasalainen, M., et al. 2008, A&A, 488, 345.
Durech, J., Sidorin, V., Kaasalainen, M. 2010, A&A, 513, A46.
Ďurech, J., Carry, B., Delbo, M., et al. 2015, In Asteroids IV (Tuscon: Univ. Ariz. Press), 183.
Hanuš, J., Ďurech, J., Brož, M., et al. 2013, A&A, 551, A67, 16 pp.
Harris, A. W., & Pravec, P. 2006, In Asteroids, Comets, Meteors (Cambridge Univ. Press), 439.
Kaasalainen, M., Torppa, J., Muinonen, K. 2001, Icarus, 153, 37.
Kaasalainen, M., Durech, J., Warner, B., et al. 2007, Nature, 446, 420.
Krugly, Yu. N., Maccone, C., Gaftonyuk, N. M., et al. 2007, PSS, 55, 449.
Krugly, Yu., Molotov, I., Voropaev, V., et al. 2015, Proceedings of GAIA-FUN-SSO 2014 Third "Gaia Follow-up Network for Solar System Objects". ISBN 2-910015-73-4. P. 93.
Kwiatkowski, T., Polinska, M., Loaring, N., et al. 2010, A&A, 511, A49, 11 pp.
Lupishko, D. F., Krugly, Yu. N., Shevchenko, V. G. 2007, Kinemat. Phys. Cel. Bodies, 23, 235.
Magri, C., Howell, E. S., Nolan, M. C., et al. 2011, Icarus, 214, 210.
Marciniak, A., Pilcher, F., Oszkiewicz D., et al. 2015. PSS, 118, 256.
Margot, J.-L., Prave, P., Taylor, P., et al. 2015, In Asteroids IV (Tuscon: Univ. Ariz. Press), 355.
Molotov, I., Agapov, V., Khutorovsky, Z., et al. 2013, Proceedings of 6th European Conference on Space Debris. ESA SP-723, ISBN 978-92-9221-287-2, 2013, id.26.
Muinonen, K., Belskaya, I. N., Cellino, A., et al. 2010, Icarus, 209, 542.
Pravec, P., Wolf, M., Sarounova, L., et al. 1998, Icarus, 133, 79.
Pravec, P., Harris, A. W., Vokrouhlicky, D., et al. 2008, Icarus, 197, 497.
Pravec, P., Scheirich, P., Vokrouhlický, D., et al. 2012a, Icarus, 218, 125.
Pravec, P., Harris, A. W., Kušnirak, P., et al. 2012b, Icarus, 221, 365.
Pravec, P., Scheirich, P., Kusnirak, P., et al. 2016, Icarus, 267, 267.
Oszkiewicz, D. A., Bowell, E., Wasserman, L. H., et al. 2012, Icarus, 219, 283.
Shevchenko, V. G., & Lupishko, D. F. 1998, Solar Syst. Res., 32, 220.
Shevchenko, V. G., Chiorny, V. G., Gaftonyuk, N. M., et al. 2008, Icarus, 196, 601.
Shevchenko, V. G., Tungalag, N., Chiorny, V. G., et al. 2009, PSS, 57, 1514
Shevchenko, V. G., Belskaya, I. N., Slyusarev, I. G., et al. 2012, Icarus, 217, 202.
Shevchenko, V. G., Slyusarev, I. G., Belskaya, I. N. 2014a, Meteor. Planet. Sci., 49, 103.
Shevchenko, V. G., Velichko, F. P., Checha, V. A., Krugly, Y. N. 2014b, Minor Plan. Bul. 41, 195.
Shevchenko, V. G., Slyusarev, I. G., Belskaya, I. N., et al. 2015, LPSC, 46, 1832, 1509.
Taylor, R.C. 1979. In Asteroids (Tuscon: Univ. Ariz. Press), 480.
Viikinkoski, M., Kaasalainen, M., Durech, J. 2015, A&A, 576, A8.
Warner, B. D., Harris, A. W., Pravec, P. 2009, Icarus, 202, 134. Updated 2015 December 7. *http://www.MinorPlanet.info/lightcurvedatabase.html*
Warner, B. D., Harris, A. W., Durech, J., Benner, L. A. M. 2016, Minor Planet Bulletin, 43, 103.
Waszczak, A., Chang, Ch.-K., Ofek, E. O., et al. 2015, Astron. J. 150, 75, 35 pp.
Zappala, V. 1981, Moon & Planets, 24, 319.

Chronicle

Victor Dzhapiashvili (1924 - 2015)

Victor Dzhapiashvili was born on June 20, 1924 in the village Daba of Borjomi(Georgia) District, where he finished a secondary school with honors.

On the very first days of the Great Patriotic War (1941-1945) he arrived in the military commissariat and went to the war as a volunteer. In 1942 he was wounded at the town Tuapse during the battle for the Caucasus.

In 1945 Victor Dzhapiashvili entered without examinations the Faculty of Physics and Mathematics of Tbilisi State University, which he graduated from in 1949. Mr. Dzhapiashvili was the first to begin since 1950 studying the Moon with an electropolarimetric method at the Abastumani Astrophysical Observatory. In 1955 he defended a candidate's dissertation on the topic: "Investigation of the Moon's Surface Structure with Electropolarimetric Measurements," which he published in the form of monograph in 1957.

Victor Dzhapiashvili in collaboration with A. Korol were the first in the world to publish in 1982 "A Polarimetric Atlas of the Moon," for which he was awarded the Bredikhin State Prize.In 1988 Victor Dzhapiashvili defended at the Sternberg Astronomical Institute of Moscow State University a doctor's dissertation on the topic: „Creation of the Polarimetric Atlas of Moon and Its Usage for the Study of Physical Properties of Lunar Surface," for which he was granted the scientific degree of Doctor of Physical and Mathematical Sciences.

Victor Dzhapiashvili's main research findings were used in many monographs and textbooks (in the works by N. Barabashov, V. Sharonov, Z. Kopal, et al.), he read scientific papers at international symposia and conferences held in the USA, Germany, Russia, Poland, Ukraine, Armenia, and Georgia.

Along the research line " Electropolarimetric studies of Moon and planets ", founded by Mr. Dzhapiashvili at the Observatory, dozens of scientists have been brought up, who for their part are bringing up young specialists.

On August 17, 2015 Victor Dzhapiashvili died at the age of 92.

On october 7-9, 2015 at Samtskhe –Javakheti State University ,Conferenec was held on: "Modern Problems of Astrophysics."

To Ms Silvia Torres-Peimbert

President of International Astronomical Union

Dear MsTorres-Peimbert!

We are bringing to your knowledge that we had in our ranks a brilliant scientist, Doctor of Sciences (Physics and Mathematics), laureate of Bredikhin State Prize, and teacher of up to ten doctors of science Professor Victor Dzhapiashvili.

Victor Dzhapiashvili was the first to begin since 1950 the study of Moon based on Electro-polarimetric method. He published a monograph and Polarimetric Atlas of the Moon (for the first time in the history of world science!). In addition he published several tens of first-class research works on the physical nature of Moon, to which he dedicated more than 65 years of his life.

He received more than one highest prizes, including the Order of Honor, Bredikhin State Prize and many others.

on 17 August 2015 at the age of 92 Victor Dzhapiashvili passed away.

Dear Ms President!

We are requesting you to take into consideration Victor Dzhapiashvili's greatest contribution to the fruitful and longtime study of the nature of Moon and to mediate and support at one of the nearest meetings of the International Astronomical Union the proposal on naming one of the nameless lunar craters after Victor Dzhapiashvili.

In the name of participants of the international conference "Modern Problems of Astrophysics":

Doctors of Sciences:

1. M. Beridze
2. O. Kvaratskhelia
3. R. Chigladze
4. G. Javakhishvili
5. E. Khutsishvili
6. A. Kvrivishvili
7. G. Mahasidze
8. R. Inasaridze
9. T. Kvernadze
10. G. Kuzkhuli
11. E. Janiashvili
12. T. Urushadze
13. A. Hukerdeak (SAO)
14. V. Shevchenko (KNU)
15. A. Rozhenko (IKI)
16. I. Belskaya (Kharkiv univ)
17. G. Kimeridze
18. R. Natsvlishvili
19. A. Sigua.

On the initiative of the conference participants a letter of the following content was sent to the President of International Astronomical Union.Based on the above letter a positive reply was received.A lunar formation,located between the areas of crisis and fertility to be named after Prof. Viktor Japiashvili.

Astronomy & Astrophysics (Caucasus) 1 (2016)

Key Words

Absorption lines, NH3, 6475 Å band

Active galactics

Afterglow

Albedo

Asteroid

Ammonia

Astropolarimeter

BL Lacertae objects

Canonical variables

CCD observations

Computer techniques

Cosmology

Evolution WR stars

Frequency

Front and rear hemispheres

Function

Galilean satellites

Galaxy model

Gamma-ray bursts

Gravitation

Groups

Groups representations

Integral of motion

Jupiter

line formation

Mass loss from stars – stars

Mass loss from stars - stars

Methods analytikal

Metods numerical

Moon

Photometry

Polarization-holographic element

Polarization- sensitive materials

Polarization degree

Positive polarization

Potential

Period

Transientes

TeV gamma-ray

Wolf-Rayet - stars

Astronomy & Astrophysics (Caucasus) 1 (2016)

Author Index for Volume 1

Astronomy & Astrophysics (Caucasus)

Scientific paper Submission

The submitted article's technical parameters are the same as in the USA leading international scientific journals.After the positive review only astronomy and astrophysical original articles will be published in this journal.
The manuscript should be presented in A4 format. The size of the article ,including bibliography and other types of enclosure should not exceed 20 pages printed with 1interval and 12 sized font.
It is possible to submit the online version of the manuscript but is should be written only in English. (Text must be typed in Times New Roman, MS word or Pdf file)
The text should be written on the whole page and not separately on twocolumns,the same as in this journal.

Structure of the paper:
Title of the paper:
Author/authors:

Name of the author/authors,firstname,secondname, working place,country and online address must be presented below the manuscript title.

Abstract

The abstract must be informative.Shouldrepresent the content of the paper,describe the goal of the research,symmerize results of the survey and show its theoretical and practical importance.The abstract should not exceed more than 250words,nearly one page.

Key words: Authors should provide key words,which are relevant to the topic.Maxium amount of the words should be 8 . Use only commonly used shortenings .

Introduction: Authors should highlight the essence of the problem, their sub-aims,what is their hypothesis,importance of their paper and what have been done peviously in this field.

Methods: The article should be build methodologically correct way. It should reflect the usage of modern research methods.

Results: Results must be described clearly and briefly**.** Each illustration should have its inscription**.** Number the tables used in the text consistently.

Analysis: This paragraph should investigate the importance of the paper results.You should compare your result to the previous ones**.**

Conclusions: The main conclusion can be written in this paragraph**.**

Acknowledgment: At the end of the paper on the separate chapter you should express your gratitute to those people who helped you during the research.

Literature citation: Consider that every source you have used in this paper is also indicated in the bibliography or vice versa.

Sources Reference Style: The literature quoted in the scientific publication should be indicated with round brackets.(Sort version:name of the author and the rule of the article publication**.**

Reference: Nominated literature where the author's identity is indicated fully,the date of the publication and appropriate page should be arranged alphabetically.

It will be published twice in a year.

The paper should be send to the following e-mail address: astronomy@sjuni.edu.ge

CONTENTS

Publishing Groupi: **L. Gurgenidze**
L. Zedginidze

Correctional: **M. Toroshelidze**

Publishing-House
„Akhaltsikhe University”

Akhaltsike, Rustaveli Street №106
Tel.: 0(365)22-19-90, 591-41-12-78
E-mail: astronomy@sjuni.edu.ge